CLALLAM MRC MEETING AGENDA

January 26th, 2026
5:30 p.m. – 7:00 p.m.
Hybrid Meeting

Zoom meeting link: https://us06web.zoom.us/j/83769639254?pwd=FmcMflhkxw6df902xa2tsxu6UAHGVB.1
Meeting ID: 837 6963 9254
Passcode: 12345
For more information about the MRC, please contact Chase O'Neil at 360-417-2361.

Welcome by Chair LaTrisha Suggs / Call to Order / Roll

- Determination of quorum

Public Comment on agenda items, *limited to 3 minutes per participant*

Approval of Minutes

- December minutes

Presentation

- Dr. Chris Bassett, PNNL: Tidal turbines and animal interactions
- Molt Search program for European Green Crab (5-10 minutes)

Announcements

- New member Rob Casey, representing Marine Related Recreation and Tourism
- Thank you departing members: Mike Doherty and Ray Kirk
- Time Log-Thank you everyone that documented their time.
- Studium Generale brief recap
- Derelict sailboat removed from Elwha Beach
- Northwest Straits Commission update – Alan Clark
- New items, consensus, staff coordination

Committee and Project Reports

- Project leads report only if an update is needed
- Advisory sub-committee

New or special business

- Potential MRC social event this spring
- Education and outreach subcommittee

Discussion of next meeting date and agenda

- Next regular meeting Monday, Feb 23 (4th Monday, due to holiday)

2026 Meetings

January 26 (4th Mon)	April 20	July 20	October 19
February 23 (4th Mon)	May 18	August 17	November 16
March 16	June 15	September 21	December 21

    - Presentations: Justine Chorley (Clallam County Emergency Management) and Cynthia Harbison (DNR Elwha Kelp and Eelgrass Priority Area)
- Call for new agenda items

Good of the Order

Public Comment *limited to 3 minutes per participant*

Adjourn

Clallam County DCD is inviting you to a scheduled Zoom meeting.
Join Zoom Meeting
https://us06web.zoom.us/j/83769639254?pwd=FmcMflhkxw6df902xa2tsxu6UAHGVB.1

Meeting ID: 837 6963 9254
Passcode: 12345

One tap mobile
+12532050468,,83769639254#,,,,*12345# US
+12532158782,,83769639254#,,,,*12345# US (Tacoma)

Dial by your location
• +1 253 215 8782 US (Tacoma)

2026 Meetings

January 26 (4th Mon)	April 20	July 20	October 19
February 23 (4th Mon)	May 18	August 17	November 16
March 16	June 15	September 21	December 21

Marine Animals Interactions with a Small Tidal Turbine in Sequim Bay

Christopher Bassett
Applied Physics Laboratory, University of Washington

Clallam County Marine Resources Committee
January 2026

Goals

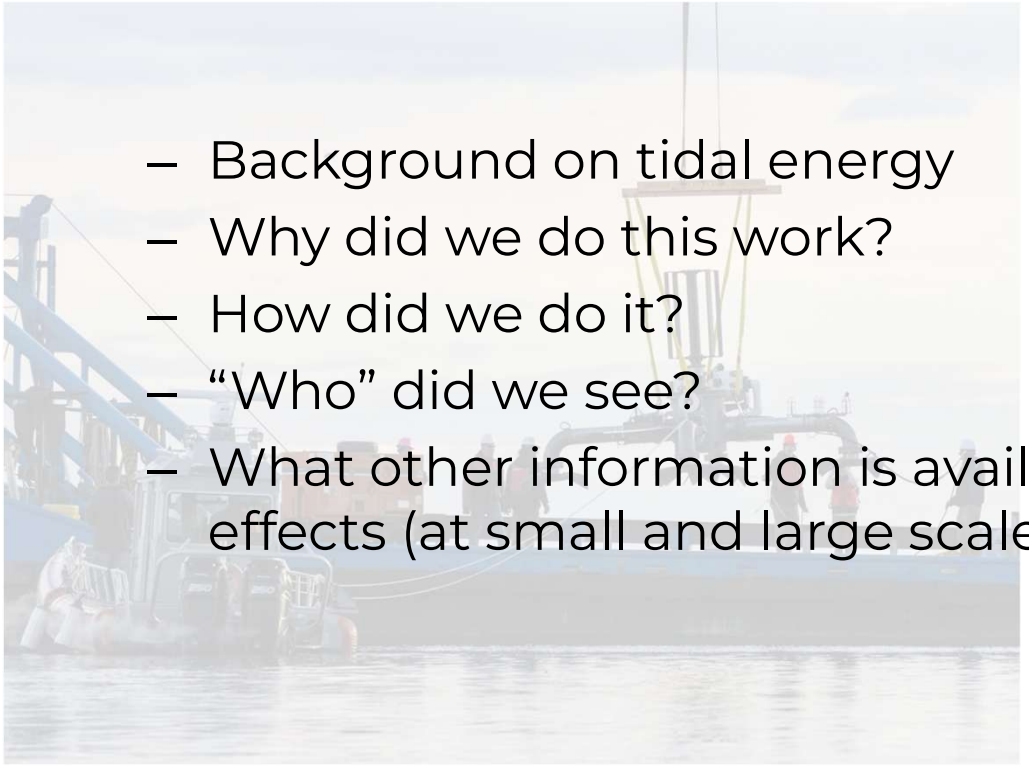

- Background on tidal energy
- Why did we do this work?
- How did we do it?
- “Who” did we see?
- What other information is available about environmental effects (at small and large scales)?

Who am I?

- UW Graduate – Passive acoustics
  - Anthropogenic noise
- Woods Hole Oceanographic Institution
  - Acoustic scattering (oil spill detection/quantification & fisheries)
- NOAA Fisheries
  - Acoustic-trawl surveys in Alaska (echosounders)
- Applied Physics Lab. (UW)
  - Scientist/engineer
  - Acoustics (passive and active)
  - Environmental effects of marine energy

What is Marine Energy?

- Offshore wind
- Offshore solar
- Waves
- Tides
- Currents
- Thermal gradients
- Salinity gradients
- Biomass

Why Marine Energy?

- Power remote ocean observing systems & vehicles
- Local communities (often remote) seeking renewable power sources
- Grid-scale power

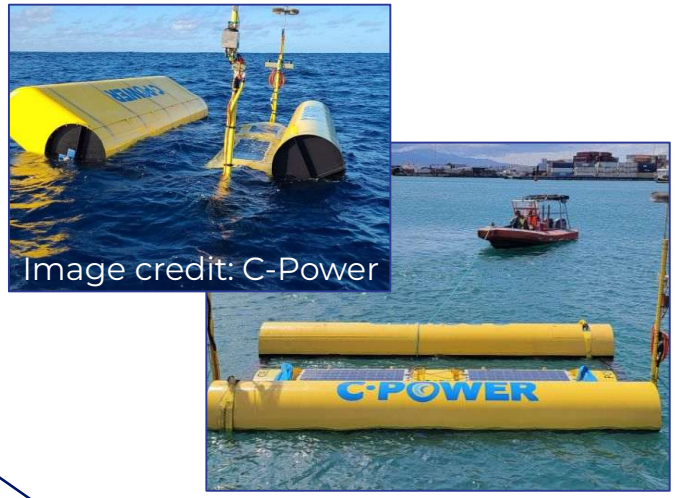

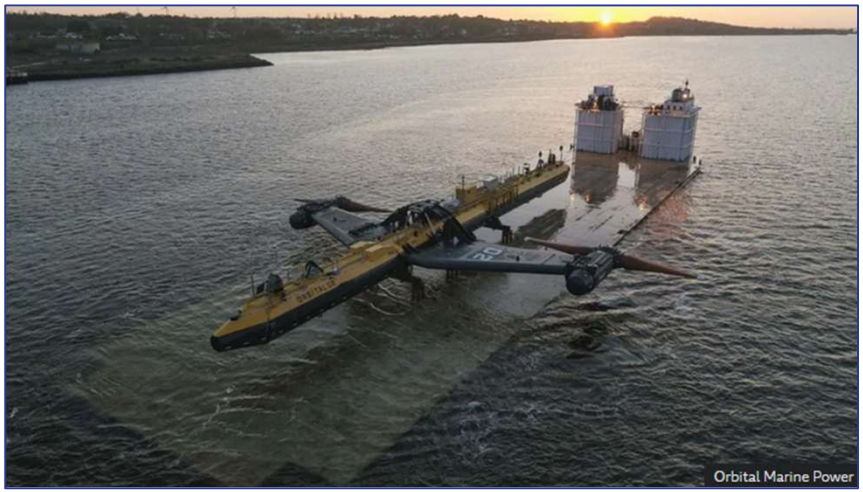

Ocean Renewable Power Company RivGen Turbine. Igiugig, AK. Photo: NOAA

Status Update

- Devices have been demonstrated at all-scales, but wave and tidal energy converters are part of a nascent industry.
  - Larger (grid-scale) wave and current (turbines) not yet deployed in the U.S.
  - Community and smaller-scales have been operated (and are currently) in U.S. waters

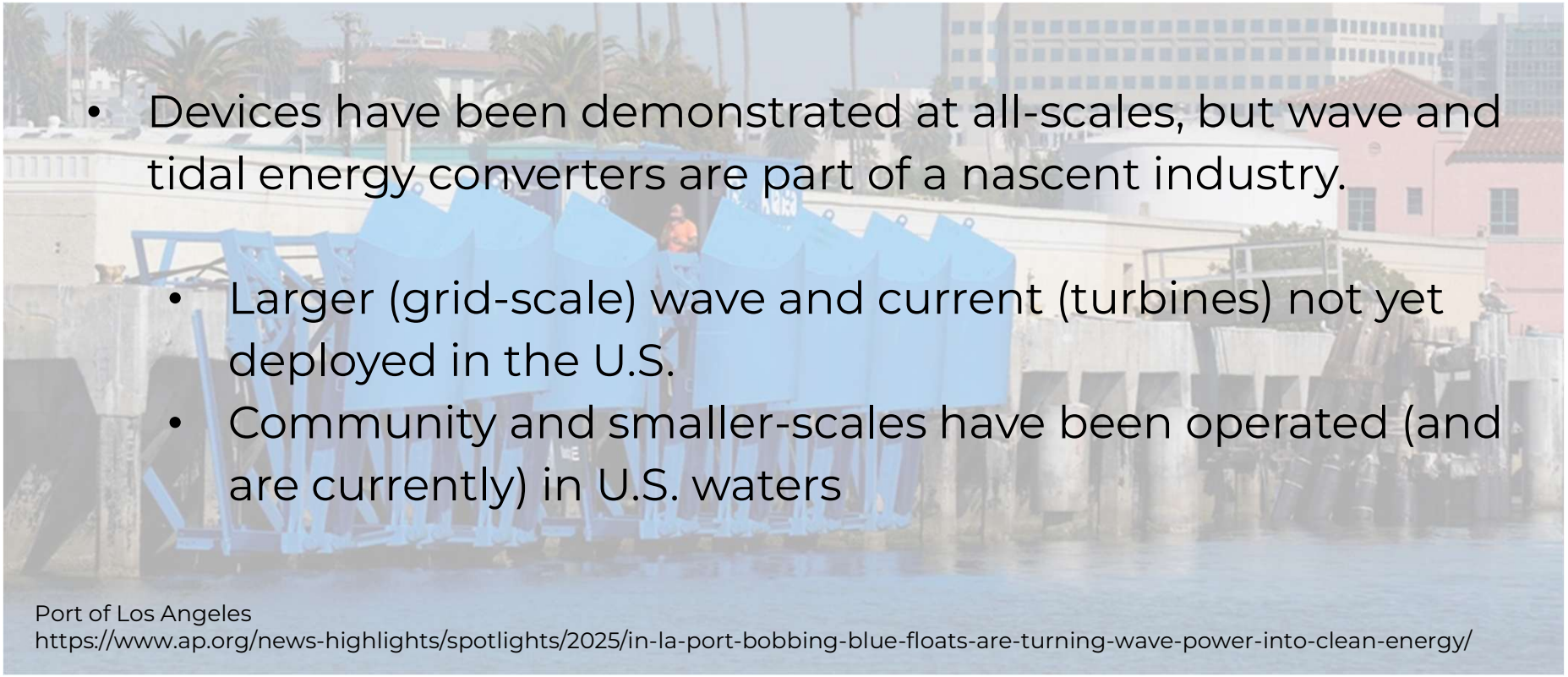

Port of Los Angeles
https://www.ap.org/news-highlights/spotlights/2025/in-la-port-bobbing-blue-floats-are-turning-wave-power-into-clean-energy/

Perceived Risks of Marine Energy

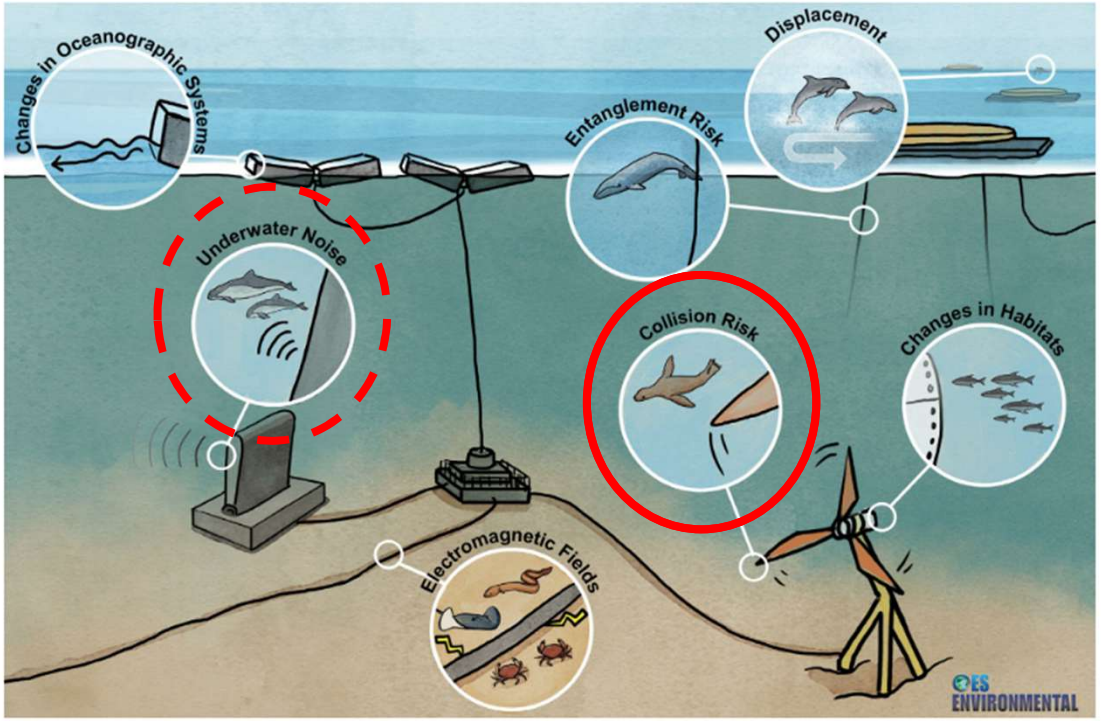

Figure 1.2. Stressor-receptor interactions potentially arising from various marine renewable energy devices. (Illustration by Stephanie King)

- Measure early
- Respond early

Collision Risk Terms

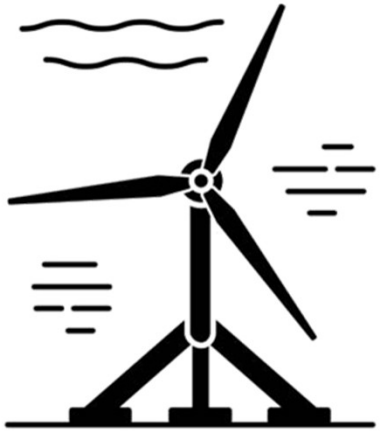

Collision Risk Terms

Avoidance:
Animal doesn't approach turbine

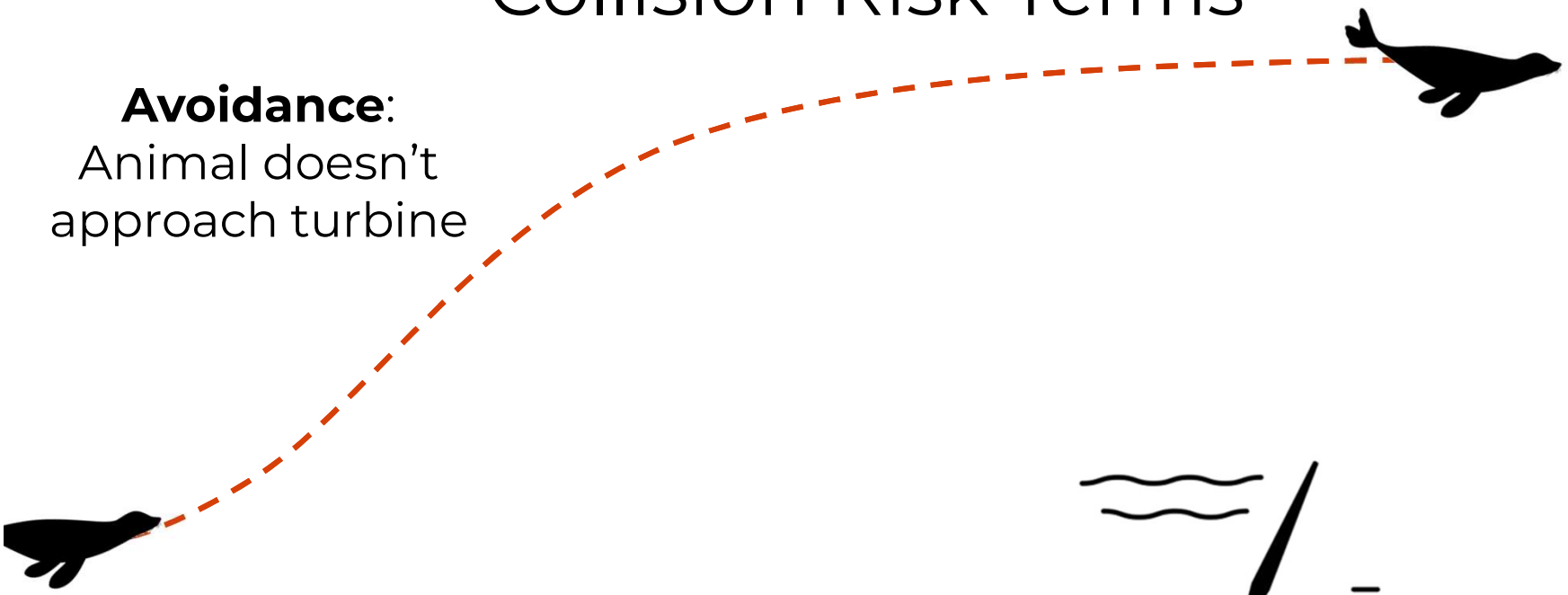

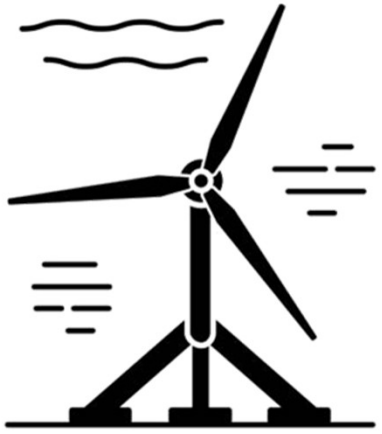

Collision Risk Terms

Encounter:
Animal approaches turbine

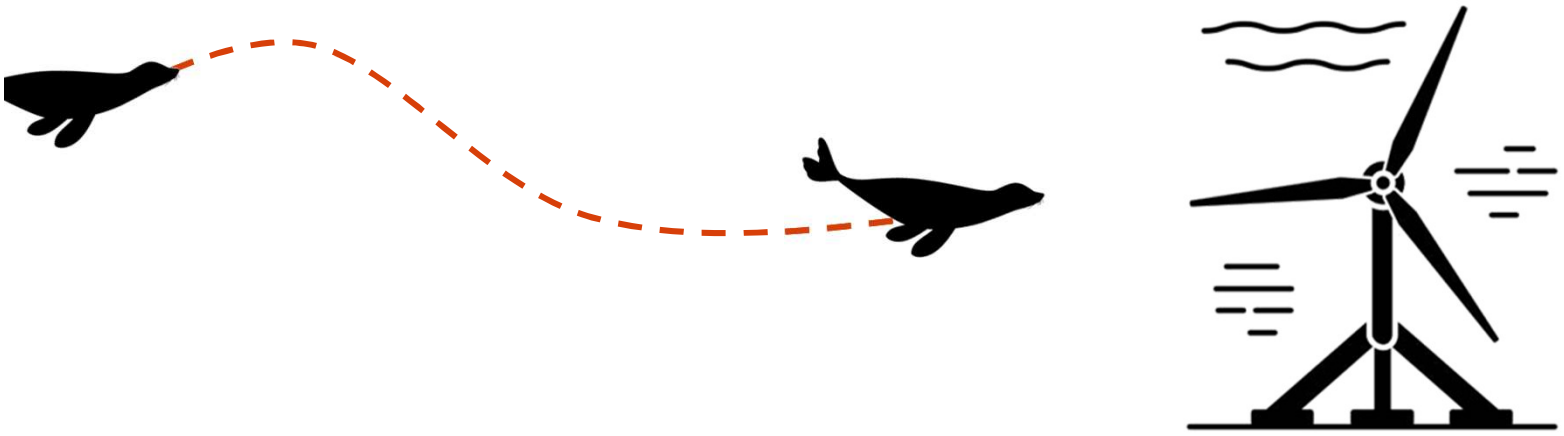

Collision Risk Terms

Evasion:
Animal changes behavior to avoid collision

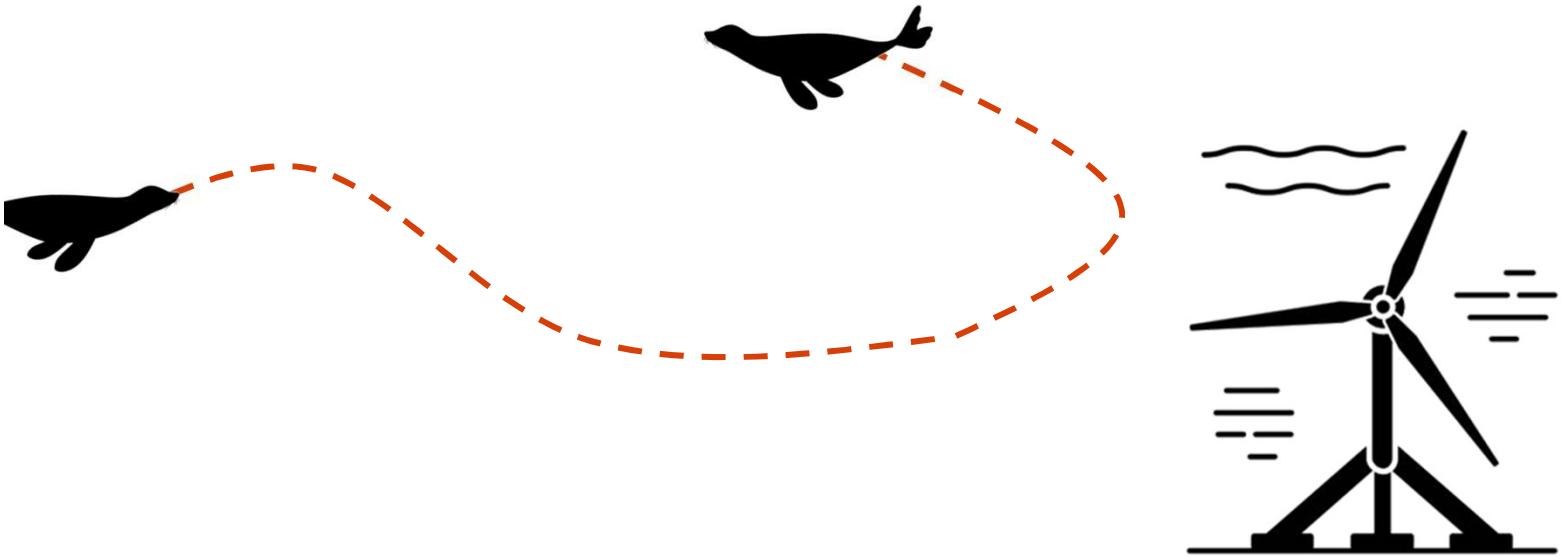

Collision Risk Terms

Collision:
Animal contacts moving parts of a turbine

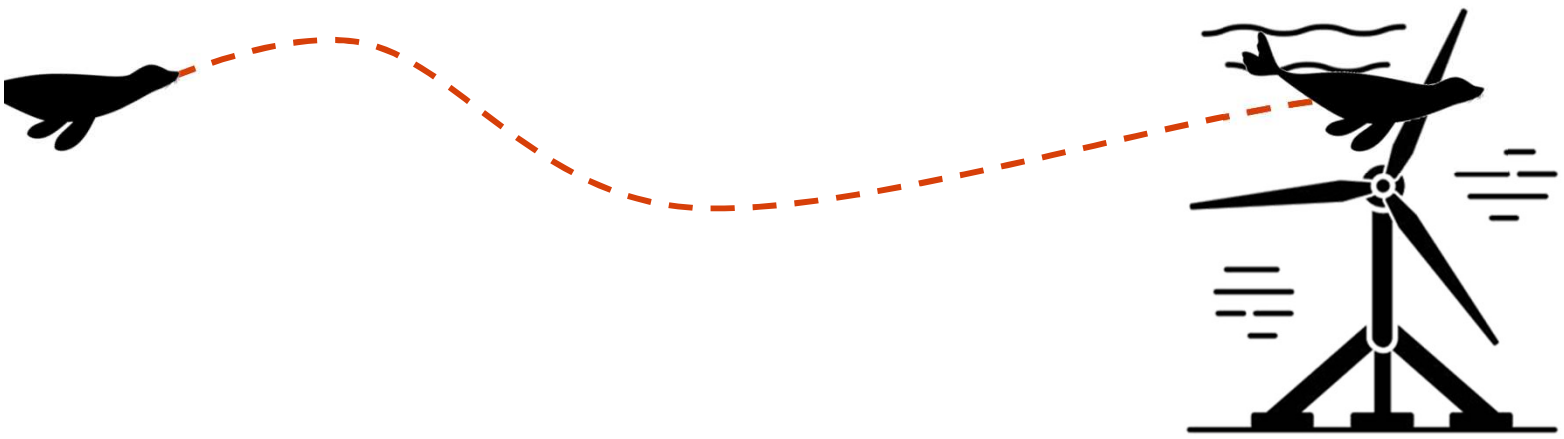

Collision Risk: Results from Prior Work?

Fish: many avoid turbine area, few cases of evasion, no collisions documented (prior to our work) *

Marine mammals: many avoid turbine area, fine-scale evasion, no collisions documented

Seabirds: habitat use in tidal channels varies, no collisions or encounters with moving turbine documented

Case Study: The Turbine Lander

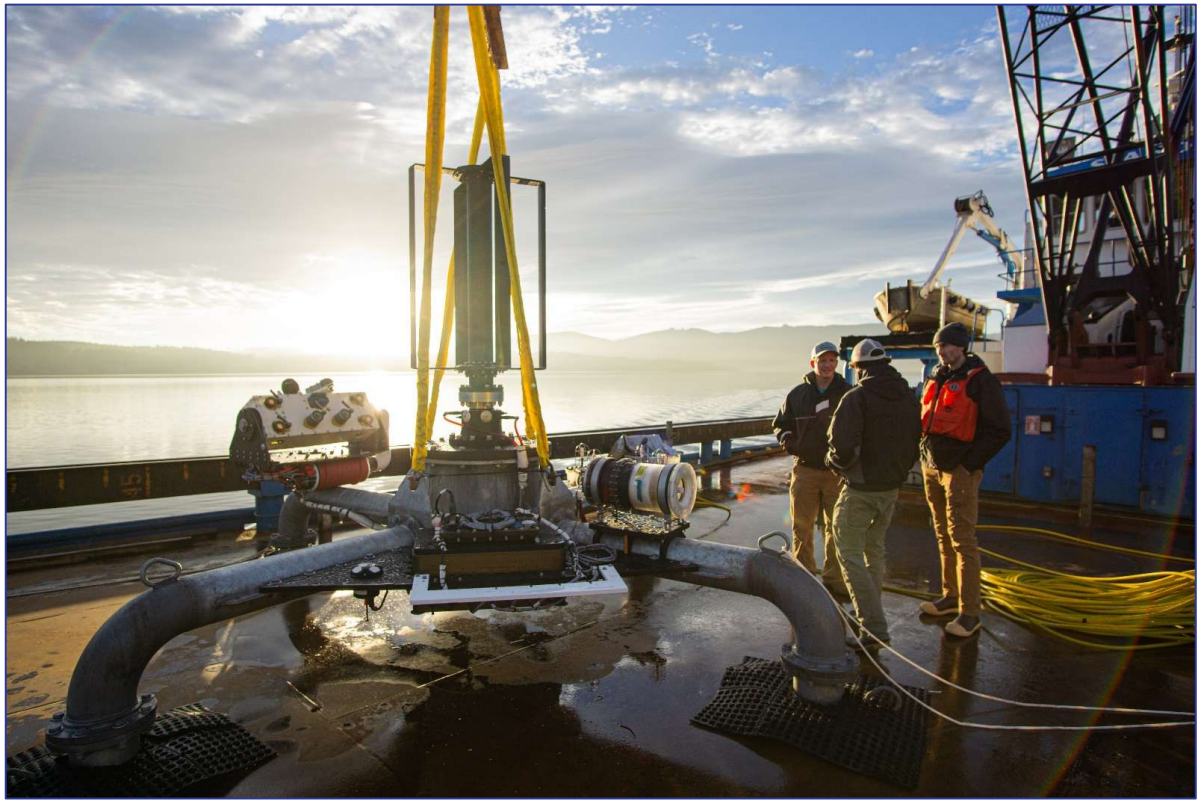

Total size:
4 m x 4 m x 2.7 m

Rotor size:
1.19 m x 0.85 m

Operations:
Currents > 0.9 m/s
RPM ~ 40 to 120

Case Study: The Turbine Lander

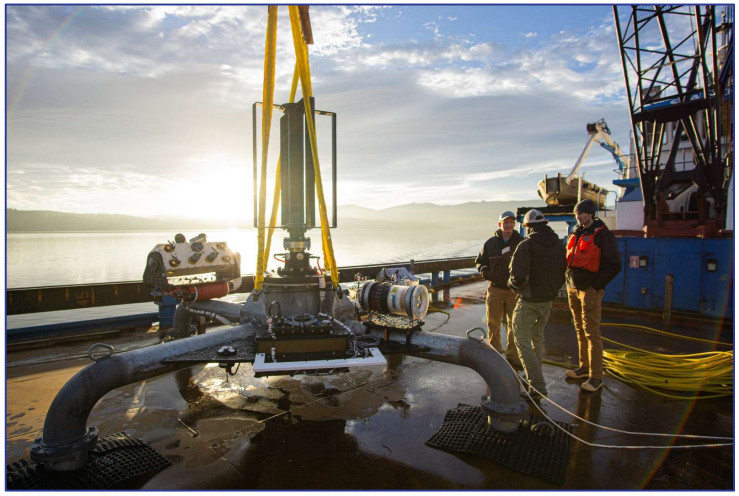

Why?

- A turbine this size might generate 100 W (on average)
- This is little power on land, but at sea this can significantly enhance our ability to use advanced sensing package, increase telemetry, or change vehicles remotely.

Case Study: The Turbine Lander

Sequim Bay, WA

- Shallow
- Infrastructure
- Support
- Previous work

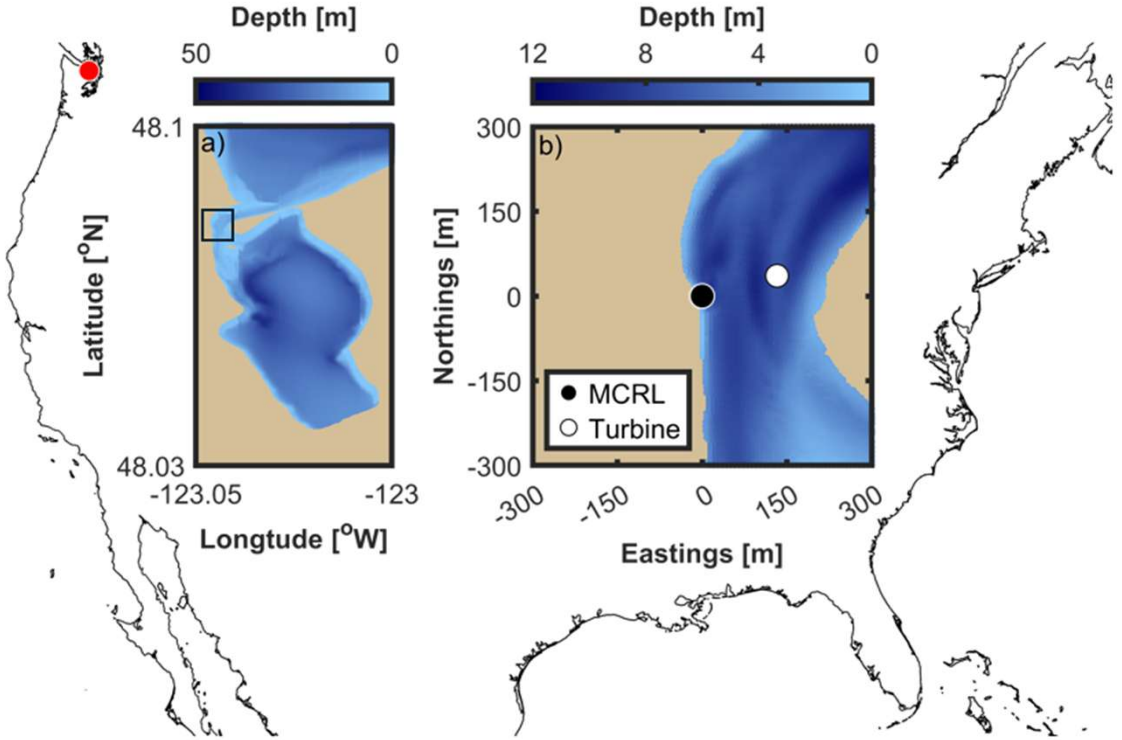

The Adaptable Monitoring Package (AMP)

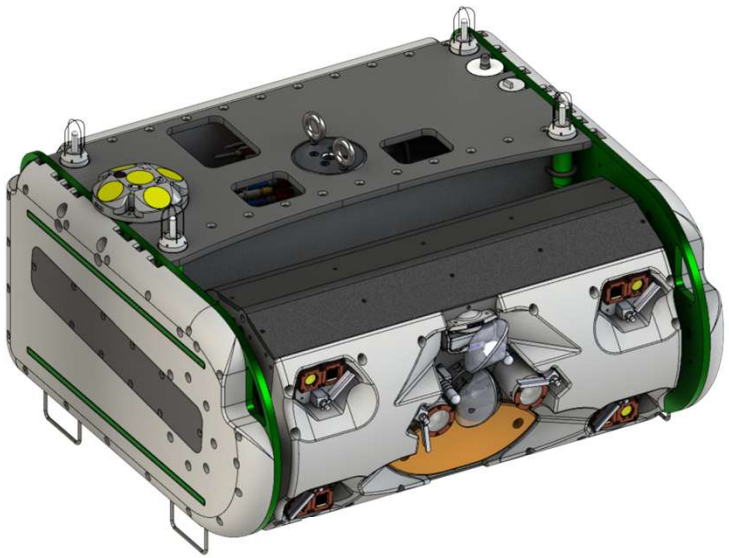

Journal of Marine Science and Engineering

Article

Adaptable Monitoring Package Development and Deployment: Lessons Learned for Integrated Instrumentation at Marine Energy Sites

Brian Polagye [1,*], James Joslin [2], Paul Murphy [1], Emma Cotter [3], Mitchell Scott [2], Paul Gibbs [2], Christopher Bassett [2] and Andrew Stewart [1]

1 Department of Mechanical Engineering, University of Washington, Seattle, WA 98105, USA; pgmurphy@uw.edu (P.M.); arstew@uw.edu (A.S.)

2 Applied Physics Laboratory, University of Washington, Seattle, WA 98105, USA; jbjoslin@uw.edu (J.J.); miscott@uw.edu (M.S.); gibbsp@uw.edu (P.G.); cbassett@uw.edu (C.B.)

3 Woods Hole Oceanographic Institution, Woods Hole, MA 02543, USA; ecotter@whoi.edu

* Correspondence: bpolagye@uw.edu

MDPI

UNIVERSITY of WASHINGTON

Applied Physics Laboratory
UNIVERSITY of WASHINGTON

MarineSitu

The Adaptable Monitoring Package (AMP)

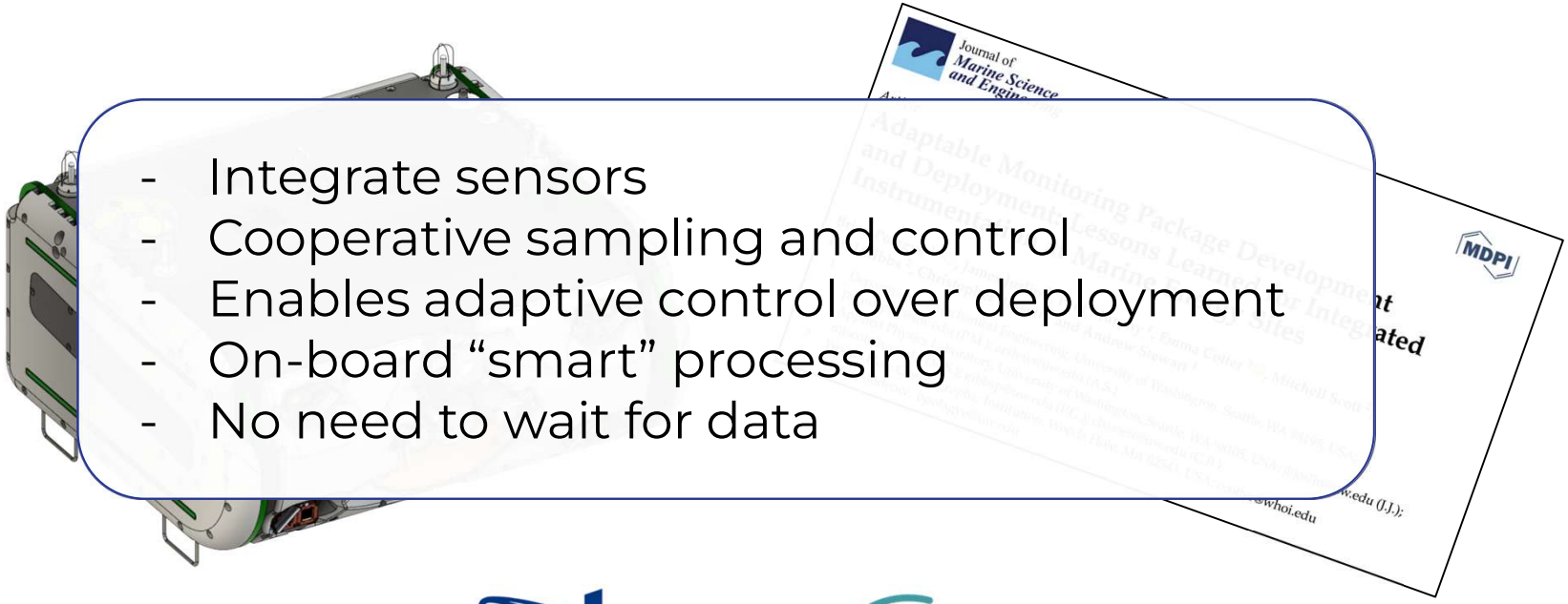

- Integrate sensors
- Cooperative sampling and control
- Enables adaptive control over deployment
- On-board “smart” processing
- No need to wait for data

UNIVERSITY of WASHINGTON

Applied Physics Laboratory
UNIVERSITY of WASHINGTON

MarineSitu

The Adaptable Monitoring Package (AMP)

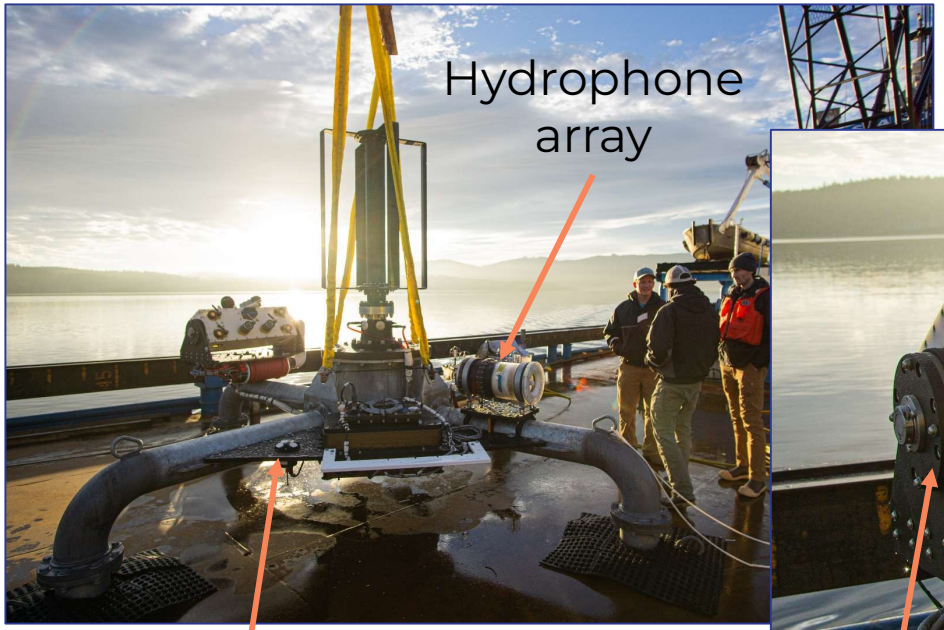

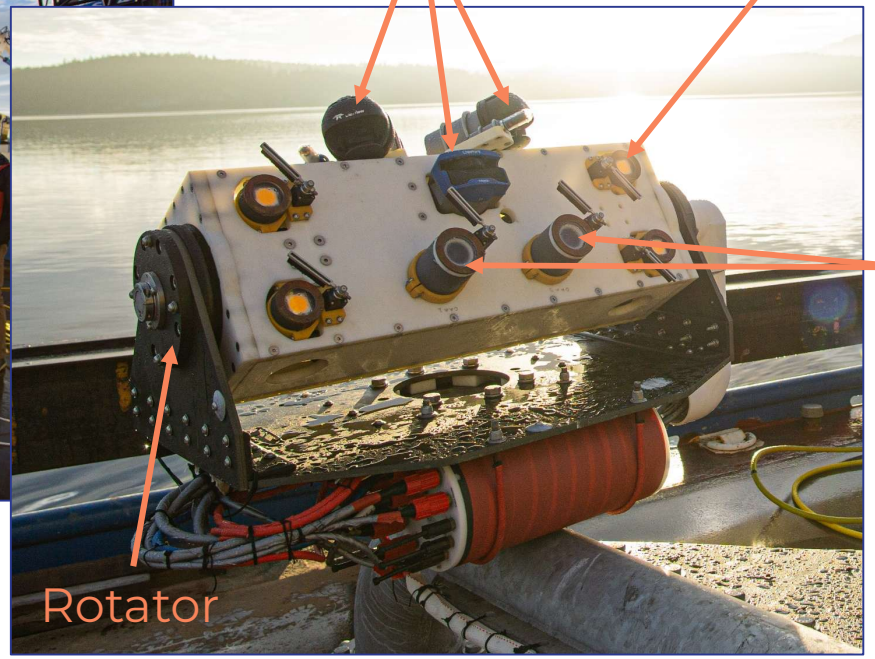

Turbine Operations

141-day deployment (curtailed near end)
Turbine spinning over 960 hours.

Current speed

Power generated

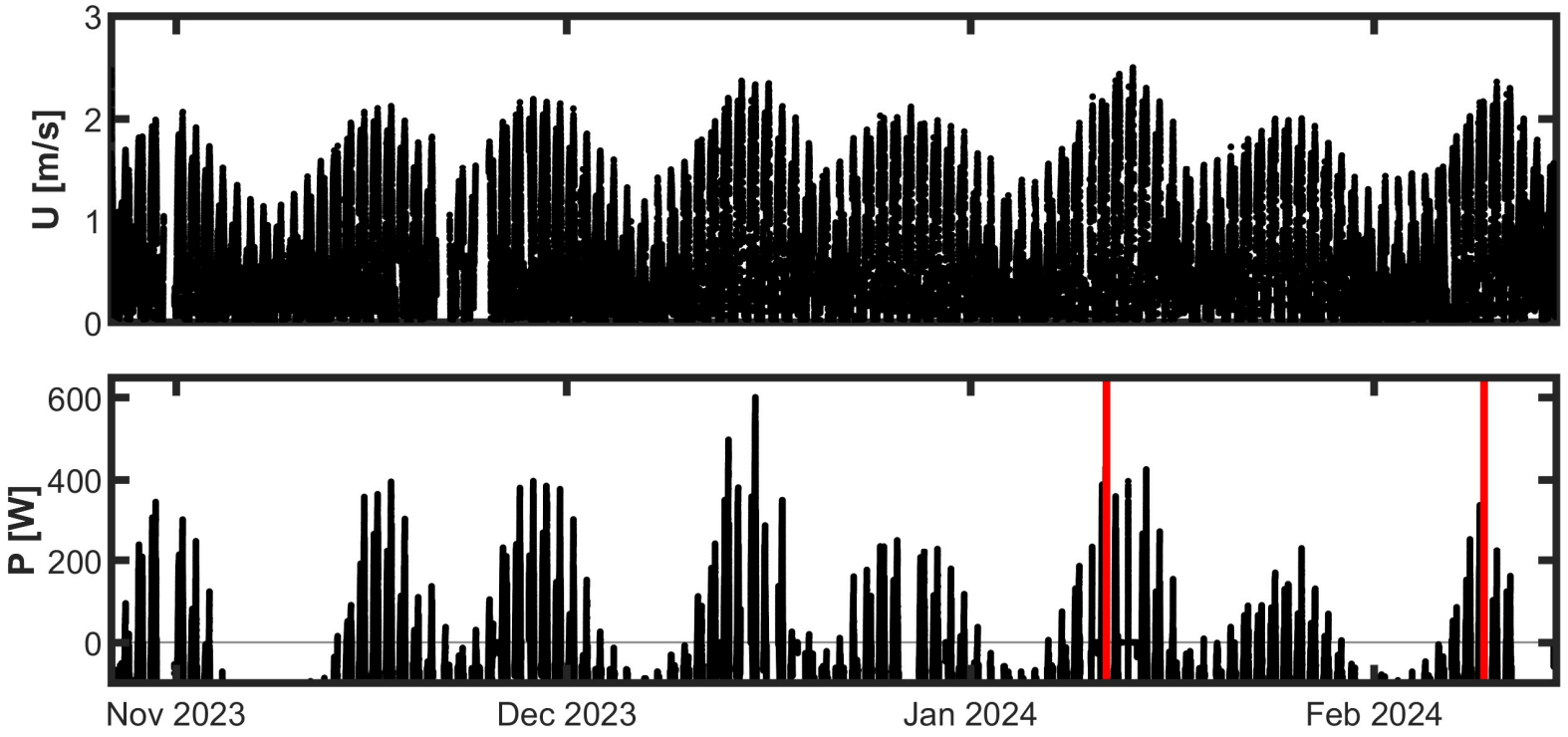

Biological

Sampling too complex for a short talk (see papers)

Over 3M images reviewed, annotated, and classified (taxonomic)

- Note: Interactions are generally relatively uncommon.

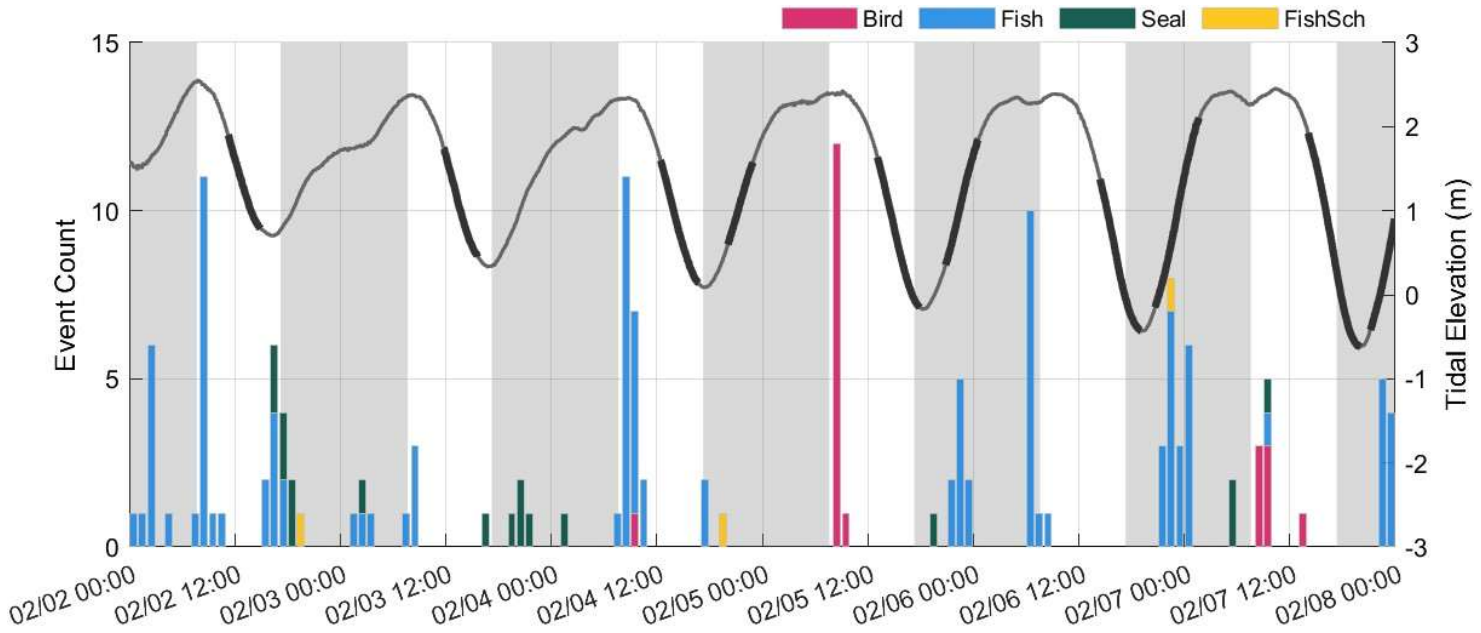

Biological

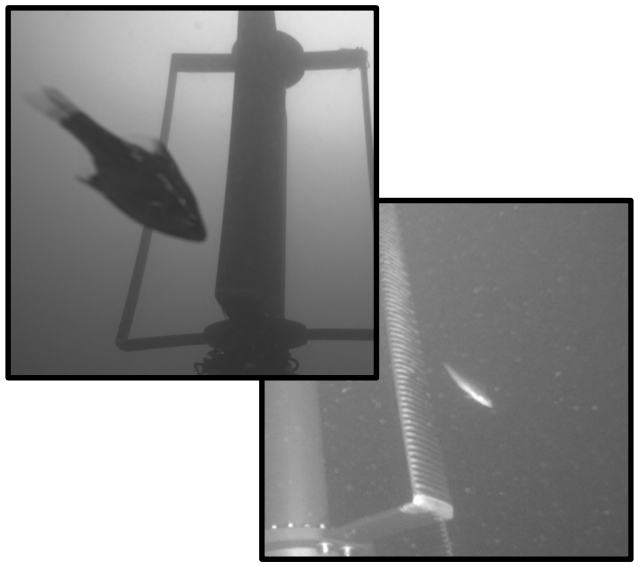

500+ Fish (*biased low*) & 19 Schools

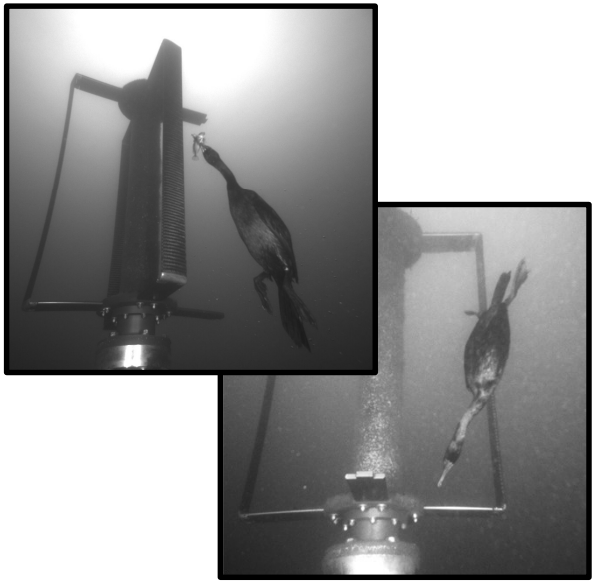

400+ Birds

90+ Seals

Sonar analysis revealed additional schools, birds, and seals beyond the field of view of the cameras.

Summary of Observations

Fish (species ID difficult) (confirmed) (likely) (possible but difficult to confirm)

- Kelp greenling (*Hexagrammos decagrammus*)
- Gunnel (sp. unknown)
- Scuplin (spp. unknown)
- Cabezon (*Scorpaenichthys marmoratus*)
- Sand lance (*Ammodytes hexapterus)*
- Starry flounder (*Platichthys stellatus*)
- Snailfish (sp. Unknown)
- *Kelp perch (Brachyistius frenatus)*
- *Shiner perch (Cymatogaster aggregate)*
- Prickleback (spp. Unknown)
- Other unidentified forage fishes:
  - Surf melt (*Hypomesus pretiosus*), *tube-snout (Aulorhynchus flavidus), Pacific herring (Clupea pallasii)?*

No endangered species (fish, birds, or marine mammals were identified)

Diving Birds

- Pigeon guillemot *(Cepphus columba)*
- Double-crested cormorant *(Nannopterum auritum)*
- Pelagic cormorant *(Urile pelagicus)*

Seals

- Harbor seal *(Phoca vitulina)*

Birds

74% pelagic or double-crested cormorants

26% pigeon guillemots

All observations during day

0 observations while turbine was rotating

Birds

Observed behaviors:

<u>Cormorants</u>

- Commonly diving around foundation
- Examples with captured prey (or pursuing prey)

<u>Guillemots</u>

- (most common) Swimming above, behind, or around rotor.
- (less common) Approach the rotor (as in this video)

Fish

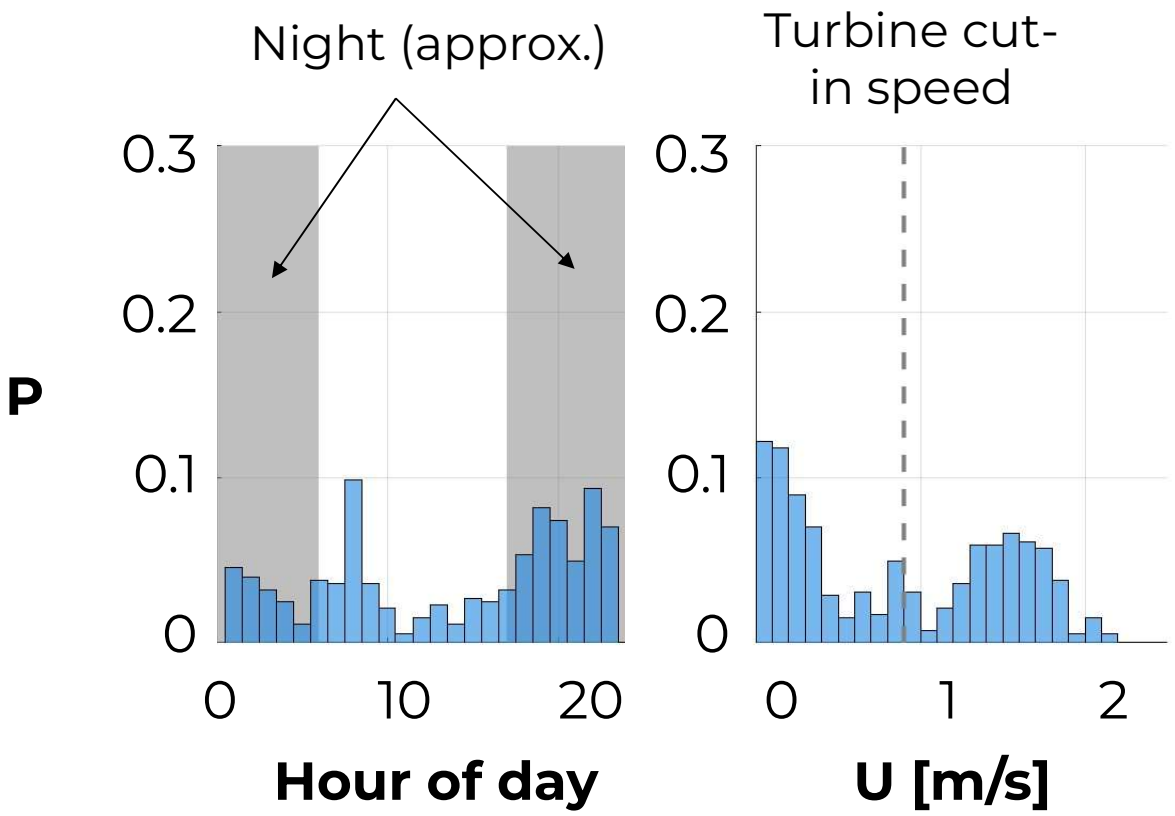

Predominately small (<30 cm) fish

No salmonids or other threatened or endangered species observed

Large Fish

We observed few large fish

Rotating: Large fish only observed high in the water column

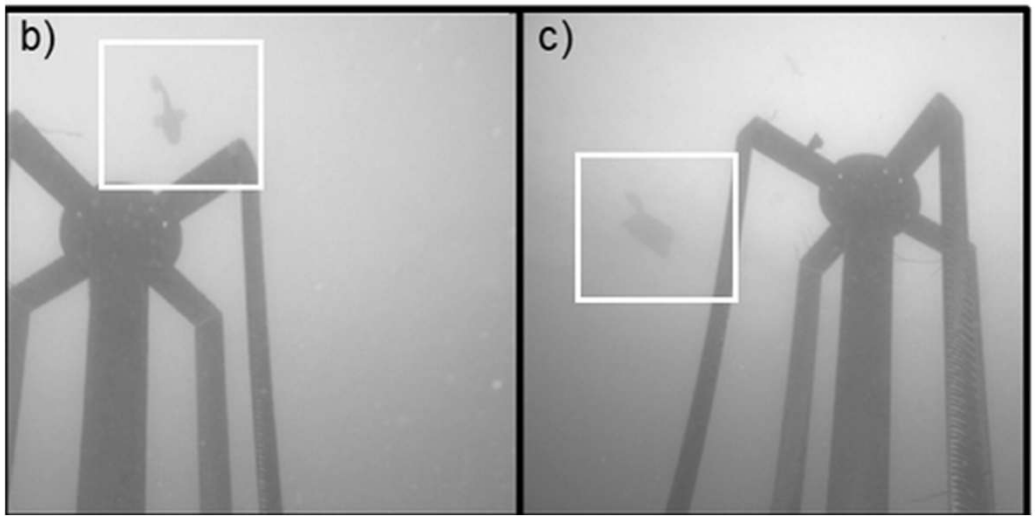

Stationary rotor

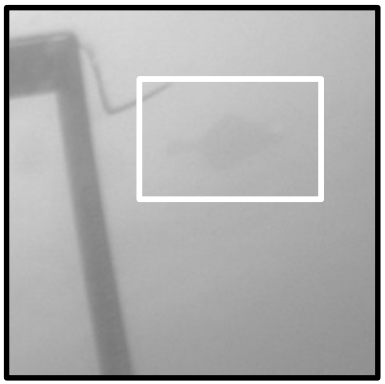

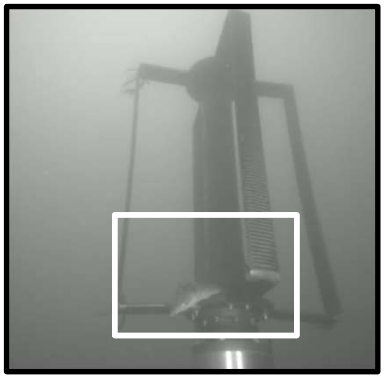

Fish

Many small fish present in and around rotor when stationary

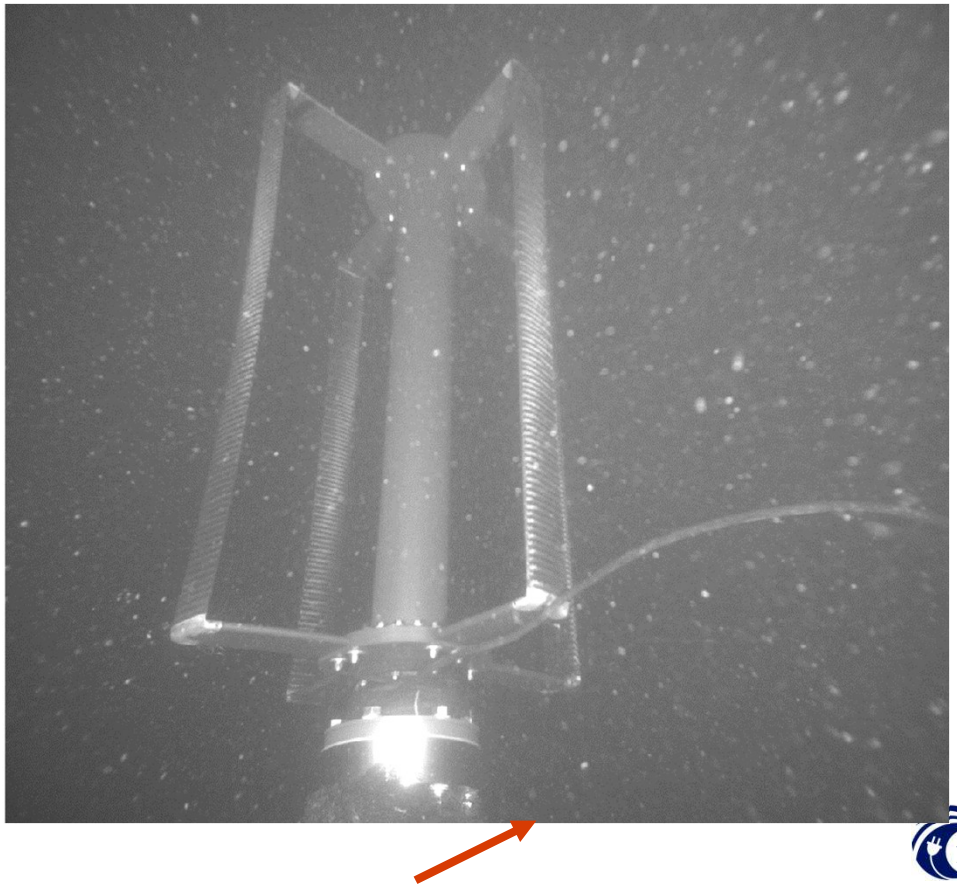

Fish

50+ fish (excluding schools) evaded the rotor using different strategies

- Swim around
- Dive down
- ~180° turn

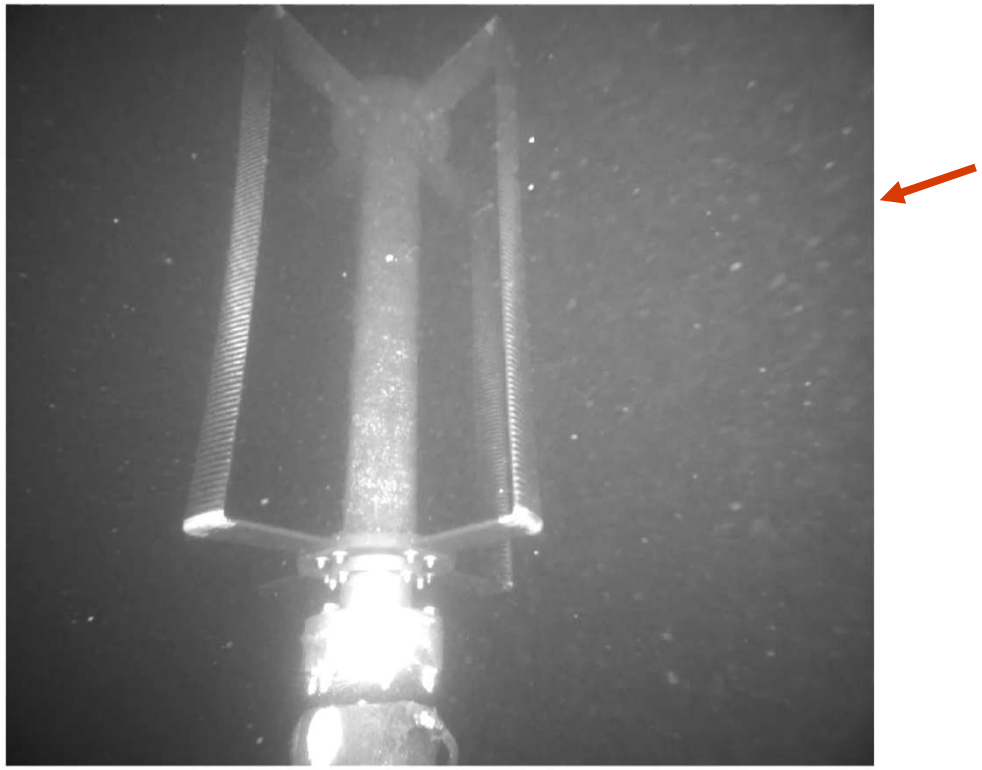

Fish

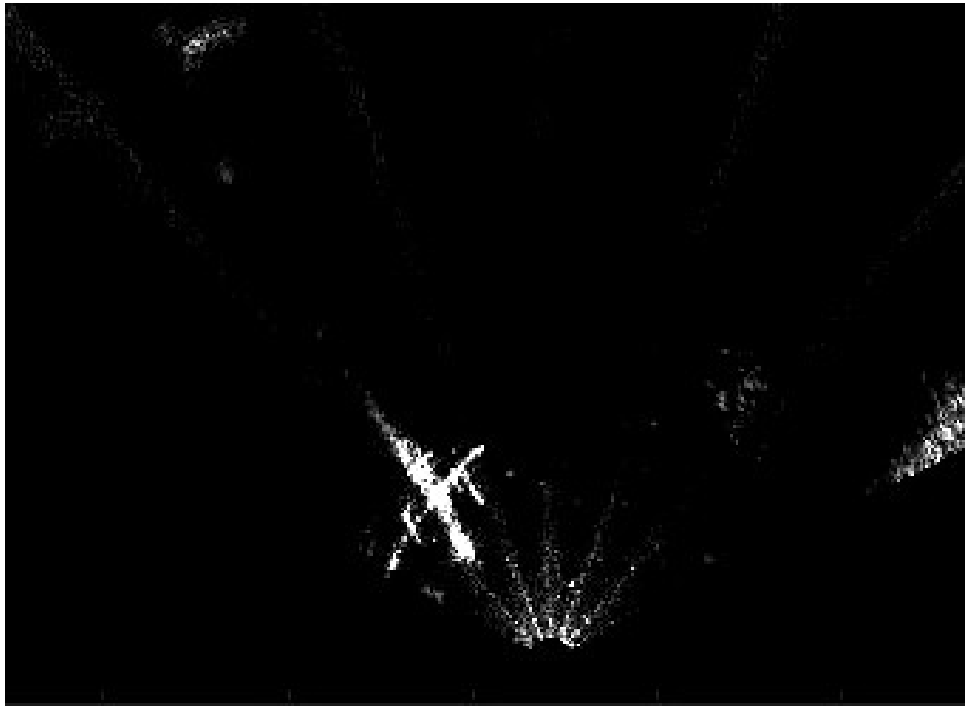

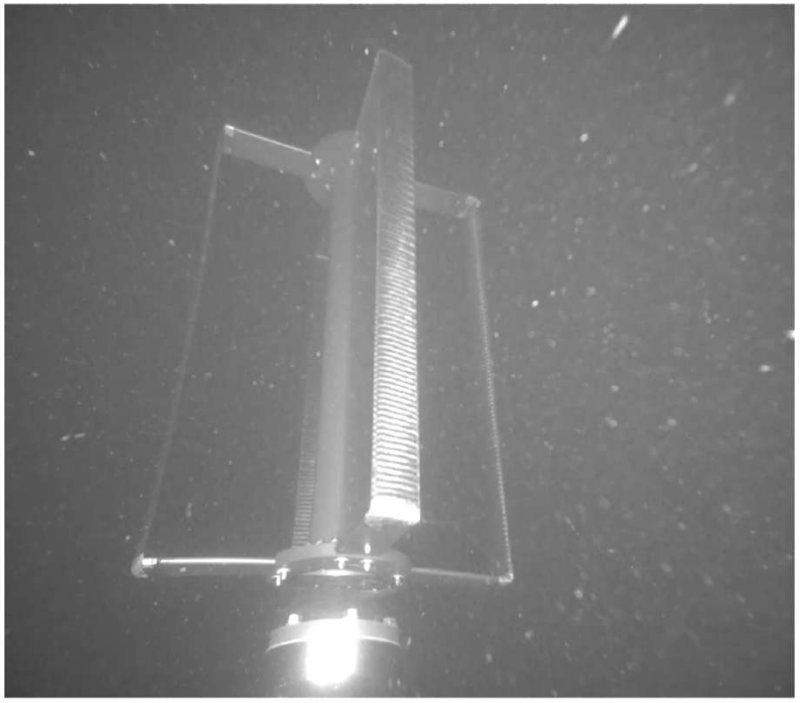

Fish

Fish collision with rotor.

Sonar reveals fish was being pursued by a seal that never entered camera FOV. Fish swimming against current.

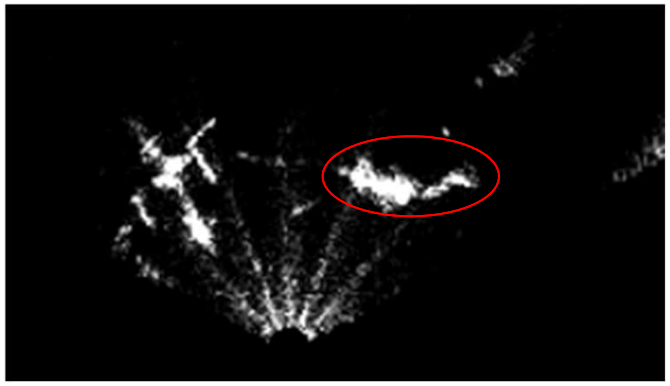

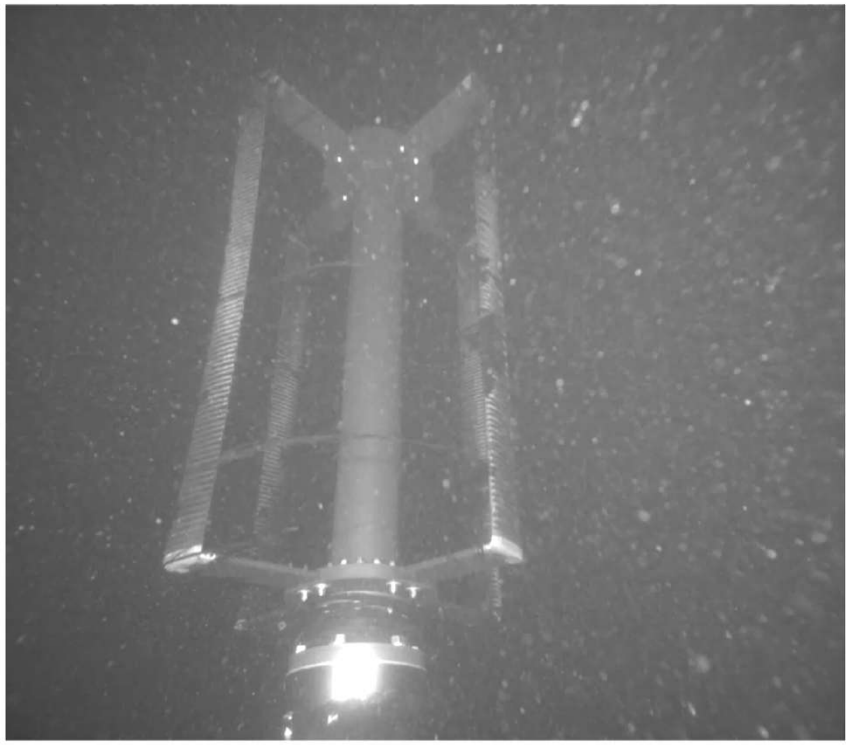

Fish

4 fish collided with the moving rotor. Three of four swam away, fate of last fish unknown.

1 fish, passively drifting with flow and collided with the turbine while it was stationary (seal in sonars).

All collisions with small fish (less than ~6 in)

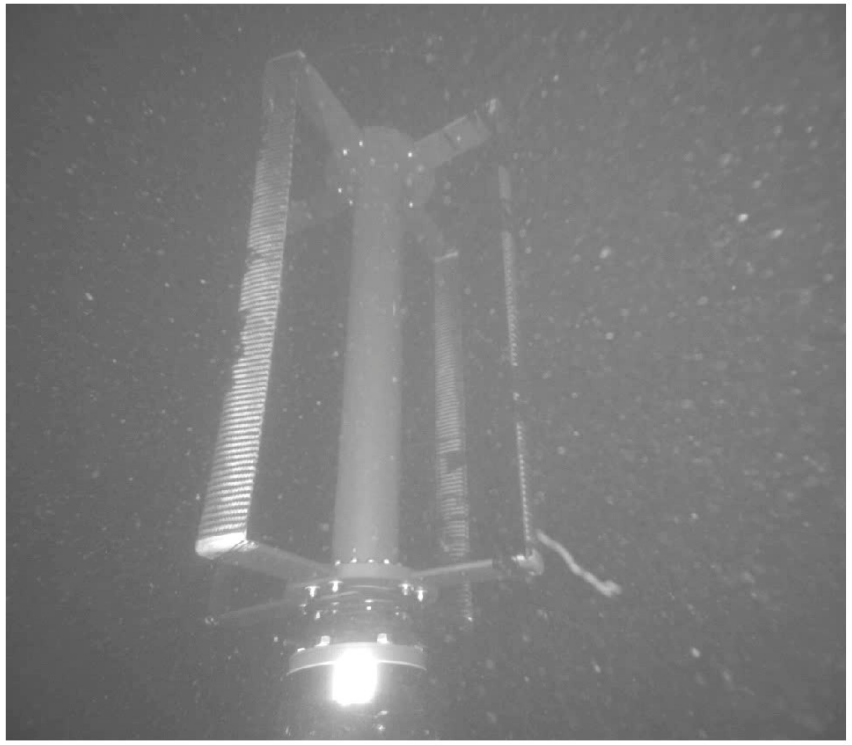

Seals

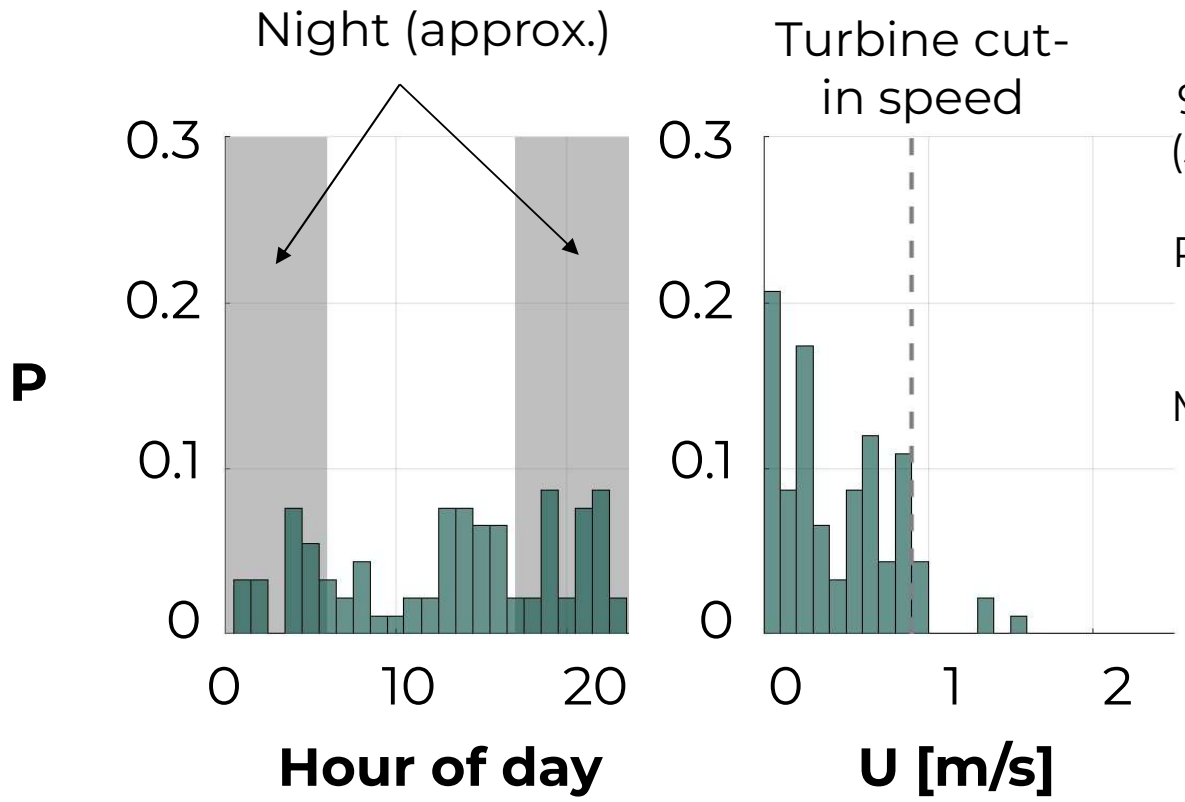

9 seals during turbine operation (3 at low flow speed due to error)

Pursuit of prey a factor in several events during operations

More seals observed in vicinity of turbine outside of optical FOV with sonars

Seals

Seal encounter with stationary turbine, no attraction

Clear case of attraction

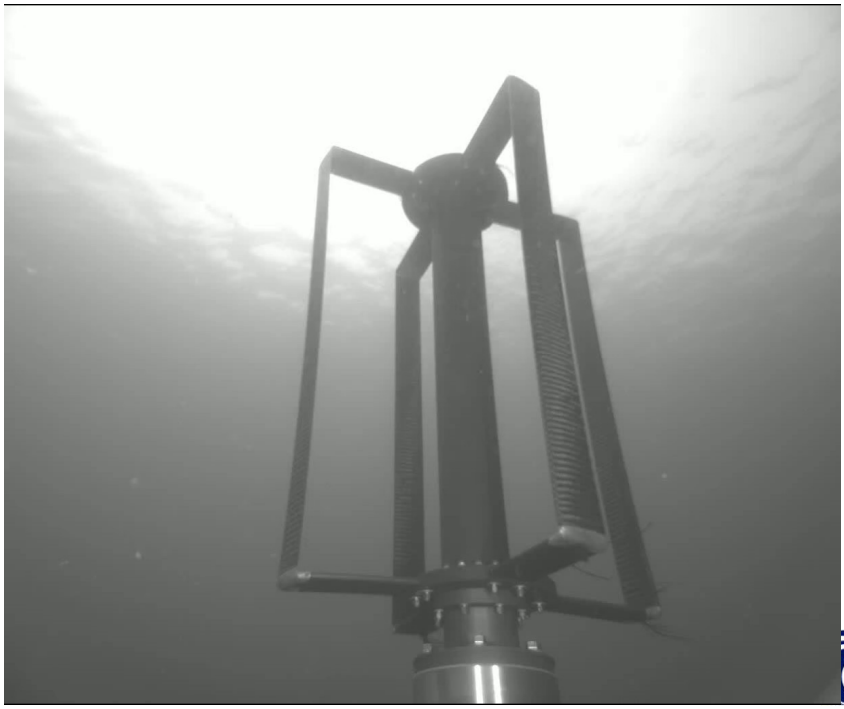

Seals

Seal predator/prey interaction during turbine operation

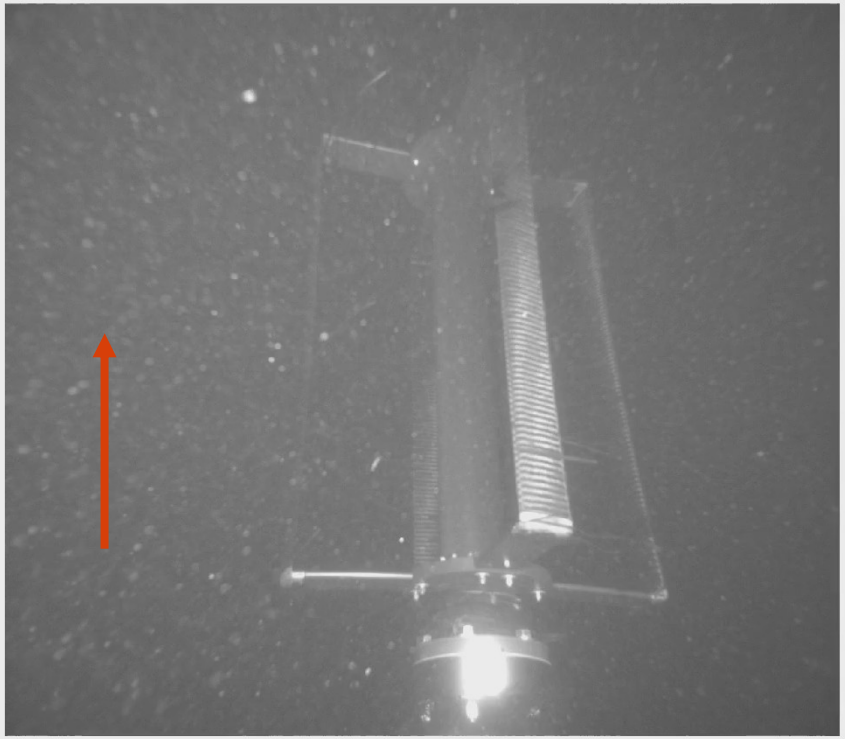

Seals

Seal encounter with operational turbine

One of two similar encounters

No collision/contact observed (reviewed positions with stereo cameras).

What about sonars?

Sonars good for imaging the following at larger ranges:

- Birds (bubbles and diving patterns)
- Seals (large)
- Fish schools (many targets of targets)
- Large fish

Repositioning to get a wider field of view is critical to better quantifying avoidance/evasion behavior.

Sound

- Note: dB in water and air are different

$$SPL = 20\log_{10}\left(\frac{p_{rms}}{p_o}\right) \qquad p_o = 1\mu\text{Pa in water} \qquad p_o = 20\mu\text{Pa in air}$$

p_{rms} = 1 Pa	SPL [dB re p_o]	Intensity [W]
Air	94.0	2.4E-03
Water	120.0	6.5E-07

Same pressure is ~3700x more intense in air

Sound

- Note: dB in water and air are different

$$SPL = 20\log_{10}\left(\frac{p_{rms}}{p_o}\right) \qquad p_o = 1\mu\text{Pa in water} \qquad p_o = 20\mu\text{Pa in air}$$

p_{rms} = 1 Pa	SPL [dB re p_o]	Intensity [W]
Air	94.0	2.4E-03
Water	120.0	6.5E-07

Same pressure is ~3700x more intense in air

- 120 dB re 1 µPa is roughly the average sound pressure level in Admiralty Inlet


DECEMBER 06 2012

A vessel noise budget for Admiralty Inlet, Puget Sound, Washington (USA)

Christopher Bassett; Brian Polagye; Marla Holt; Jim Thomson

Check for updates

J. Acoust. Soc. Am. 132, 3706–3719 (2012)

https://doi.org/10.1121/1.4763548

- Same SPL in air is associated with intense sound like police sirens or concerts (i.e., general discomfort)

Sound

- The turbine produces noise, but it is relatively low intensity
  - Audible to ranges of a few hundred feet since the site isn't particularly noisy
    - We measured this at range and near the turbine

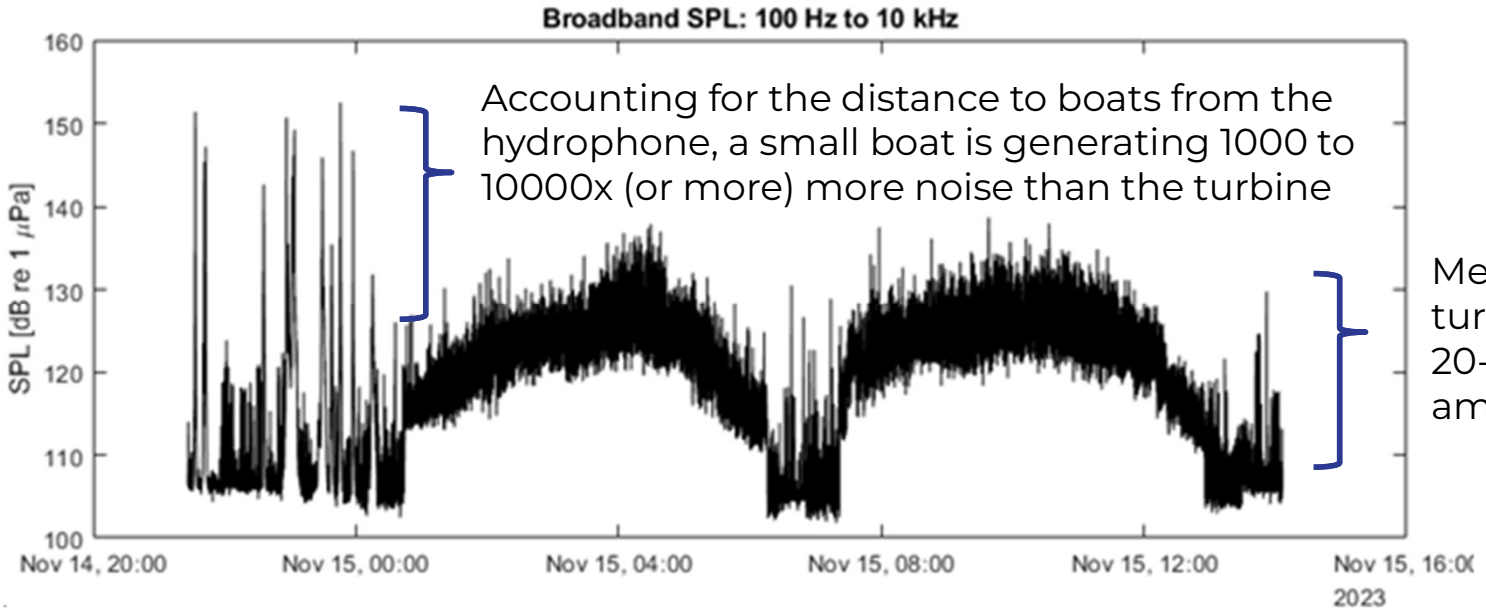

Lessons learned

- ~~Manual review~~: 1+ TB/day
  - One simply can't review everything at a high sampling rate, so what can/should we do?

  - We care about two things:
    1. Identifying potential collisions or other behaviors
    2. Acquiring data to build processing pipelines

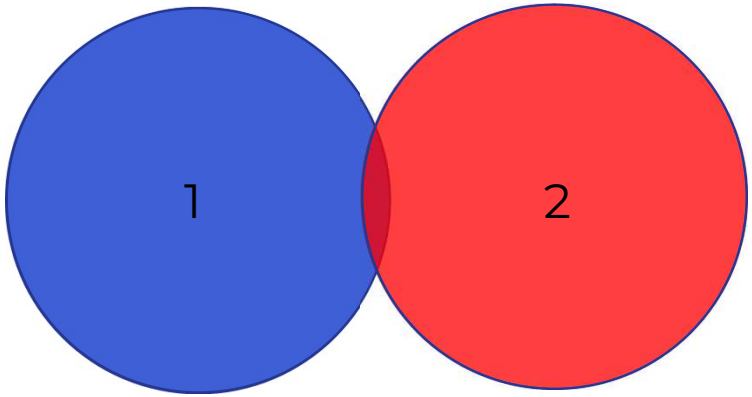

Lessons learned

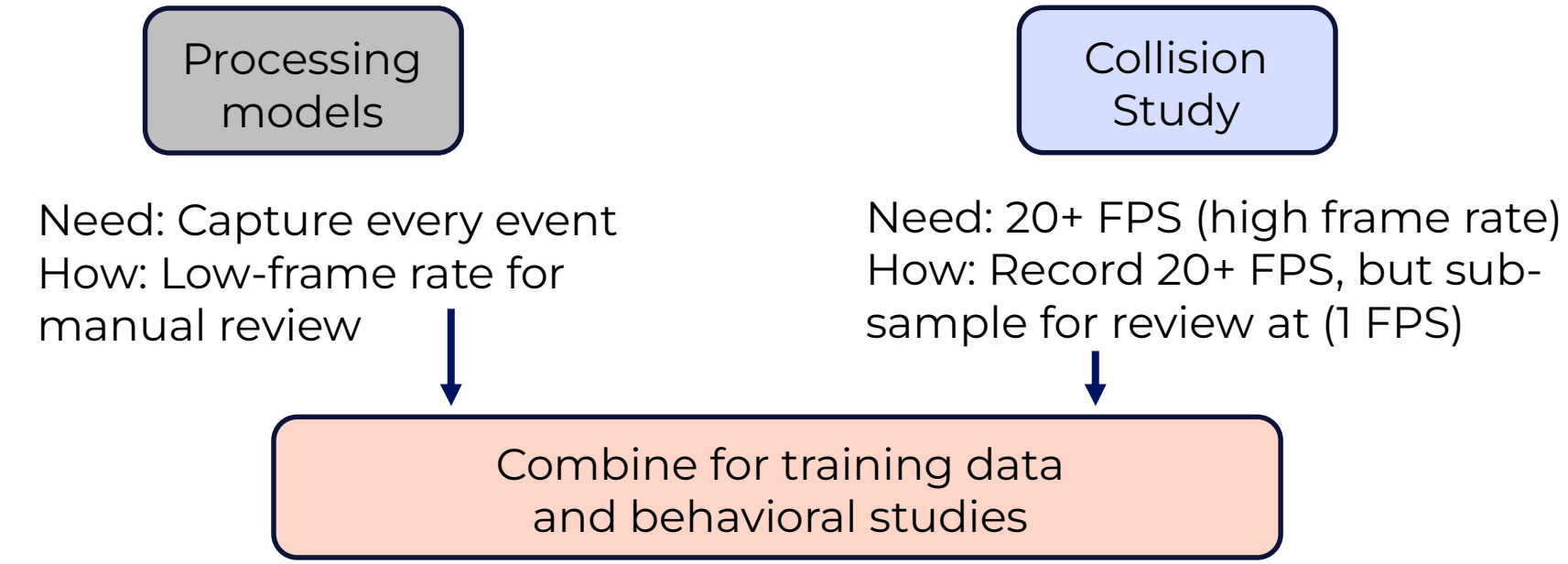

We do not expect additional data (deployments) to result in different conclusions, just an improved quantitative understanding of behavior.

Lessons learned

Optical (ML) models worked well for seals and birds even with small training sets

- Small fish are challenging

Automated processing for sonar data with moving turbine

- Work in progress

Risks seem low given the observations, but there is still work to do.

What about a larger turbine?

Information to-date suggests similarities across geographic scales and sizes.

- Grid-scale turbines have been deployed and monitored for years (in Europe)
  - Marine mammals including seals and porpoise

- Documented avoidance and evasion

- Examples of decreased presence in immediate vicinity of turbine while operating

Credit: Ampeak Energy

What about a larger turbine?

Further reading (and references therein)

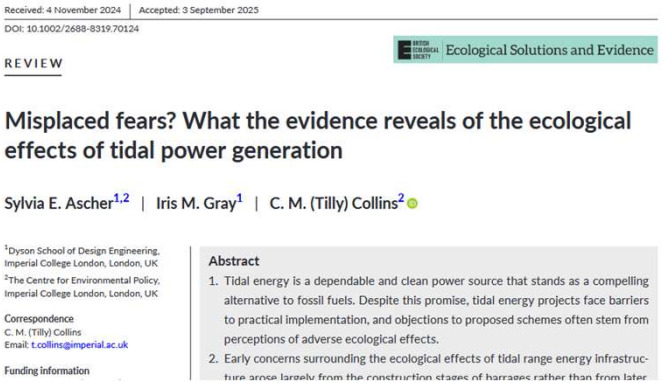

Received: 4 November 2024 | Accepted: 3 September 2025

DOI: 10.1002/2688-8319.70124

Ecological Solutions and Evidence

REVIEW

Misplaced fears? What the evidence reveals of the ecological effects of tidal power generation

Sylvia E. Ascher[1,2] | Iris M. Gray[1] | C. M. (Tilly) Collins[2]

[1]Dyson School of Design Engineering, Imperial College London, London, UK
[2]The Centre for Environmental Policy, Imperial College London, London, UK

Correspondence
C. M. (Tilly) Collins
Email: t.collins@imperial.ac.uk

Funding information

Abstract

1. Tidal energy is a dependable and clean power source that stands as a compelling alternative to fossil fuels. Despite this promise, tidal energy projects face barriers to practical implementation, and objections to proposed schemes often stem from perceptions of adverse ecological effects.
2. Early concerns surrounding the ecological effects of tidal range energy infrastructure arose largely from the construction stages of barrages rather than from later

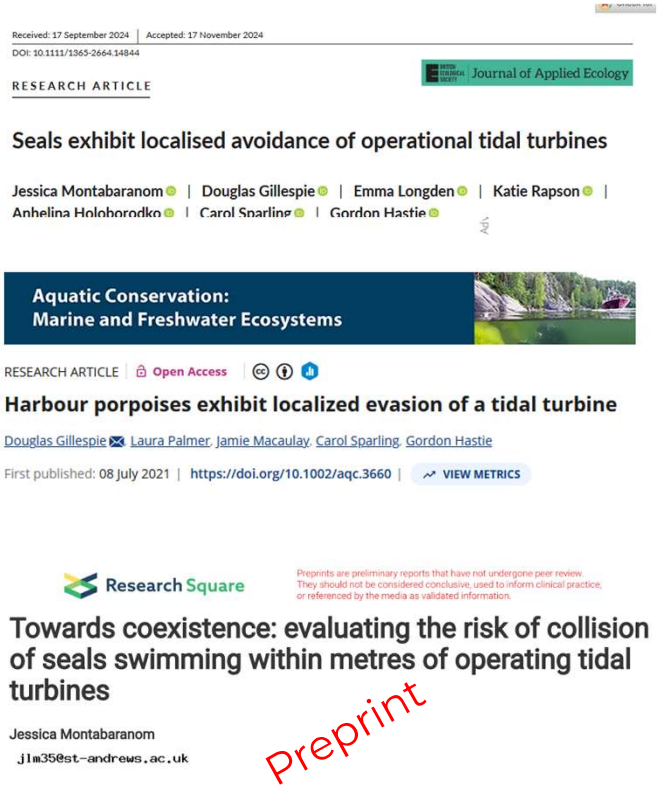

Received: 17 September 2024 | Accepted: 17 November 2024

DOI: 10.1111/1365-2664.14844

Journal of Applied Ecology

RESEARCH ARTICLE

Seals exhibit localised avoidance of operational tidal turbines

Jessica Montabaranom | Douglas Gillespie | Emma Longden | Katie Rapson | Anhelina Holoborodko | Carol Sparling | Gordon Hastie

Aquatic Conservation: Marine and Freshwater Ecosystems

RESEARCH ARTICLE | Open Access

Harbour porpoises exhibit localized evasion of a tidal turbine

Douglas Gillespie, Laura Palmer, Jamie Macaulay, Carol Sparling, Gordon Hastie

First published: 08 July 2021 | https://doi.org/10.1002/aqc.3660 | VIEW METRICS

Research Square

Preprints are preliminary reports that have not undergone peer review. They should not be considered conclusive, used to inform clinical practice, or referenced by the media as validated information.

Towards coexistence: evaluating the risk of collision of seals swimming within metres of operating tidal turbines

Jessica Montabaranom
jlm35@st-andrews.ac.uk

Preprint

Contains a nice literature review summarizing prior observations for fish, birds, and seals.

Videos and metadata:

https://mhkdr.openei.org/submissions/599

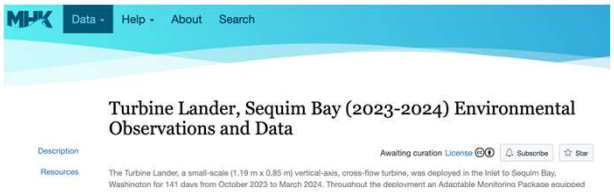

Note that this contains 600+ videos, most of which are not exciting. I've taken the "full disclosure" approach.

File structure: By event type/rotating vs not rotating
- Greatest hits includes, notable collision/evasion events and other interesting observations

Videos and metadata:

https://mhkdr.openei.org/submissions/599

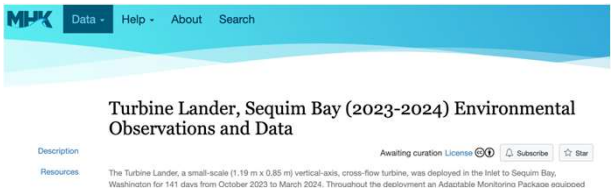

Analysis:

Bassett, C. et al. Lessons learned from the design and operation of a small-scale cross-flow tidal turbine. *J. Ocean Eng. Mar. Energy* (2025). https://doi.org/10.1007/s40722-025-00411-y

Bassett, C. and E. Cotter. Observations of fish, birds, and harbor seals around an operating cross-flow turbine. 16th *European Wave and Tidal Energy Conference*, Funchal, Portugal, September 7–11, 2025.

Cotter, E. *et al (2026)*. Observations of fauna interactions with a small tidal turbine. *PLoS One, 21(1): e0338376 DOI: 10.1371/journal.pone.0338376. (Published 14 January 2026)*

Acknowledgements

AMP Analysis: Paul Murphy, Mitchell Scott, Alexa Runyan, James Joslin, Jood Almokharrak, Lucy Kao, Suni McMillan, Lillian Ovall, Lenaïg Hemery

Lander Deployment: Rob Cavagnaro, Jesse Dosher, Brian Polagye

Software and Data: Mitchell Scott, Emily Paine, Sadie Kass

NAVFAC
Naval Facilities Engineering Systems Command

TEAMER
Testing & Expertise for Marine Energy

U.S. DEPARTMENT OF ENERGY

Questions and Discussion…

Journal of Ocean Engineering and Marine Energy
https://doi.org/10.1007/s40722-025-00411-y

RESEARCH

Lessons learned from the design and operation of a small-scale cross-flow tidal turbine

Christopher Bassett[1] · Paul Gibbs[1] · Harlin Wood[1] · Robert J. Cavagnaro[3] · Ben Cunningham[1] · Jesse Dosher[1] · James Joslin[1] · Brian Polagye[2]

Received: 19 February 2025 / Accepted: 27 May 2025

Abstract

In 2023, a first-generation prototype of a small-scale marine current turbine was operated in Sequim Bay, Washington (USA) for 141 days. The system, referred to as the Turbine Lander, was the product of a laboratory-to-field effort to develop a system that enables enhanced ocean sensing or vehicle recharge in remote, energetic settings. The turbine consists of a vertical-axis, cantilevered rotor (1.19 m × 0.85 m) with four foils installed on a gravity foundation. A broader range of constraints including the deployment strategy, site characteristics, and estimated loads, drove the system's design. This work presents the design, characterization, operation, and post-recovery engineering assessment of the Turbine Lander. Pre-deployment characterization efforts yielded a peak power coefficient of approximately 0.3 for the rotor, although system losses resulted in much lower water-to-wire efficiencies under most operating conditions. The results demonstrate the importance of co-design among key components of the powertrain and control systems to achieve acceptable system efficiency across operating conditions.

Keywords Cross-flow turbine · Field deployment · System design · Survivability · Efficiency · Co-design

1 Introduction

Marine energy conversion has the potential to catalyze latent opportunities in offshore environments that are currently unexplored or under-subscribed due to existing power constraints (Whitt et al. 2020; Cavagnaro et al. 2020). When stationary offshore systems lack a grid connection their endurance and range of capabilities are limited to onboard energy storage and the ability to harvest energy from the environment. At present, solar photovoltaics are the most common generation technology, but the higher energy density of marine energy resources could widen operational capabilities (Dillon et al. 2022). However, given the nascent state of small-scale marine energy converters, realizing these benefits requires overcoming challenges related to their design, operations, and maintenance.

Reliable design in ocean applications often seeks to minimize the number of moving parts. Design around this principle makes sense given the forces acting on objects in environments where biofouling, particulate, corrosion, and other floating objects are factors and maintenance

✉ Christopher Bassett
cbassett@uw.edu

Paul Gibbs
pgibbs@uw.edu

Harlin Wood
hdw3@uw.edu

Robert J. Cavagnaro
robert.cavagnaro@pnnl.gov

Ben Cunningham
bpcham@uw.edu

Jesse Dosher
jdosher@uw.edu

James Joslin
jbjoslin@uw.edu

Brian Polagye
bpolagye@uw.edu

[1] Ocean Engineering Department, Applied Physics Laboratory, University of Washington, 1013 NE 40th St, Seattle, WA 98105, USA

[2] Mechanical Engineering Department, University of Washington, 3900 E Stevens Way NE, Seattle, WA 98195, USA

[3] Pacific Northwest National Laboratory, 1529 W. Sequim Bay Rd., Sequim, WA 98382, USA

Published online: 01 July 2025

opportunities are both rare and costly. Unfortunately, to efficiently extract power from sources like waves and currents, dynamic components exposed to the environment are generally required. The relatively slow pace of progress in this area, demonstrated by the small number of operating marine energy converters at any scale, is driven by both the engineering challenges and high costs when compared to existing mature sources of power.

Faced with these limitations and increasing interest in marine energy technology our project team designed, fabricated, characterized, deployed, and operated a small-scale prototype tidal turbine. The unit was a vertical-axis, cross-flow turbine mounted on a gravity foundation. The system as a whole is simply referred to as the "Turbine Lander". Mean, time-averaged power generation targets for the unit are on the scale of 100 W at sites with moderately strong tidal currents (peak instantaneous velocities less than 3 m/s). This first-generation design aimed to demonstrate proof of concept for the design and system components and involved cabled operation without integrated energy storage. Projects with comparable scope must overcome a broad range of design challenges and fundamental design trade-offs inherent to transitioning laboratory-scale research to field operations. However, these topics are not discussed in the marine energy literature, leading to a repetition of common mistakes, duplication of non-recurring engineering effort, and limited knowledge transfer between groups. Here, we seek to address this transparency gap by providing detailed design information, broader discussions of engineering decisions, and lessons learned through the process of end-to-end system characterization and field deployment.

The paper adopts a structure that chronologically follows the design lifecycle from constraint definition to post-deployment engineering review. We first provide background on general terminology and performance metrics for current turbines. Section 3 describes fundamental constraints and associated considerations that informed system design. Section 3.3 provides an overview of the design of the Turbine Lander and its subsystems, as shaped by the constraints. Next, in Sect. 4, we provide an overview of pre-deployment efforts to characterize system losses, rotor performance, and system integrity. Section 5 presents an overview of a field deployment in Sequim Bay, WA and the following section discusses the outcomes of a post-deployment engineering assessment of the system. The paper concludes with a discussion of lessons learned, pathways for improving system performance, and a deployment-informed assessment of challenges for power generation from currents at this scale.

2 Background: current turbine terminology and metrics

Throughout this paper we regularly describe system performance through specific terminology and engineering shorthand. Key among these include losses, efficiencies, load and power coefficients, and control strategies. For a turbine occupying a relatively small fraction of a channel, the kinetic power incident on the turbine's rotor sets the baseline for potential power extraction. The kinetic power of a current P_u is

$$P_u = \frac{1}{2}\rho A U_o^3, \tag{1}$$

where A is the projected area of the rotor, ρ is the water density, and U_o is the free stream water velocity at the height of the rotor. The mechanical power associated with rotor rotation is described by

$$P_r = Q_r \omega, \tag{2}$$

where Q_r is the hydrodynamic torque generated by the rotor and ω is its angular velocity. P_u, P_r, and derived quantities are time-varying as a consequence of the oscillatory nature of cross-flow turbine hydrodynamics (Polagye et al. 2019) and temporal variations in inflow (Thomson et al. 2012).

The non-dimensional performance of a rotor, or its ability to convert the available kinetic power in the flow to mechanical power, is described by the power coefficient, C_P, according to

$$C_P = \frac{P_r}{P_u} = \frac{Q_r \omega}{\frac{1}{2}\rho A U_o^3}. \tag{3}$$

This does not, however, account for power conversion losses, which decrease electrical power output relative to the mechanical power generated by the rotor. C_P may be presented as an instantaneous value, a phase-resolved quantity representing instantaneous values at different angular positions of the rotor, or as time-averaged values representing the mean over one or more full revolutions.

For a direct coupling between rotor and generator (i.e., no speed-increasing gearbox), the mechanical power input to the generator, $P_{\text{gen,in}}$, is related to the shaft speed of the rotor and the torque applied to the generator shaft after any torque losses between the two. This is described by

$$\begin{aligned} P_{\text{gen,in}} &= \eta_{\text{trans}} P_r = P_r - \omega Q_{\text{loss}} \\ &= \omega \left(Q_r - Q_{\text{loss}}\right) = \omega Q_{\text{gen,in}}, \end{aligned} \tag{4}$$

where the subscript $_r$ is used to represent the torque or mechanical power associated with the rotor, η_{trans} is the efficiency of the transmission of torque from the rotor to the

generator shaft, Q_{loss} represents torque losses in the system, and $Q_{\text{gen,in}}$ is the torque applied to the generator shaft. The electrical power produced by the generator is given as:

$$P_e = \eta_{\text{gen}} P_{\text{gen,in}}, \tag{5}$$

where η_{gen} is the efficiency of the generator and includes power conversion inefficiencies and resistive losses in the windings. The total power take-off (PTO) efficiency is then $\eta = \eta_{\text{trans}}\eta_{\text{gen}}$.

Water-to-wire system efficiency, η_{ww}, varies from C_P in that it accounts for all losses occurring during power conversion in the PTO and is defined by

$$\eta_{\text{ww}} = \frac{P_e}{P_u} = C_P \eta. \tag{6}$$

If system losses are well characterized, it is possible to estimate power coefficients when only measures of electrical power and inflow are available (Cavagnaro and Polagye 2016) and identify pathways to increase system performance.

The PTO efficiency is characterized using a dynamometer across a broad range of operationally relevant speeds and torques (Sect. 4). By characterizing baseline frictional losses of the system and combining them with mechanical inputs, the generator efficiency can be estimated according to

$$\eta_{\text{gen}} = \frac{(P_e - L_{\text{seal}})}{Q_c \omega}, \tag{7}$$

where L_{seal} represents losses between the rotor and generator (primarily seals) and Q_c represents the torque applied to the shaft. Here, Q_c is referred to as the control torque as it is modified by controls algorithms during operations. Equations 6–7 and dynamometery measurements of η_{gen} are used herein to assess factors impacting power generation under highly variable inflow. By combining previous equations, C_P can be estimated directly from time averaged inflow velocity and control torque noting that $Q_r = Q_c + Q_{\text{loss}}$:

$$C_P = \frac{\omega\,(Q_c + Q_{\text{loss}})}{\frac{1}{2}\rho A U_o^3}, \tag{8}$$

where $Q_{\text{loss}} = P_{\text{loss}}/\omega$. Thus, measured system losses and the control torque applied by the generator can be used to estimate the power coefficient.

Hydrodynamic forces acting on the rotor produce time-varying forces in the direction of the inflow (thrust force) and perpendicular to the inflow (lateral force). These can be non-dimensionalized as force coefficients, C_L and C_T, respectively:

$$C_T = \frac{T}{\frac{1}{2}\rho A U_0^2} \quad \text{and}$$
$$C_L = \frac{L}{\frac{1}{2}\rho A U_0^2},$$

where T denotes a thrust force and L denotes a lateral force. As with C_P, C_T and C_L may be presented in instantaneous, phase-averaged, or time-averaged forms. A generalized force coefficient, C_F, represents the vector sum of C_T and C_L and provides critical estimates of instantaneous loads for several aspects of design including the bearings to the foundation.

Parameters including C_P, C_T, and others are often presented as a function of a non-dimensional rotation rate. The tip-speed ratio, defined as

$$\lambda = \frac{\omega r}{U_o}, \tag{9}$$

where r is the radius of the rotor, represents the tangential blade speed relative to the inflow.

Two approaches for controlling a cross-flow turbine are speed and torque control (Pao and Johnson 2011; Forbush et al. 2017; Polagye et al. 2019). Under speed control, the control torque, which is the torque applied by the generator and electrical load, is modulated to maintain a constant rotation rate. Under torque control, the speed of the rotator modulates based on the control torque applied by the system and oscillatory hydrodynamic torque. Newton's 2nd Law for a rotational system in which the net torques acting on the system are the hydrodynamic torque on the rotor, any torque losses from components like seals, and the control torque imposed by the generator is described by

$$Q_r - Q_{\text{loss}} - Q_c = J\dot{\omega}, \tag{10}$$

where J is the rotational moment of inertia of the rotor, driveshaft, and generator, and $\dot{\omega}$ is the rotor's angular acceleration. Under constant speed control, the rotor is regulated to hold the rotational speed constant (i.e., $\dot{\omega} = 0$) and Q_c will oscillate in response to the oscillatory hydrodynamic torques. In contrast, under ideal torque control, the rotor will accelerate or decelerate based on instantaneous hydrodynamic torques generated by the rotor and system control gains. In theory, either approach can generate comparable system performance under ideal conditions (Polagye et al. 2019), but each has unique challenges. Torque control can cause the rotor to stall while speed control can necessitate power input to the rotor (i.e., operating the generator as a motor) if the commanded speed results in negative, phase-resolved C_P at some point throughout a cycle. This can occur even if the time-averaged C_P is positive.

3 Constraints and design

3.1 Constraints

The identification of constraints, driven by external factors and project objectives, played a significant role in the development of the Turbine Lander. Here we summarize several important design constraints, the motivation or justification for selecting them, and the implications of these decisions. For reference, a picture of the system is shown in Fig. 1 and Fig. 2 includes an annotated rendering.

Minimize environmental impact: The potential environmental impacts of marine energy include, but are not limited to, collision risk, benthic habitat disturbance, and radiated noise (Copping and Hemery 2020; Garavelli et al. 2024). A conservative approach towards minimizing potential impacts drove multiple design decisions. First, we selected a vertical-axis, cross-flow turbine instead of an axial-flow turbine because the former operates efficiently at lower tip-speed ratios (Bhutta et al. 2012), which may lower risk to animals in the event of a collision. A gravity foundation was selected to avoid a ground-penetrating foundation and disturbance to the underlying substrate. To address key environmental concerns including collision risk for marine animals, an environmental monitoring system called the Adaptable Monitoring Package (Polagye et al. 2020) was integrated into the platform.

Vessel selection: We elected to design the system to be deployed and recovered with a relatively small, well-equipped oceanographic research vessel with a length overall of approximately 20 m. Although somewhat arbitrary, vessels of this size are common at institutions with oceanographic research programs and comparably sized vessels built for other applications (e.g., fishing) often have similar capabilities. While each vessel is different, setting a bound on the length of the vessel (or choosing one outright) provides constraints on equipment, lift capacity, and deck space. These vessel constraints subsequently constrain many design features including rotor size and geometry, foundation size and weight, and deployment/recovery operations. For example, over-the-side lift capacity plays a significant role by limiting the size and weight of the package, which impact a gravity foundation's ability to resist overturning moments generated during operations. This, in turn, constrains maximum rotor force, which depends on rotor geometry and blade count.

In the case of APL-UW's R/V *Jack Robertson*, the target deployment vessel, the aft deck space has a width of approximately 5 m (3.66 m clearance beneath the A-frame) and an A-frame lift capacity of approximately 2700 kg. This defines the maximum working load permitted to occur during deployment and recovery and is the sum of the load being lifted (i.e., the in-air or in-water weight), drag forces and added mass inertial loads (if submerged), wave loads (during transition through the sea-surface), biomass accumulated during operations, suction forces (if lifting components embedded in the seafloor), and ship-motion induced inertial loads. We therefore targeted a maximum in-air mass of 2460 kg. Because this is close to the A-frame's working load, it also restricts the conditions under which the system could be safely deployed and recovered.

System survivability: A system survivability of 18 months with 6-month maintenance intervals was targeted. This interval informed material selection for corrosion resistance, designs to limit stress concentrations and prevent fatigue failures, and robust measures to mitigate salt-water or particulate accumulation in the bearing pack and generator housing. In addition, prior research has shown that biofouling can substantially decrease rotor performance (Stringer and Polagye 2020), thus methods for mitigating biofouling on the rotor were required.

With these general constraints in mind, additional factors informing design included site selection, targeted mean power generation, commercial off-the-shelf component availability, and deployment/recovery methods.

Site selection: Numerous sites in Salish Sea have currents suitable for power generation, including some sites exceeding peak tidal currents of 3 m/s (Thomson et al. 2012; Polagye and Thomson 2013). However, many suitable sites lack supporting infrastructure and are relatively deep, making operations more difficult. For health, operations, and environmental monitoring purposes, we opted to deploy the system with a single cable supporting 480 Vac power, communications, and data transfer. To limit costs, a site relatively close to accessible facilities, requiring minimal infrastructure upgrades, was preferable. Diver accessibility during the unit's first deployment was also preferable given that the cabled needed to be secured to the seabed. This also has the added advantage of simplifying deployment and recovery operations.

Before the system design could be completed, the constraints were used to identify the deployment site. The inlet to Sequim Bay was selected despite the fact that sites with stronger currents are encountered in the region. Based on the prior measurements (e.g., Harding et al. 2016; Polagye et al. 2020), the rotor was designed for continuous operations at a peak current of 2.34 m/s assuming the controller maintained operations at the peak tip-speed ratio. A detailed site description is included in Sect. 5.

Mean power generation: There was no specific target for mean power generation that informed the design process. Rather, the objective was to maximize power generation within the bounds of the other project constraints. From a practical perspective, time-average generation on the order of 100 W would be meaningful. Coupled with suitable energy

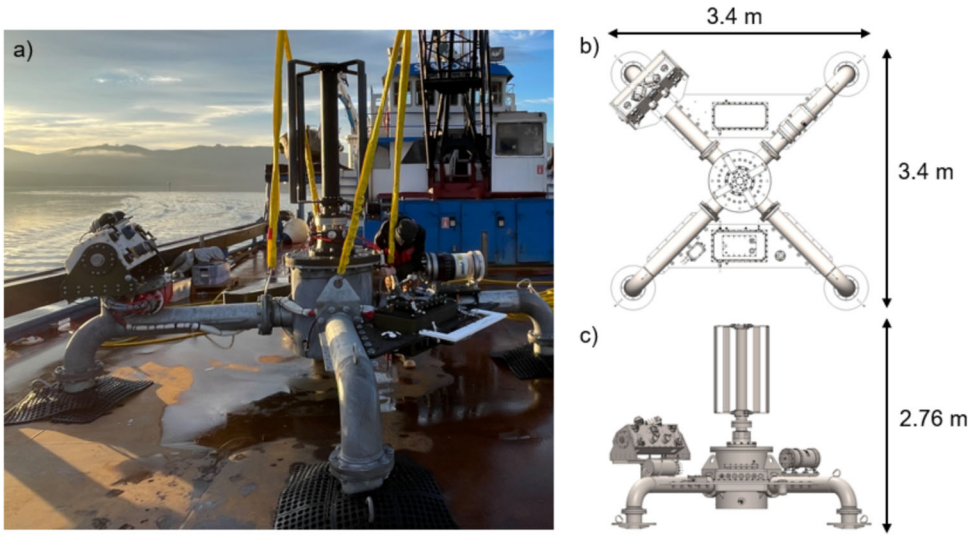

Fig. 1 **a** The Turbine Lander prepared for deployment in Sequim Bay, Washington. Plan (**b**) and elevation (**c**) views of the Turbine Lander showing its length, width, and height when fully assembled

storage, such a system could support advanced sensing systems or vehicle charging capabilities in regional waters.

Power electronics: The Turbine Lander was designed to generate not only power, but also high-quality and well-resolved data streams to assess its performance. Thus, any power electronics and controls systems needed to support relatively high-frequency ($>$ 500 Hz) data acquisition of key system parameters. We chose to limit our options to commercial-off-the-shelf components as a means of minimizing engineering costs associated with developing custom pulse-width modulation motor controls and high-voltage ac/dc conversion.

3.2 Rotor design considerations

Minimizing system complexity and associated modes of failure was a driving factor in the rotor design. A vertical-axis, cross-flow design was chosen given that it is agnostic to inflow direction (Hand et al. 2021). In contrast, horizontal-axis cross-flow and axial-flow turbines require additional components to maintain rotor alignment with inflow direction. For the same reason, a vertical-axis cross-flow turbine also avoids the need to control the orientation of the foundation during deployment, which would introduce significant operational complexity and vessel capability requirements, especially at deeper installation depths (e.g., $>$ 20 m).

For a cross-flow turbine, rotor geometry design decisions that affect forces and torques include the aspect ratio and blade count. Rotors with relatively few straight blades (e.g., one or two) are more efficient than those with more blades, but have substantially higher peak-to-average power and force ratios within a single rotation (Li et al. 2015; Rezaeiha et al. 2018; Hand et al. 2021; Hunt et al. 2024). A higher rotor solidity (defined as the ratio of the number of blades times the chord length divided by the rotor circumference) can reduce the peak-to-average ratios, but comes at the cost of added manufacturing costs and poorer performance. In addition, higher solidity turbines operate at lower tip-speed ratios (Rezaeiha et al. 2018; Hunt et al. 2024) and may achieve optimal efficiency over a narrower range of tip-speed ratios (Brusca et al. 2014). Based on prior scale-model experimental results described by Hunt et al. (2024), a four-bladed rotor was selected because it considerably reduces peak-to-averages force and torque ratios without significantly reducing optimal efficiency. Further reductions in peak-to-average ratios could be achieved with helical or twisted-swept blade geometry (Shiono et al. 2002; Castelli and Benini 2011; Marsh et al. 2015; Hand et al. 2021), albeit by increasing manufacturing complexity and reducing optimal efficiency.

To avoid potential negative impacts of the surrounding superstructure on performance but also accommodate lifting the full package from a single pick point on the shaft, the Turbine Lander rotor was ultimately designed with a cantilevered rotor shaft in-line with the bearing pack and PTO. The choice of a direct-drive system was primarily driven by a desire to minimize the complexity and stack height of the PTO housing coupled with the rotor. An added benefit of the direct-drive architecture is the lack of a gearbox. A vertical axis rotor operating in a constant speed control regime may undergo torque reversals as the hydrodynamic torques drop and the control torque switches sign to maintain rotation (Polagye et al. 2019). These torque reversals, which could occur once per cycle per blade, could result in premature failure of the gearbox.

The anticipated peak, instantaneous inflow conditions were used in load estimates for structural components of the rotor and overturning moment calculations. When relevant, minimum safety factors of 1.5 or greater were used in the in the design process.

3.3 Turbine Lander design

This section provides a high-level overview of the system's mechanical and electrical design. Additional technical information including dimensioned figures and off-the-shelf component specifications are included as supplemental material. An annotated rendering of the final system is shown in Fig. 2. The foundation's footprint is approximately 3.7 m by 3.7 m. Scour-prevention mats (1 m by 1 m non-slip, flexible rubber mats) added approximately 1 m to each dimension of the final footprint. The maximum height above the seabed is 2.76 m and its total weight in air was approximately 2270 kg. While a four-legged foundation is unstable on a solid surface, the approach maximizes the static stability potential of the foundation on a deformable seabed. The risk of one leg not making contact with the seabed when deployed is ameliorated by the nature of reversing load conditions at the site, which causes the feet to work themselves into the cobble layer on the seabed, as had been evidenced by previous deployments of an environmental monitoring system at the site (Polagye et al. 2020).

The rotor dimensions were 1.19 m by 0.85 m (cross sectional area of 1.01 m^2). The NACA 0018 foils (chord length 10 cm) were constructed with a solid, uniaxial carbon fiber core wrapped in a carbon fiber twill. This choice was driven primarily by the stiffness to weight ratio. The intended preset pitch angle (toe out angle between the blade chord and tangent to rotation) was $-6°$, but due to a miscommunication during the design process, they were fabricated with a $-9°$ pitch angle. This mistake likely resulted in decreased power production (Hunt et al. 2024). A ClearSignal (Severn Marine Technologies, LLC.) coating was later applied to the foils to mitigate biofouling without substantially altering hydrodynamic performance.

A combination of end plates and struts was chosen given prior research suggesting decreased performance with solid end plates (Strom et al. 2018). The foils were secured to the struts using a 3D-printed titanium (Ti) hinge assembly. The interface between the carbon fiber blades and the central shaft is a sensitive area for two reasons. First, even with unidirectional carbon fiber, oscillatory blade deflection would fatigue a rigid connection point. Second, hydrodynamic disturbances at the rotor periphery impose a significant parasitic torque (Strom et al. 2018). To address this, a streamlined "living hinge" assembly consisting of a titanium insert in the blade, titanium pin, galvanic protection, and aluminum strut was employed. The remainder of the rotor assembly was constructed from hard anodized 6061 aluminum while the driveshaft was machined 2507 duplex stainless steel. Additional technical information about the blades and struts, including a cut-away rendering, is included in the supplementary material.

The generator was a Siemens 1FW3202 permanent-magnet synchronous torque motor with a rated power of 7.9 kW. This motor, which is considerably oversized for the application (maximum expected time-averaged power generation of $\sim$ 1 kW), was selected, in part, to minimize active cooling requirements during periods of peak power production. The generator housing was air-filled and isolated from the environment using redundant face and piston seals. A magnetic coupling connected the driveshaft to the generator, thereby avoiding a rotary seal on the generator housing, which could be a critical failure point. The magnetic coupling does, however, introduce an additional constraint. Its static tear torque (i.e., the torque at which the coupling slips), is approximately 390 N m, which is substantially lower than the rated torque of the generator (500 N m).

Two tapered roller bearings housed in an oil-filled chamber were used to maintain the shaft alignment while two lip seals and an exclusionary v-seal were used to isolate the bearings from salt water and particulate and to prevent lubrication oil egress into the environment. The lip seals can support a maximum pressure differential of 48 kPa relative to ambient conditions. Given the tidal range at the site (up to 3.8 m) and deployment depth, this required an oil-filled pressure compensator, which provided an additional 13.8–27.5 kPa of positive gauge pressure relative to ambient pressure at depth. A biodegradable oil (PANOLIN TURWADA SYNTH 46) was selected as the lubricant for the bearing pack in the event of a seal failure. The drive shaft's sealing surface was coated with alumina-titania ceramic to increase the resistance to wear, which also reduces friction at the sealing surface. A labeled rendering of the driveline and generator housing is included in Fig. 3.

Four custom housings were designed and fabricated to accommodate the power electronics, load dump, and an underwater junction bottle (images of the housings are included as supplemental material). These housings all had rectangular form factors, which were designed to maximize the in-water weight of the system while retaining the convenience of air-filled housings (i.e., cylindrical form factors would have been higher volume, producing more buoyancy). At the Turbine Lander, the shore cable terminated at a small junction housing, where copper conductors and optical fibers were split and distributed to the ac housing, dc housing, and Adaptable Monitoring Package (AMP). This was an inexpensive plastic housing filled with mineral oil that served as a "weak link" with a low failure consequence if a high strain was placed on the cable (e.g., it was dragged by a vessel anchor). The ac housing accommodated the ac power and passed the required dc power to the dc housing. This included 720 Vdc (Seimens DCLink) and 48 Vdc to support instrumentation. Power generated by the system was dissipated using a load dump constructed using three 42Ω, 600 W resistors wired in parallel to dissipate up to 1.8 kW of power.

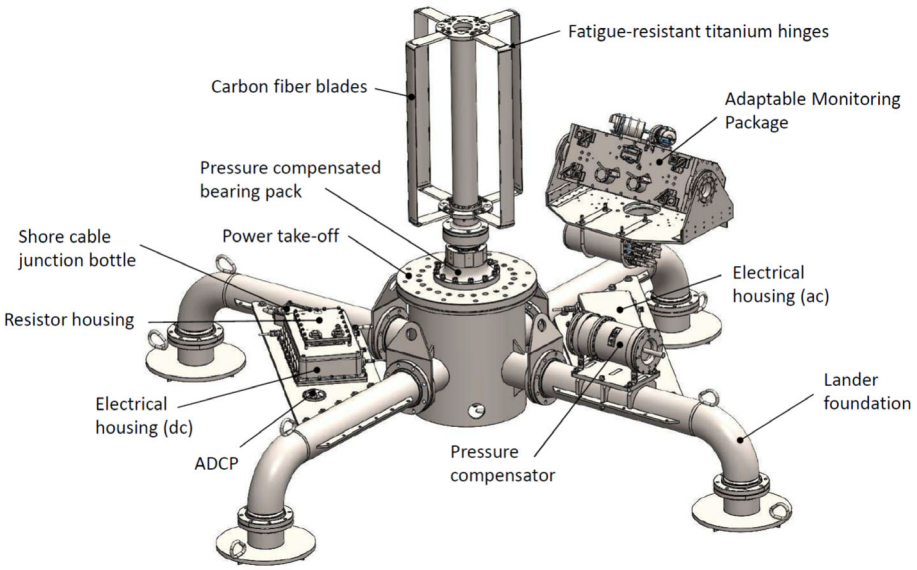

Fig. 2 A labeled rendering of the Turbine Lander lacking only the scour mats, hydrophone array, electrical cables, and hoses. The pear links welded to the foundation's legs and feet were included to facilitate assembly and deployment

Components from the Siemens SINAMIC S120 family formed the foundation of the system's power electronics and management. This included active interface and line modules deployed in the ac housing and, in the dc housing, a control unit and two single-unit 9A motor modules. The remaining components of the system included numerous ac–dc and dc–dc converters, a relay board, a network switch, a PC/104 computer, and health monitoring sensors (e.g., ground fault monitoring equipment, thermocouples). One feature requested during the permitting process was the ability to control the turbine by ensuring that it could not self-start or continue to operate if power was lost. While self-start was not expected under the conditions at the deployment site, if shore power was lost, the rotor could rotate at its "free wheel" condition until the currents fell towards slack. To address this, an Altech C-TEC2405-5 24 Vdc ultra-capacitor was added to the dc housing. In the event of shore power loss, this provided sufficient energy storage for the onboard computer to initiate a controlled shutdown, with a final step of short-circuiting the motor windings with a set of relays. This provides sufficient resistive torque to preclude self re-start and could also be leveraged to prevent rotation the system if operating in currents that exceed the design conditions.

System controls and data acquisition were implemented in C++ with custom software running on a real time Linux PC/104 system that interfaced with the Siemens electronics over Profinet. The custom software permitted the implementation of arbitrary control schemes and modifications to acquisition parameters within the limitations of the electronics. The relative ease of implementing arbitrary control schemes in future research (e.g., intracycle control, Strom et al. 2017), was an additional motivating factor for selecting the Siemens equipment and direct-drive architecture. During operations, data including shaft speed, voltage, control

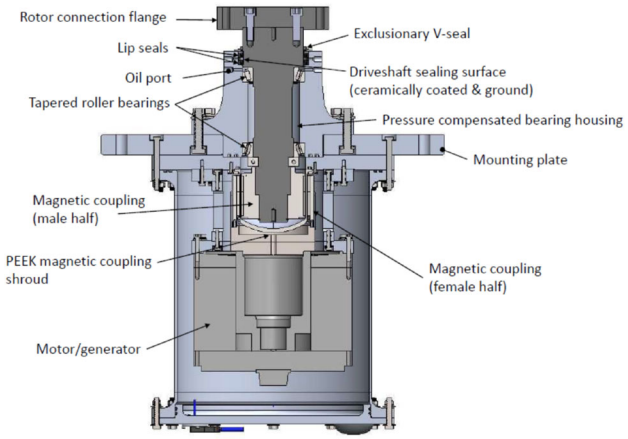

Fig. 3 A labeled rendering of the driveline assembly and generator housing

torque, winding current, absolute encoder position, incremental encoder position, generator winding temperature, oil levels in the pressure compensator, and control set points were recorded. Data were recorded at sampling rates between 100 Hz and 1 kHz.

An AMP was mounted on one leg of the Lander's foundation for environmental monitoring purposes and to allow local measurements of the tidal currents with an acoustic Doppler profiler (ADCP, Nortek Signature1000). ADCP data were processed in real-time and time-averaged inflow conditions measured 3.1 m above the seabed were passed to the onboard computer and used to control the turbine. While upgrades to the AMP's instrumentation, packaging, and software were made before the deployment, the system architecture and functionality was functionally identical to the MSL-2 configuration described in Polagye et al. (2020).

Since a variety of materials (e.g., titanium, galvanized and stainless steel, and aluminum) were used in the rotor, foundation frame, and housings, efforts were made to prevent corrosion from mixed metal contact. Unless otherwise stated, 316 stainless steel fasteners were used to secure components and sub-assemblies. Mixed metals were isolated using garolite tubes, fiberglass gaskets and washers, and custom machined Polyether ether ketone (PEEK) isolators. In addition, all housings, the bearing pack, and the rotor were generously equipped with sacrificial anodes (aluminum).

4 System characterization and performance

Several tests were performed to characterize the system before the field deployment. These efforts measured the water-to-wire performance of the rotor, estimated losses, and verified component integrity. Testing was performed in the laboratory without a rotor, on a dynamometer, in a saltwater tank, and on a research vessel under propulsion to simulate in situ operations.

4.1 Laboratory testing

Torque losses were measured in the laboratory by driving the generator as a motor with the magnetic coupling and bearing pack assembled and attached to the generator housing. In this arrangement, the electrical power input to the generator represents generator inefficiency and frictional losses from the bearing pack and seals. Mechanical torque supplied to the magnetic coupling was estimated by the manufacturer's torque constant and rotation was measured by the generator's encoder. The tests were performed by stepping through shaft speed setpoints from 10 to 120 RPM for one minute each. Thirty seconds of data at each setpoint were isolated as representative of steady-state conditions. These tests were performed with no seals on the bearing pack and then again after each seal was installed. At each setpoint the power required to drive the assembly was nearly constant, with small intracycle fluctuations attributed to the bearing pack and magnetic coupling.

The results of these tests (Fig. 4a) show that baseline losses for the system range from approximately 60 to 120 W for operating conditions from 50 to 100 RPM. Installing a second seal increases losses by approximately 30 W at 50 RPM and close to 80 W at 120 RPM. The addition of the final lip seal and v-seal resulted in total frictional losses ranging from 100 to 300 W. Increases in power input requirements correspond to parasitic torques of 3–5 N m with the addition of each seal. While relatively small, these losses values are not insignificant near cut-in speed and represent the cost of balancing survivability with power generation.

The baseline conditions include a dust seal on the manufacturer's generator housing. As part of the post-deployment review, we performed additional testing without that seal and found this to reduce parasitic torque by approximately 10 N m, which translates to losses of 50–120 W across operating states (Fig. 4b). This seal, therefore, constituted an unexpectedly high fraction of the baseline losses.

Winding temperatures during sustained operations and the impact of sustained operations on viscous losses in the bearing pack were also measured and details are included in the supplemental material. These tests showed that sustained operations at levels of power generation within the design performance envelope were not expected to cause thermal issues and that the overall changes in viscous losses in the bearing pack were not likely to significantly impact operations.

To characterize the Lander PTO efficiency as a function of rotation rate and input torque, APL-UW developed a dynamometer (see the supplemental material for details) consisting of a second motor that emulated the turbine power input and a rotary torque cell positioned between the PTO shaft and second motor. Characterization was carried out with the Lander generator in speed control over a range of speeds from 20 to 140 RPM and the dynamometer motor in torque control over a range from approximately 10 to 360 N m, distributed logarithmically to obtain a higher density of set points at low torque conditions. As for the loss characterization tests, individual tests were one minute long and 30 s steady-state periods were isolated for further processing. The mechanical power provided to the Turbine Lander's shaft was calculated from the torque cell and encoder mounted to the prime mover's shaft. They were used to calculate PTO efficiency (Fig. 5a) and estimate the motor efficiency using knowledge of the seal losses (Fig. 5b). Efficiency depends strongly on the input torque with modest decreases as rotational speeds increase. Torque inputs above approximately 20 N m are required to overcome system losses and generate power. At relatively low torques, these losses drive the system's efficiency to zero, while at higher rotation rates, frictional losses increase. Over the range of operational conditions for the Turbine Lander, PTO efficiency varies from approximately 0 – 0.7 when the system losses are included. Over the same range, excluding those where no electrical power is generated, η_{gen} ranges from approximately 0.6 – 0.87. This is slightly lower than the theoretical maximum efficiency of 93% provided by the manufacturer, but the full operational range of the motor was not tested.

In summary, we anticipate low PTO efficiency near cut-in conditions due to the combination of relatively low rotation rates and low torque input from the rotor (lower left corner of Fig. 5a). PTO efficiency generally improves as speeds and torques increase, but the full system does not actually operate

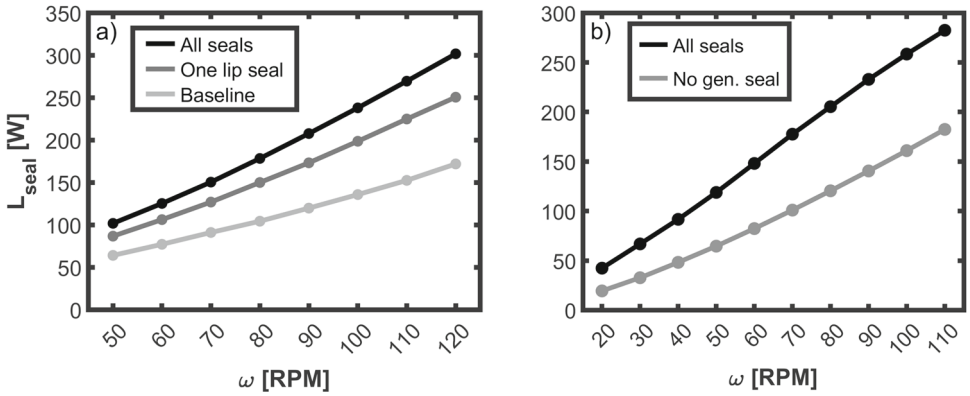

Fig. 4 **a** Measurements of baseline and seal-related system losses. "All seals" curve represents the total losses measured including baseline operations, both lips seals, and the v-seal. **b** A comparison between system losses with both lips seals and the v-seal installed when the generator dust seal was both installed and removed. Note the measurements in **a** were performed prior to the system deployment while the measurements in **b** were performed when the system was reassembled after the deployment

in the most efficient portions of the parameter space due to the rotor dynamics.

4.2 Testing under propulsion

R/V *Russell Davis Light* (RDL) is a specialized, purpose-built research vessel owned by APL-UW. The shallow draft, twin-hulled vessel's forward section is equipped with a gantry/frame system for test articles (see Supplemental Material). A turbine installed on the frame and lowered below the water line is clear of the hydrodynamic impacts of the vessel hull. This allows for tests of turbines with characteristic length scales up to 1.5 m at inflow speeds expected in situ (up to 3 m/s depending on the rotor).

The water-to-wire efficiency was characterized by installing the PTO and rotor on RDL's gantry. An acoustic Doppler velocimeter (Nortek Vector) was deployed approximately 1 m forward of the rotor to measure the inflow velocity at 64 Hz. The recorded data were despiked (Goring and Nikora 2002) and the magnitude of the inflow velocity taken as the representative speed incident on the rotor. During individual tests, vessel heading and speed (ranging from approximately 0.5 to 2.5 m/s) were maintained at constant values while stepping through different rotor rotational speeds under constant speed control. These conditions correspond to tip-speed ratios between 1 and 2.6. Each setpoint was maintained for a three-minute dwell time. In post-processing, these data were manually trimmed to select one minute steady state conditions. Data were processed to produce a single, time-averaged water-to-wire efficiency for each set of vessel and rotor rotational speeds.

Results for the time-averaged water-to-wire efficiency and electrical power generation under test conditions are shown in Fig. 6. At inflow speeds of 1 m/s, $\lambda > 2$ is required for net positive power generation, with peak $\eta_{\mathrm{ww}} < 10\%$. This is a consequence of low PTO efficiency under these conditions (Fig. 5a). Optimal tip-speed ratios decreased slightly and η_{ww} exceeded 20% when inflow speeds were 2 m/s or greater. Phase-resolved (4° resolution) control torque, power, and efficiency (see supplemental material) were consistent with a priori expectations and yielded no significant signs of fabrication or assembly issues (e.g., deviations from expected periodicity due to alignment issues).

Accounting for the PTO efficiency (Sect. 4.1) during rotor characterization tests, peak C_P was ≈ 0.3 (Fig. 6b). Bachant et al. (2016a) and Miller et al. (2018) demonstrated that C_P becomes independent of flow speed for $Re_D > 1.5\mathrm{e}6$. For $Re_D = \frac{U_o D}{\nu}$, where ν is the kinematic viscosity (1.027 m^2/s in freshwater at 19°C), rotor operation at 1 m/s, 1.5 m/s, and 2 m/s corresponds to $Re_D = 8.5\mathrm{e}5$, 1.2e6, and 1.7e6, respectively. Rotor performance is consistent with expectations for Reynolds independence at inflow velocities greater than 2 m/s (Fig. 6b), but $C_P - \lambda$ behavior is appreciably influenced by inflow velocity below this threshold.

4.3 Salt-water tank testing

Salt-water tank testing was performed to verify the integrity of the housings and to test for ground faults before the field deployment. One particular concern was that ground faults would accelerate the corrosion of the housings. During this testing, the PTO and all housings were wired as deployed in the field, rigged, and submerged to a depth of 2 m. Power was provided by the shore cable, wired with a Littlefuse SB6000 ground fault monitor/interrupt, and the system was operated (motored). No ground faults or housing issues were identified, so no further modifications were made to the assemblies prior to deployment. However, one serendipitous outcome

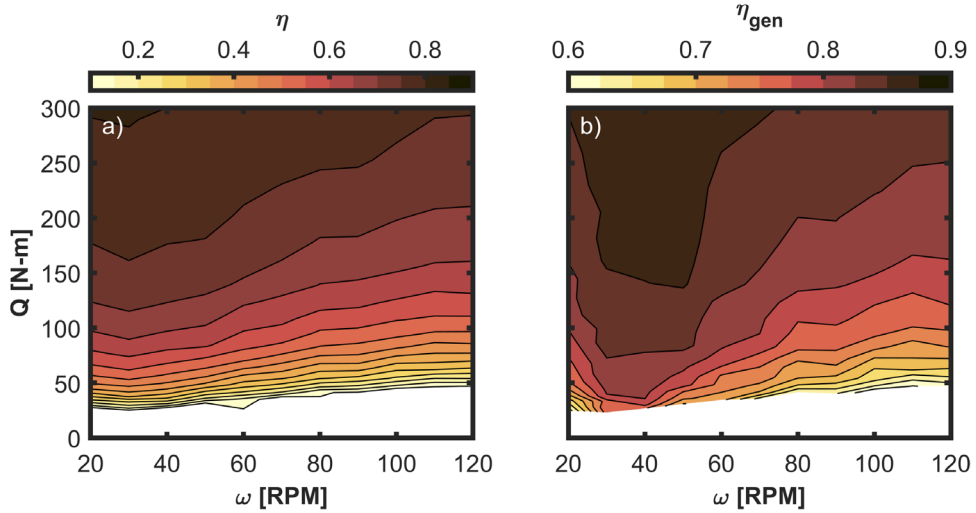

Fig. 5 Results from the dynamometer measurements. **a** PTO efficiency estimated as P_e/P_m. **b** Estimates for η_{gen} using Eq. 7, which accounts for mechanical losses. The y-axis is the torque input to the driveshaft as measured by the torque cell. This can be used to estimate the control torque at the same operating state by subtracting 20 N m, which is an approximation to the baseline parasitic torque present in the system

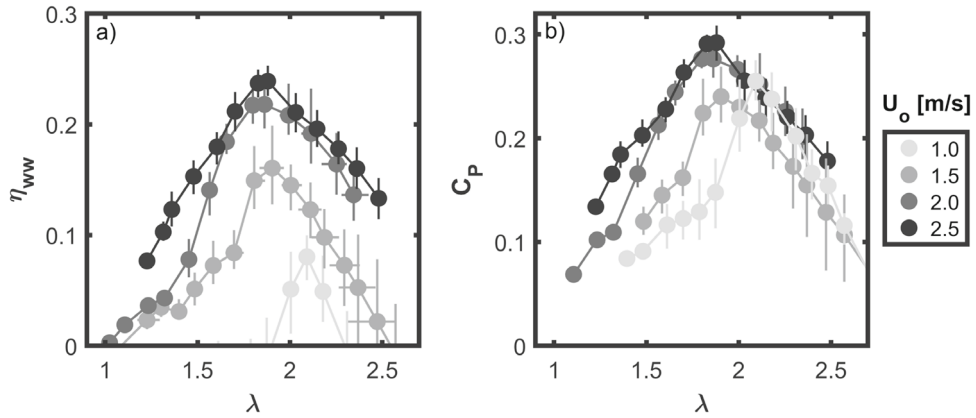

Fig. 6 **a** Water-to-wire efficiency versus tip-speed ratio as a function of inflow speed from 1 to 2.5 m/s. **b** C_P using control torque and seal loss measurements (Eq. 8). The mean and 5–95th percentile bounds for the tip-speed ratios in **(a)** and **(b)** are calculated from the rotational speed and smoothed (2-s) moving mean inflow. Note that the legend denotes targeted vessel speeds. Measured speeds for each test were used in the calculations and were generally within 5% of the vessel speed

of these tests revealed issues with the installed anodes, all of which were thought to be aluminum. Upon entering the water there were immediate signs of electrolysis and associated anodes were later identified to be magnesium, which is only suitable for freshwater deployment. All anodes were therefore replaced before the salt water deployment. Whether these were misplaced in storage or shipped improperly cannot be confirmed given the anodes are not labeled to differentiate their materials.

5 Field deployment—Sequim Bay, WA

The inlet to Sequim Bay, WA (Fig. 7) satisfied all project siting constraints (Sect. 3). Sequim Bay is a relatively large and shallow bay that is connected to the Strait of Juan de Fuca by a shallow (< 10 m MLLW), narrow inlet. With peak tidal ranges exceeding 3 m, parts of the inlet to the bay experience peak tidal currents greater than 2 m/s (Harding et al. 2016). Pacific Northwest National Laboratory's (PNNL) Marine and Coastal Research Laboratory (MCRL) is located on the west side of the inlet and hosts accessible shore-side facilities, including access to 480 Vac power, and staff with experience with marine operations and oceanography. Due to its position and facilities along the waterfront, it was feasible to install a

relatively short cable (< 160 m) from the deployment location to the dock and then to an electrical box installed on a shore-side building. From there, systems were networked for remote access.

The Turbine Lander was deployed on 18 October 2023 and was recovered on 7 March 2024 (141 days). The system was deployed using *Sea Horse*, a 33 m construction barge equipped with a high-capacity crane. Rather than anchoring, the vessel is equipped with two spuds (up to 15 m) that can be lowered into soft substrates. Since the site was accessible to divers who could remove deployment hardware, four of the lifting eyes on the foundation were equipped with shackles and slings secured to a spreader beam, leading to a balanced pick while the unit was lifted from the deck to the water. Deployment operations consisted of anchoring the vessel with the spuds approximately 10 m from the intended deployment location, a single lift to set the system on the seabed, and passing the shore cable to a support vessel that laid it on the seabed while transiting to shore. Once communications were established, the cable was secured by divers using sand anchors. The original plan of deploying the Turbine Lander from a research vessel was discarded relatively late in the process out of concern for the potential to accidentally damage a nearby telecommunications cable if the currents caused the vessel to drag anchor.

The deployment location was 46°4.761′N, 123°2.589′W, which is just east of mid-channel at a depth of approximately 8 m MLLW. The footprint of the Turbine Lander was oriented with the AMP facing west-southwest (∼ 260°), placing the ADCP northwest of the rotor. This approximate orientation was intentional and chosen to orient the environmental monitoring packaging roughly perpendicular to both the ebb and flood currents.

Time-varying currents are driven by the region's mixed semi-diurnal tides, which, in the inlet to Sequim Bay, result in tidal cycles with relatively strong currents that are often followed by multiple cycles with currents below 1 m/s. The cut-in/out speeds were set to 0.9 m/s for most of the deployment. While below the anticipated inflow speed required for net power generation was approximately 1 m/s, we chose to intermittently run the system in a net power consumptive state to increase the total operation time and cycle count that critical components would experience. Over the deployment period, the system had an up-time exceeding 95%. Downtime was a consequence of power outages and network maintenance at the site and system software modifications. In total, the rotor was spinning for approximately 960 h, corresponding to approximately 3.4 million revolutions.

The ADCP sampled velocity profiles at 4–8 Hz with 0.2 m vertical resolution from 66 cm above the seabed to the surface. Raw data were stored in 10-min .txt files by the AMP control computer located on shore. For rotor control, the AMP processed the ADCP profiles, removing pings with correlations below 50%, and then provided a 2-min moving average velocity at 3.1 m above the seabed. This is above the height of the rotor, which extends to a height of 2.76 m above the seabed, and consequently minimizes the impacts of the rotor wake on estimated inflow during ebb tides. In post-processing, velocity data were reprocessed to produce short-time averages (24 ping ensembles; 3–6 s in length). Before calculating ensemble averages, bins with correlations less than 50% were removed, as were velocity spikes exceeding the mean values in each 10-min sample by greater than three standard deviations.

As shown in Fig. 8, the site's mixed semi-diurnal tides result in periods of 12–18 h each day when currents are too weak for power generation, while the spring-neap cycle drives significant variability in peak currents associated with a given day's largest exchanges. Peak currents were nearly 2.5 m/s during both ebb and flood tides, but are not representative of the general conditions at the site. Vertical shear corresponding to approximately 10% of the mean current measured at 3.1 m was regularly observed across the depths spanned by the rotor (see the supplemental material). In addition, post-deployment analysis of the flood tide boundary layer suggests that mean inflow conditions averaged across the rotor height were typically on the order of 80–90% of the measured inflow at 3.1 m.

The reference inflow velocities and 2-min averaged power generated by the system are shown in Fig. 9. For the majority of this time, the turbine was operating in constant speed control with target tip-speed ratios of $1.7 \leq \lambda \leq 1.9$. Throughout the deployment, control settings were regularly modified to better understand the performance in situ. For example, speed control settings from $1 \leq \lambda \leq 3$ were iterated upon during multiple tidal cycles to verify that the standard settings were optimal. Similarly, we tested torque control using $K\omega^2$ (Pao and Johnson 2011), but were only successful in avoiding stall at relatively high mean inflow velocities. The maximum electrical power generated during a 2-min moving average was over 600 W. While many of the periods where power input was required (i.e., $P_e < 0$ in Fig. 9) correspond to periods with currents below 1 m/s, in other cases, power input also occurred due to suboptimal control strategies or poorer than expected rotor performance.

Relative to vessel-based testing, power generation in Sequim Bay was substantially reduced and net power generation was not generally achieved until the reference inflow exceeded 1.3 m/s. We attribute this to several factors including biofouling and variability in the inflow conditions. Biofouling had both intermittent and sustained impacts on the system's operations, which could be verified using the AMP. Within 48 h of the system's deployment, strands of eelgrass had become lodged in the narrow (< 0.3 cm) gaps between the struts and rotor blades at the living hinge interface. Attempts to remove this fouling by temporarily

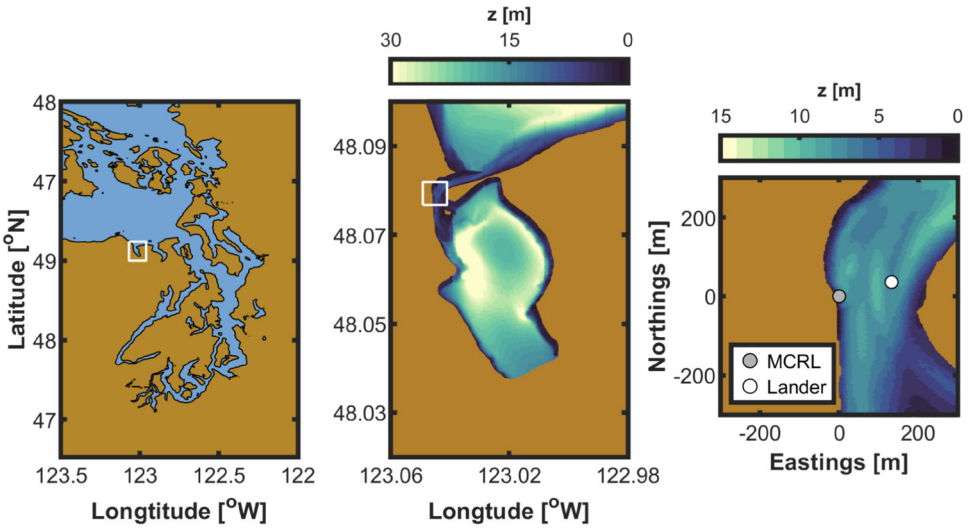

Fig. 7 (left) The Salish Sea region with an inset highlighting Sequim Bay. (middle) Sequim Bay with the inset highlighting the inlet. (right) Deployment area with points indicating the location of the research pier at MCRL and the Turbine Lander

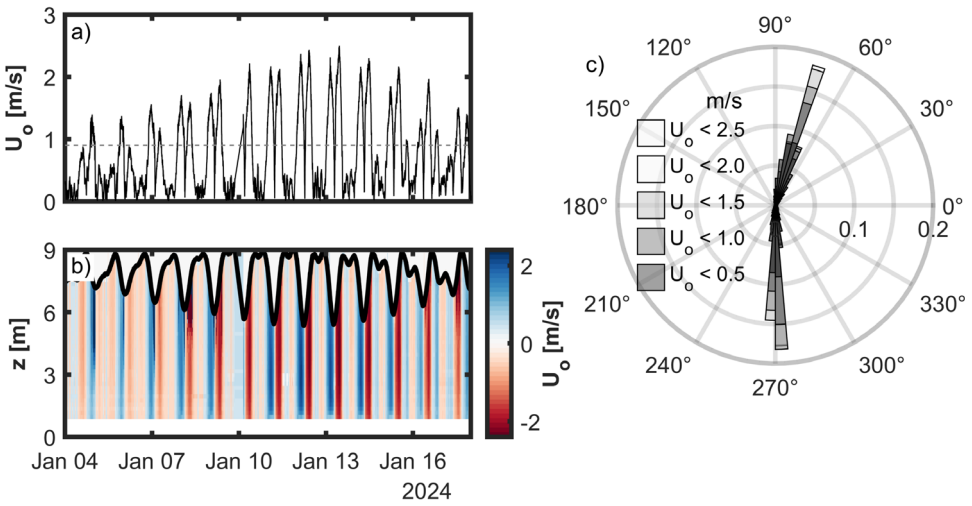

Fig. 8 **a** Measured tidal currents 3.1 m above the seabed. The dashed line shows the cut-in speed. **b** Profiles of tidal currents for the same period shown in **a**. The black line tracks the surface. **c** Probability density functions for inflow velocity and direction. Note that this period includes some of the strongest exchanges expected in a given 1-year period

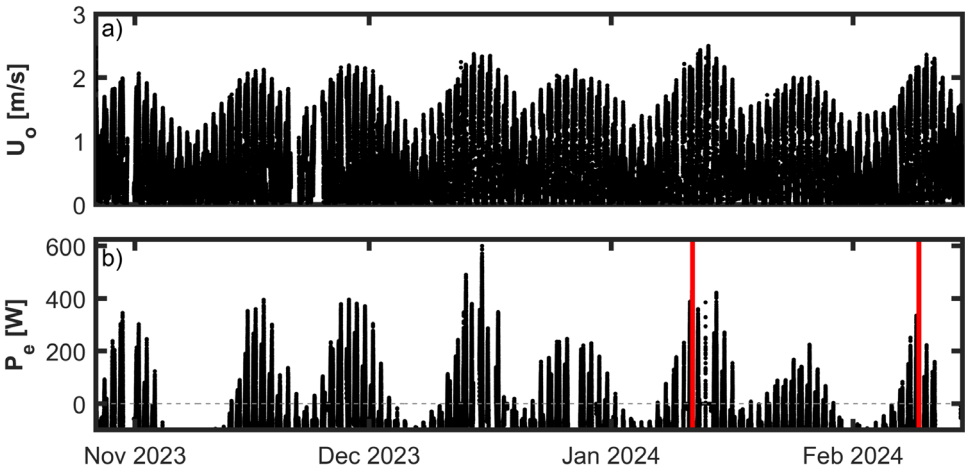

Fig. 9 **a** Reference inflow velocities (2-min average) measured 3.1 m above the seabed and **b** power generation (2-min average) throughout the deployment. In **b** the two vertical red lines correspond to the blade loss events. Note also that the figure includes periods where the system was operating at a net loss of power (i.e., power input was required to operate the rotor)

reversing the rotor's direction of rotation were unsuccessful and periods with modest fouling of the foils were regularly observed. A less common form of biofouling was kelp wrapped around the entire rotor. When this occurred, it typically resolved itself within a tidal cycle. The final form of biofouling observed was slow growth of algae on the rotor's struts, shaft, and endplates.

We estimate that modest biofouling reduced power production by between 50 and 200 W over the range of inflow conditions based on measurements of the power required to motor the rotor with and without fouling during quiescent conditions. A review of periods when the rotor was fully wrapped in kelp strongly suggests that this type of fouling of the rotor was far more consequential in terms of power losses, but also more intermittent. We hypothesize that the algae growth had relatively minor impacts on power production because most of the fouled area was located relatively close to the axis of rotation. Further information on power loss estimates attributed to fouling and images of fouling are included in the supplemental material.

Even without notable biofouling, the Turbine Lander performance would have been impacted by the complex inflow conditions and choice of a reference velocity timescale for constant speed control at a nominal tip-speed ratio. The instantaneous inflow measured by the ADCP can be decomposed into a mean velocity varying with the stage of the tide, turbulence, and instrument noise (Thomson et al. 2012). A 2-min moving average is sufficiently long to filter out instrument noise, while admitting fluctuations associated with the tidal cycle and "aharmonic" currents (Polagye and Thomson 2013). However, turbulence will affect the rotor in a similar manner to the mean flow when turbulent length scales are greater than or equal to the turbine length scale (i.e., an "engulfing gust") (Medina et al. 2017). For a rotor length scale on the order of 1 m and mean velocity on the order of 1 m/s, Taylor's frozen field hypothesis (Taylor 1938) suggests that the smallest engulfing gust would have a timescale on the order of 1 s. While a shorter averaging time would have admitted more of these engulfing gusts into the reference inflow condition, the lag in processing time and control system response would have resulted in the controller continually chasing inflow features that had already passed the rotor, possibly degrading performance beyond what was observed here. This would be compounded by the mismatch between currents experienced at the rotor depth and those reported at 3.1 m elevation.

To interpret the implications of this averaging and control strategy, shorter timescale velocity measurements and system performance are shown in Figs. 10, 11 and 12 for a 5-min, flood tide with mean current velocities exceeding 2 m/s. We observe a strong correlation between electrical power generation and velocity profiles (Fig. 10), with decreases in power generation corresponding to drops in inflow velocity. While mean, time-averaged velocities exceeded 2 m/s at 3.1 m, within the rotor height, inflow velocities varied from more than 2.4 m/s to less than 1.6 m/s over relatively short timescales (e.g., < 10 s). We hypothesize that this variability is driven by eddies associated with horizontal shear layers generated by the complex bathymetry as suggested by the figures in Harding et al. (2016). In this example, despite the relatively high mean inflow, the system temporarily required power input to maintain rotation during this period. Sentchev et al. (2020) observed similar short-term variability in the field deployment of a cross-flow turbine roughly twice the size of the Turbine Lander and, through analysis of co-temporal acoustic Doppler velocimetry data, were able to correlate variability in power output with turbulent length scales. Variability associated with turbulence and the transfer function by which different scales of turbulence affect turbine power output has been a general topic of interest in the wind (Tobin et al. 2015) and tidal energy community (Druault et al. 2022).

The observed decreases in power generation over short timescales when inflow speeds drop, and the lack of significant increases in power generation during analogous periods of higher velocity, reveal the role that the system characteristics (i.e., η_{ww} vs. λ curves) and controls play in power generation. Figure 11 shows the time series of inflow conditions at the top and bottom of the rotor, shaft rotation rate, tip-speed ratio, control torque, and electrical power. Over the period, the targeted rotor rotation rate based on the 2-min average inflow conditions was approximately 88 RPM. However, the 6-s averaged inflow spanned a much larger range, resulting in periods when parts of the rotor experienced $\lambda < 1.6$ or $\lambda > 2.7$. Both decreases in Q_c required to maintain rotor speed and the corresponding power generation are correlated with periods when the tip-speed ratio experienced by at least part of the rotor increases significantly. This is due to decreases in the kinetic power incident on the rotor and the inadvertent shift away from optimal λ to higher tip-speed ratios, both of which decrease the electrical power generation. To offset the decrease in hydrodynamic torque generated by the rotor, the control torque is reduced to maintain the system's rotation rate. In contrast, when the inflow increases, the tip-speed ratio drops. However, when this occurs, significant drops in power generation are not observed because the decreased C_P is offset by an increase in the kinetic power of the inflow.

Figure 12 dissects this further by showing time series of control torque, electrical power generation, water-to-wire efficiency, and PTO efficiency. Notably, for this time period, the mean η_{ww} in Sequim Bay was approximately half of that observed during vessel-based testing. Some of this difference is attributed to biofouling, but PTO efficiency dependence on ω and Q_c is also a factor. During the relatively high power generation periods, the rotation rates and control torques

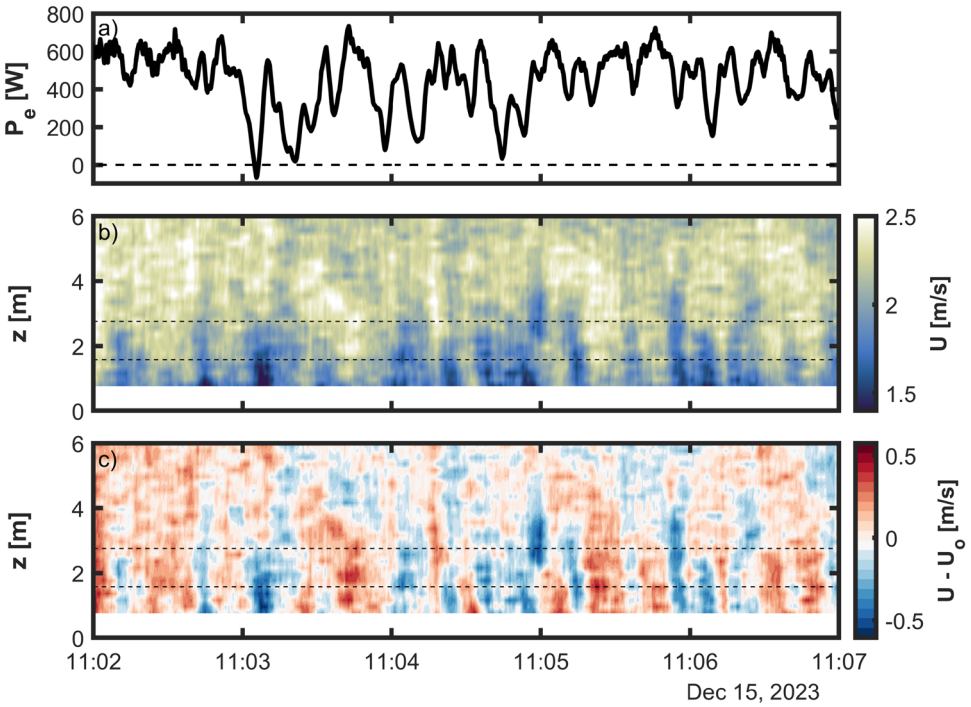

Fig. 10 **a** Turbine Lander electrical power generation calculated using a 6-s moving average. **b** Inflow velocity profiles using 6-s moving averages. The dashed black lines show the height of the bottom and top of the rotor. Over the 5-min period, there is a clear correlation between the generated power and the fluctuating velocities. **c** Velocity profiles show the deviations of the 6-s averages from the mean of all profiles shown in **b**

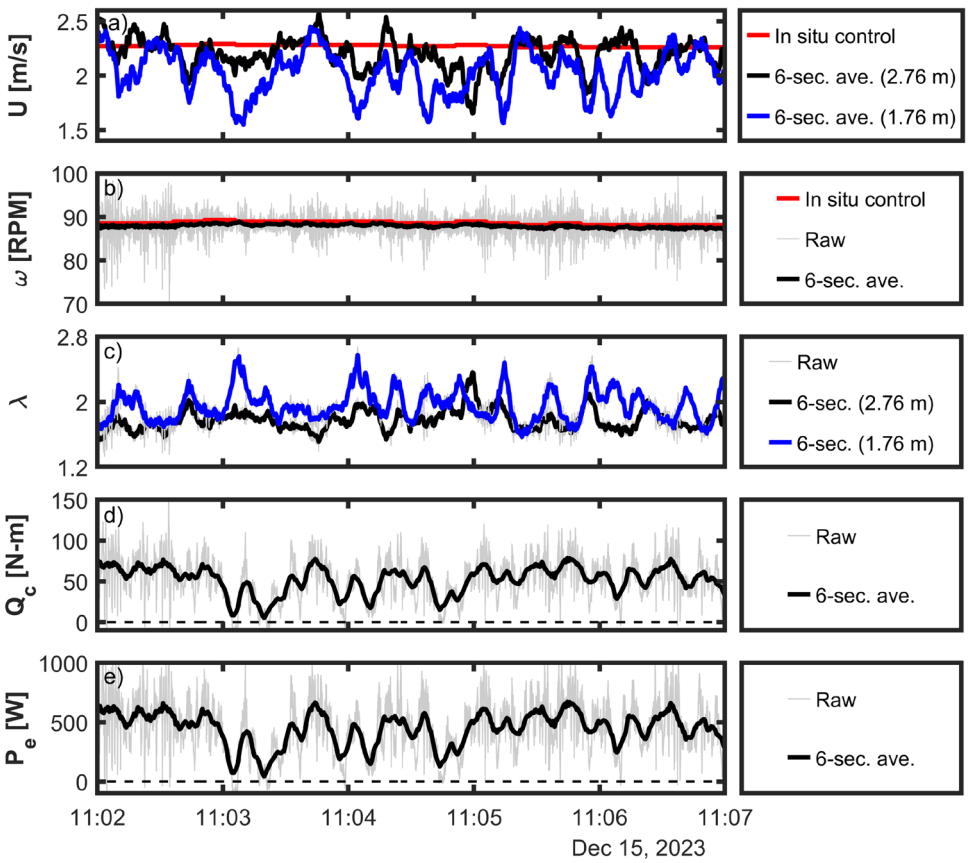

Fig. 11 **a** Inflow conditions (2-min and 6-s moving averages). Raw and 6-s averaged rotor speed (**b**), tip-speed ratios at the top and bottom of the rotor (**c**), control torque, and (**d**), electrical power. The data 2.76 m above the seabed correspond roughly to the top of the rotor while the data at 1.76 m are near the bottom of the rotor. Raw data were sampled at 100 Hz. All subplots correspond to the same time periods in Fig. 10

result in PTO efficiencies of about 0.5–0.6. However, when the control torque drops as a result of an increase in λ, the PTO efficiency decreases drastically. This is a result of two factors: mechanical losses (e.g., seals) increase relative to the production of hydrodynamic torque and the generator efficiency drops. These decreases in overall system efficiency become most significant when Q_c drops below approximately 30 N m. While Figs. 10, 11 and 12 correspond to a single 5-min period, similar measurements were obtained across the range of inflow conditions. Sustained deviations in inflow speeds of ± 0.5 m/s were regularly observed. For $U_o = 1.5$ m/s, these ± 0.5 m/s fluctuations would cause a rotor operating targeting a constant $\lambda = 1.9$ to fluctuate between approximately $\lambda = 1.4$ and $\lambda = 2.9$. The implications of this are significant given the narrow range of tip-speed ratios under which the system operates efficiently (Fig. 6). The observed decreases in system efficiency driven by the variable inflow clearly demonstrate why the performance of the system was poorer under constant speed control using 2-min inflow averages than under controlled inflow speeds during vessel testing.

During the deployment, the Turbine Lander lost two blades in separate events. The first occurred on 11 January and the second on 9 February, which correspond to 85 and 114 days after the deployment, respectively. These blades were not replaced during the deployment. Both events were associated with perigean spring tides, which often entrain debris from local beaches. AMP cameras with artificial illumination were not operating, but other sensors suggest the events were driven by the combination of a collision and a failure of the lower pin/hinge assembly. More analysis of the probable failures is included in Sect. 6.1 and the supplemental material. After both blade loss events, the system was able to continue generating power without modifications to the rotor controls. However, using experimental data from the laboratory-scale model, we were able to determine that modest increases to tip-speed ratios following each blade loss event were required to maintain optimal operations. However, a rigorous exploration of parameter space for controls was not explored following the blade losses. Notably, following the blade losses the temperatures measured in the generator windings increased, which we attributed to increased bi-directional current in the windings (see Supplemental Material for additional information). This increase in temperature represents an higher electrical inefficiency while operating constant speed control with fewer blades.

On 11 February, approximately two days after the loss of the second blade, we opted to curtail operations to minimize the probability of a third loss event, therefore allowing us to perform detailed assessments on the two remaining blades and associated assemblies. The system was recovered by *Sea Horse* on 7 March 2024.

6 Post-recovery assessment

Following recovery, a full mechanical breakdown of the system was carried out to investigate its health. This involved cleaning the system to identify superficial problems, investigations to identify factors contributing to the blade losses, and breakdown of the bearing pack to review the condition of the bearings and seals. An assessment of corrosion, biofouling, and biofouling mitigation techniques was also performed. The results presented in this section are limited to components critical to system performance (e.g., the bearings and housings) or unanticipated problems. A more detailed summary of other findings and supporting pictures are included in the supplemental material.

6.1 Blade losses

Post-recovery analysis of the rotor was sufficient to constrain the mechanisms leading to the blade failures. There is evidence that these events were triggered by collisions (e.g., foreign objects observed in the acoustic imaging and collision sounds preceding the blade loss of the blade by 1–3 s). However, the condition of the rotor revealed that the system may have been primed for failure before the inferred collisions. Mechanical issues with the lower strut/hinge assemblies appear to be the root cause. On the two remaining blades, the set screws holding the pins in place on the lower struts had backed out and the pins had begun "walking" towards the leading edge of the blade. Some slop in the bushings, which were installed to avoid mixed-metal contact, had also developed, which we hypothesize occurred as the cyclic load rounded the through holes in the hinges, allowing the pin to walk. We have not developed a working hypothesis to explain why this problem was only observed on the lower hinges.

The most logical explanation for the failure sequence is that, prior to each event, the pin had walked forward enough to be only partially seated in the hinge/bushing assembly. Consequently, the impulse from the debris collision may have ejected the pin. Damage to the interior of one bushing suggests that when this occurred the pin levered itself before falling out. Once freed from the lower strut, the blade swung up, rotating around the pin in the upper strut, cyclically loading the stress concentration at the hinge mounting point. After a short period, the blade rotated a full 180°, camming the titanium hinge against the strut, and levering the upper pin out of the strut (Fig. 13). Audio and post-recovery images reveal this was a catastrophic failure (i.e., no signs of fatigue were observed) but that some cyclic forcing on the upper joint occurred prior to the failure. Both struts with the failures have clear signs of damage to the anodized surface that are attributable to direct contact between the hinge and strut.

This mode of failure points to a design flaw that needs to be addressed in future systems. Poor tolerances in the 3D-

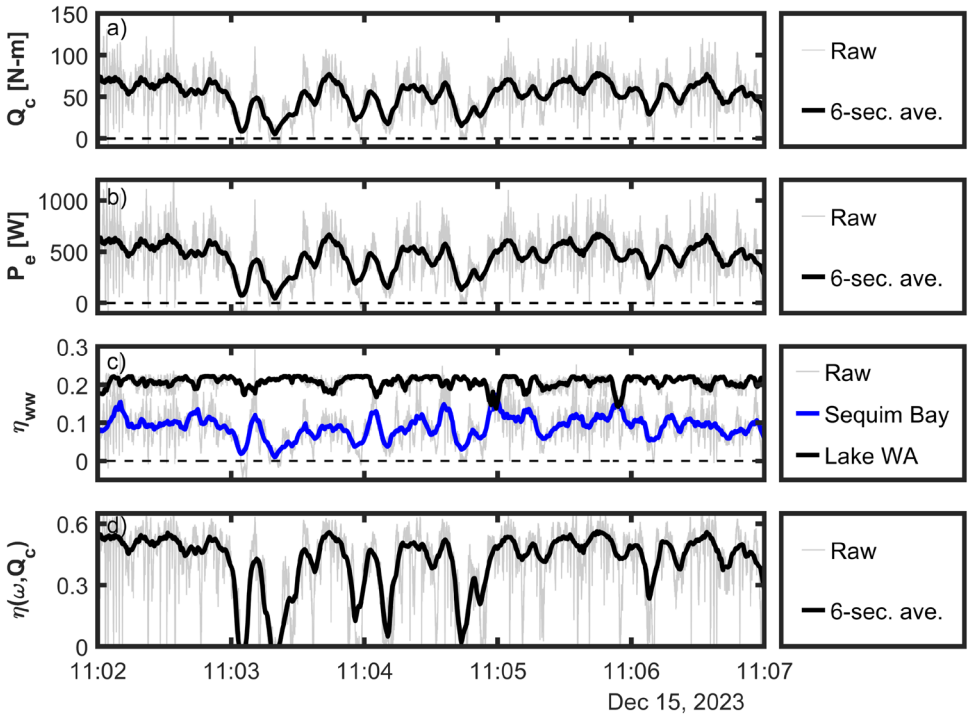

Fig. 12 Raw and 6-s averaged control torque (**a**) and electrical power (**b**). **c** Wire-to-water efficiencies as a function of time. The black line shows the expected η_{ww} based on the vessel-based measurements (Fig. 6) given the averaged inflow velocities and rotor speeds (Fig. 11a–b). The blue line shows the wire-to-wire efficiencies calculated from the electrical power and inflow velocities. **d** Estimates of PTO efficiency interpolated from the dynamometry data for the measured rotor speed and control torque after accounting for frictional losses (Fig. 5a). All subplots correspond to the same time periods in Figs. 10 and 11. The differences between the lines in **c** are attributed to a combination of biofouling, operational inefficiencies, and the spanwise variations in λ across the blades due to shear in the water column

printed titanium hinges, despite post-machining the parts, may have attributed to this failure by allowing some wobble under load. The design and layup of the composite blades to reduce stress concentrations at the hinge is also complicated. A redesign of this entire system should include a more robust mechanism to retain fasteners and could decrease manufacturing costs.

6.2 Bearing pack and driveline

The bearing pack was deconstructed and all components including the seals, bearings, shaft, and oil were investigated. Throughout the deployment the rotor completed rotated through more approximately 3.4 million revolutions, or greater than 1600 km of linear travel at the sealing surfaces. When the system was recovered, the exclusionary v-seal was found to have been displaced from the installation location. This is attributed to kelp that wrapped around the shaft early in the deployment and remained there throughout. This allowed sediment (sand) to accumulate above the upper lip seal, but no unexpected particulate was found between the seals or in the bearings. The upper lip seal had some wear we attribute to this sediment accumulation, but the primary sealing surface was in good condition. We estimate that less than 10 mL of water had entered through the upper lip seal and that no additional oil had been lost from the bearing pack or pressure compensator. The lower lip seal was found to be in good condition and no water had intruded into the bearing pack. The ceramic sealing surface was measured with a dial indicator and revealed no apparent surface roughness associated with wear. Lastly, the bearing appeared in good condition with no clear signs of unanticipated wear. The oil drained from the bearing pack was discolored, likely due to wear of the seals. Lines of particulate were encountered on the magnetic coupling suggesting that ferrous "dust" worn from the bearings had accumulated on the surface of the magnetic coupling. However, no larger fragments of ferrous material indicative of more serious mechanical wear were found.

Overall, the seals, bearings, magnetic coupling, and oil were recovered in good condition. The most obvious path for improving this assembly is better seating and securing of the v-seal to exclude particulate from the bearing pack. While removing one of the two lip seals could reduce parasitic losses, given that some water intruded past the first seal, this would likely reduce survivability. Given that the seal on the generator in the PTO housing is not needed, and that losses attributed to it are comparable to those from the two lip seals combined (Fig. 4), the most effective way to improve performance without impacting survivability would be to remove it but both leave external seals in place.

6.3 Corrosion and biofouling

The biofouling observed on the Turbine Lander was generally consistent with a priori expectations. Design to avoid small cracks and protruding objects (e.g., fasteners) will ultimately reduce parasitic drag losses. Coating the blades with ClearSignal™ resulted in clean blades when recovered while

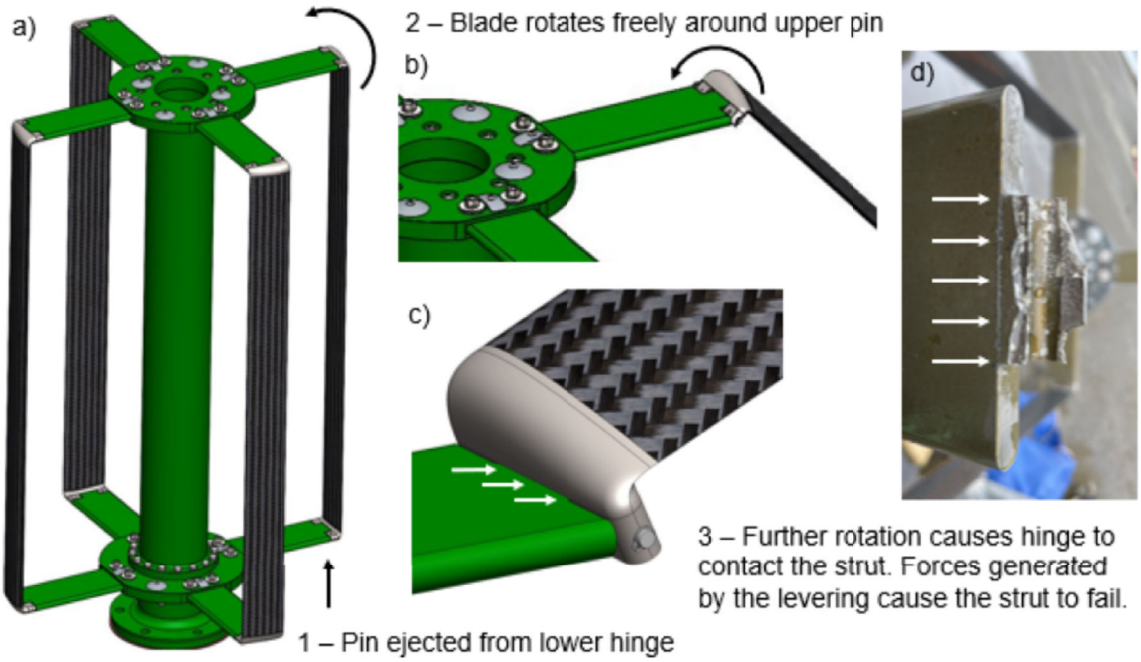

Fig. 13 **a** A drawing of the intact rotor with blades installed in their proper positions. **b** With the lower pin missing, the foil can rotate around the upper pin. **c** If the foil rotates greater than 90° degrees the titanium hinge eventually contacts the strut. **d** A picture of one strut with a missing foil. Note the damage to the anodized surface of the strut where the hinge makes contact in (white arrows in **c** and **d**) and that the material around the through hole has failed up and away from the strut as would be expected for the forces generated if the hinge contacting the strut. The supplemental material contains additional drawings of the hinge assembly and a picture of the damage to the other strut

the struts and shaft were colonized by barnacles and macroalgae. In future applications, we would likely coat additional components to further minimize fouling and associated drag losses. We were surprised by the amount of floating eelgrass that was caught in the narrow gaps in the pin/hinge assembly on the blades and how often drifting eelgrass and kelp wrapped itself around individual blades or the entire rotor. Limited review of camera data suggest that this plant matter was observed throughout the water column. Future quantitative analyses could assess whether significant differences in fouling potential exist throughout the water column by evaluating the observed concentrations of plant matter using stereo camera images like those obtained by the AMP. Such an analysis could inform decisions to adopt additional fouling mitigation strategies.

Little to no corrosion was identified while disassembling the system except for the ac housing, which had developed several large pits, suggesting inadequate grounding. This was later confirmed when the housing was reopened and a clear ground path to the seawater through the housing from an improperly grounded chassis was identified. We believe that we should have identified this during pre-deployment tank testing as the system likely had a weak ground fault that failed to trip the Littlefuse's ground fault current interrupt circuit. This oversight likely resulted from considerable turnover in core project staff due to project delays, a failure to develop and fully implement a robust test plan, and distractions driven by time constraints and the installation of the wrong anodes. The supplemental material contains several pictures of biofouling and corrosion on the recovered system.

7 Discussion

By most measures, the development and deployment of the Turbine Lander was a success, as indicated by sustained operation throughout its first 141-day deployment. Valuable lessons have been learned regarding the Turbine Lander's design that can be addressed in future work and are relevant to other hypothetical small-scale current energy systems. In addition, the benefits and uncertainties associated with transitioning a concept from the laboratory to the field are clear.

The Turbine Lander, and various aspects of its performance in situ, demonstrated numerous ways in which specific project constraints impact system design and performance. As designed, the best estimates for drag from the foundation and rotor's force coefficients resulted in a safety factor of approximately 1.5, and the use of additional weight risked violating the project constraints set by vessel over-the-side handling capabilities. This ultimately limited the

rotor's size and peak, phase-resolved force, which varies with rotor aspect ratio, blade count, rotation rate, and inflow velocity. The rotor shaft was sized to accommodate lifting the full system from the top of the rotor, while minimizing shaft deflection, accommodating the tapered roller bearing's radial force specifications, and meeting the maximum height requirements. The selected generator was ultimately chosen, despite being oversized for the system, to minimize thermal load management requirements. The redundant lip seals and exclusionary V-seal were chosen to minimize water and particulate intrusion into the bearing peak while the magnetic coupling was selected to eliminate the risk of water intrusion into the generator housing. Rotor geometry was optimized to maximize energy captured from the expected probability distribution of inflow conditions, subject to the maximum allowable moment created by the rotor on the foundation, and the maximum torque that could be transmitted through the magnetic coupling. With the information now available, we believe that the decisions made during the design process were generally good, but that with the benefit of hindsight, there is room for improvement.

The Turbine Lander was designed with four blades. This was selected not to optimize power production, but to reduce peak-to-average forces and minimize torque reversals under speed control. A two-bladed rotor could achieve higher time-averaged C_P values but at the cost of increased thrust loads, which would push the system closer to overturning under design conditions. While a four-bladed design may decrease the performance, the operational benefits were made clear by an increase in platform vibration measured by the AMP's inertial measurement unit following both blade loss events. An unforeseen benefit of the four-bladed geometry was the system's ability to continue operating and generating power following blade loss, meaning that the higher blade count provided a degree of unanticipated redundancy. Given these trade-offs, the four-bladed design is one we would choose to adopt again in future deployments. An additional benefit of the four-bladed rotor, discussed in greater detail in the supplemental material, is that it results in smaller variations in control torque throughout the cycle compared to a two-bladed rotor. These torques are associated with lower winding currents and therefore smaller resistive losses in the windings that would otherwise increase generator temperature. In fact, this temperature increase was observed following the blade losses events (see supplemental material). With the current design, there was no need to manage thermal loads, but this would not necessarily be true if a combination of a smaller generator, a larger rotor, and fewer blades had been selected.

Inefficiencies and hotel loads are inherent to any system but are particularly challenging for systems with power generation levels $<$ 1 kW. Take, for example, a hypothetical small rotor (1 m^2) with a cut-in speed of 1 m/s. The available kinetic power at that speed is approximately 500 W. Assuming a C_P of 0.3 at optimal tip-speed ratio, this means approximately 150 W of mechanical power is delivered to the PTO. Without increasing the rotor size, this constrains acceptable losses in the system. Short of increasing the C_P, which may be difficult as the current C_P appears reasonably high for a straight-bladed rotor in unconstrained flows, the avenues for decreasing losses are the generator, bearings, seals, and biofouling reduction (e.g., preventing eel grass build up at the rotor periphery). In addition, further streamlining to reduce hydrodynamic losses from the physical structure (shaft and struts) could improve the efficiency (Bachant et al. 2016; Strom et al. 2018).

While many options for improving the Turbine Lander efficiency exist, the clearest ways to reduce losses, such as removing the redundant seals or reducing the cross-section geometry of components, would come at the cost of long-term survivability. The seals and current power electronics are good examples. Multiple seals protect the bearing packs and laboratory analysis of their losses suggests that each lip seal results in losses on the order of 20–40 W over the operational conditions of the rotor. If the system were larger and regularly generated 1 kW of power, this loss would be relatively small, but at currents on the lower end of operating conditions, these losses increase the cut-in speed and represent a considerable reduction to the mechanical power delivered to the generator. A smaller shaft diameter and correspondingly small seals could mitigate these losses, but would need to be balanced against the need to minimize shaft deflection and maintain adequate factors of safety within the bearing pack.

The analytical estimates of the viscous losses within the bearing peak suggests that they are relatively small compared to the other systems losses. Nonetheless, an alternative biodegradable oil with a viscosity 50% lower is available. Our estimates suggest this might reduce losses by on the order of 10–15 W. While small, overcoming even minor inefficiencies is a necessity for systems seeking to generate small amounts of power with appropriately sized marine energy converters.

Similarly, commercial-off-the-shelf power electronics designed for industrial automation have high hotel loads when compared to power generated over a tidal cycle. While insignificant in many contexts, the constant consumption of many tens of watts is unacceptably high for small-scale generation. The next step for this system is to move to alternative power electronics. We have been exploring the use of the custom components from the MBARI-WEC (Hamilton et al. 2021), which were custom designed for small-scale wave energy converters. Initial estimates suggest that this could reduce hotel loads tens of watts, but at the cost of a reduction in capabilities relative to the Siemens equipment. Similarly, we are also working to integrate a suitable battery with the system. Integrating battery management systems with minimal hotel loads is an important consideration. As shown here,

given the performance of the system and inflow conditions, an energy storage system must be capable of accommodating rapid charge/discharge cycles, particularly if power input to the rotator is periodically required within each cycle (e.g., speed control near cut-in conditions). This, coupled with general safety concerns, restricts the pool of candidate battery chemistries.

Size, efficiency, and serviceability often conflict with design goals. In this case, water-lubricated bearings would avoid the use of redundant lips seals, but analysis showed that this would have required an increase in overall system height that would violate project constraints. The short-term implications of a seal failure are unclear, but the long-term implications (particulates and corrosion) would be problematic. There is no perfect solution to this problem and the "correct" balance depends on desired outcomes. Higher power output (fewer losses) with shorter deployments or regular maintenance intervals may be preferred in some cases while lower levels of power generation and greater survivability may be preferable at other times. Establishing project objectives and acceptable trade-offs is critical to narrowing the number of variables that must be balanced.

The Turbine Lander did not perform as well in Sequim Bay as it did in vessel-based measurements. This is less indicative of a flaw in our laboratory-to-field development than specific in situ conditions that could not have been discovered through additional pre-deployment testing. However, these performance challenges could have been predicted based on a site-specific resources assessment. Improved inflow measurements and improved controls algorithms that can more rapidly respond to inflow conditions would likely yield considerable performance improvements. Given that the rotor regularly stalled under torque control except during strong currents, minimizing system losses and redesigning the rotor and foils to produce higher torque could be beneficial. Regardless, if inflow conditions are informing system controls, more robust inflow measurements would be beneficial. This will ultimately be challenging at sites with rapidly varying inflow given that, by the time velocity data has been sampled, processed, and averaged, the flow incident on the rotor may have changed. While feed-forward controls are appealing in principle, implementing them at this scale would be difficult. The size of the rotor compounds this problem, as turbulent length scales that can engulf the rotor and material affect power production have a timescale on the order of 1 s in currents of 1 m/s. Recognizing this limitation, we would approach this problem by maximizing the sampling and attempting constant speed control using moving averages on the order of five seconds. With a sampling rate of 8 Hz, even after removing suspect pings in quality control, this would be sufficient to reduce Doppler noise and establish a robust measurement of the inflow. The result would still be a lagging indicator of the inflow, but given the rapid changes observed in Sequim Bay would likely push the tip-speed-ratio closer to the optimal value. An alternative approach would be to pursue a rotor geometry with a lower, broader C_P maximum (e.g., lower solidity rotor). While velocity fluctuations would still cause fluctuations in power output, these would be less pronounced if not also amplified by substantial changes in C_P.

In addition to general inflow conditions, temporary biofouling of the foils from plant matter in the water column poses a significant operational challenge. While fouled power production will inherently be reduced and fouling is likely to pose further limitations on control strategies as a heavily fouled rotor would be more likely to stall when operated under torque control. It is difficult to evaluate how much of the observed fouling is directly attributed to high levels of suspended plant matter at the specific site versus the general challenges associated with fouling on a vertical-axis cross-flow turbine in coastal environments.

The vertical shear observed in situ also has significant implications for power generation. Decreases in mean inflow conditions on the order of 10–20% were regularly measured across the rotor height (see supplemental material). Maintaining an optimized tip-speed ratio under strong shear with turbulence is challenging (Fig. 11), but is necessary for optimizing the performance of systems deployed near the seabed. While locating the rotor higher in the water column would reduce this impact, that cannot be easily achieved under the same project constraints and it would also increase conflict with vessel traffic in the area.

Increasing the size of the rotor to augment power generation will require care with regards to the overturning moment, magnetic coupling torque limit, and bearing loads, but preliminary analyses based on the data presented here suggest a 10% increase in swept area, coupled with a change in aspect ratio to make the rotor shorter and wider is achievable within existing constraints. A wider rotor, with optimal preset pitch angles, is expected to increase the torque production while reducing the shaft speed and associated torque losses from the seals. It is difficult to the predict gains associated with adjusting the present pitch angle across the operating space of the rotor, but results discussed by Hunt et al. (2024) suggest that a preset pitch angle of $-6°$ would maximize power production and that the $-9°$ preset pitch may have reduced cycle-averaged performance a few percent. With these changes the system's mechanical efficiency would be expected to increase and operate at more favorable PTO efficiency. The remaining system changes are generally expected to yield only modest performance improvements. However, in aggregate, if this set of improvements yields increases in power generation of only a few 10 s of watts over the broad range of inflow conditions, this would be meaningful when integrated over long periods.

8 Conclusions

The Turbine Lander, a small (1 m^2 swept area) vertical-axis, cross-flow turbine on a gravity foundation, was designed and deployed in a laboratory-to-field effort. Before in situ deployment, the system was characterized through dynamometry and vessel-based testing aboard a research vessel. During its 141-day deployment in Sequim Bay, WA, the system operated with 90%+ system up-time with the rotor operating for more than 960 h. The deployment site is characterized by shallow (< 10 m depth) water with moderate mixed semi-diurnal tides in which currents exceed 1 m/s approximately 40% of the time. In situ performance was lower than observed in vessel-based testing, attributable to a combination of biofouling and complex inflow conditions coupled with inadequate control response times. The deployment demonstrated the robust design of the Turbine Lander, as it was recovered in relatively good condition and continued to produce power even after two blade loss events. Post-deployment assessments, coupled with lab-based characterization, suggests improved power generation and survivability with relatively modest redesign tasks that minimize losses and modifications to the rotor.

Supplementary Information The online version contains supplementary material available at https://doi.org/10.1007/s40722-025-00411-y.

Acknowledgements This work was sponsored by Naval Facilities Engineering Command (NAVFAC) under Naval Sea Systems Command contract N00024-20-F8708. Additional engineers and graduate students at the University of Washington that contributed to early design decisions, conceptualization, and other engineering activities include Andy Stewart, Ben Strom, Tim McGinnis, Cassie Riel, Carl Stringer, Aidan Hunt, Greg Talpey, and Gemma Calandra. The efforts of Cam Fisher and Deb McKay were critical to acquiring project permissions. We also thank PNNL staff, particularly John Vavrinec, for field and operational support. It is difficult to imagine carrying out similar work without the efforts of APL's administrative staff, particularly Larry Joireman, Kasey Gausnell, and Autumn Salazar. We would also like to thank Paul Bieker for valuable discussions regarding the fabrication of the rotor blades.

Data availability Processed data from this paper is available at https://datadryad.org/dataset/doi:10.5061/dryad.d51c5b0dq and additional data products can be made available upon request.

References

Bachant P, Wosnik M (2016) Effects of Reynolds number on the energy conversion and near-wake dynamics of a high solidity vertical-axis cross-flow turbine. Energies 9(2):1–18

Bachant P, Wosnik M, Gunawan B, Neary VS, Roh M-I (2016) Experimental study of a reference model vertical-axis cross-flow turbine. PLoS ONE 11(9):1–20

Bhutta MMA, Hayat N, Farooq AU, Ali Z, Jamil SR, Hussain Z (2012) Vertical axis wind turbine—a review of various configurations and design techniques. Renew Sustain Energy Rev 16(4):1926–1939

Brusca S, Lanzafame R, Messina M (2014) Design of a vertical-axis wind turbine: how the aspect ratio affects the turbine's performance. Int J Energy Environ Eng 5:333–340

Castelli MR, Benini E (2011) Effect of blade inclination angle on a Darrieus wind turbine. J Turbomach 134(3):031016

Cavagnaro RJ, Copping AE, Green R, Greene D, Jenne S, Rose D, Overhus D (2020) Powering the blue economy: progress exploring marine renewable energy integration with ocean observations. Mar Technol Soc J 54(6):114–125

Cavagnaro RJ, Polagye B (2016) Field performance assessment of a hydrokinetic turbine. Int J Mar Energy 14:125–142

Copping A, Hemery L (eds) (2020) OES-environmental 2020 state of the science report: environmental effects of marine renewable energy development around the world. Pacific Northwest National Laboratory (PNNL), USA. https://doi.org/10.2172/1632878

Dillon T, Maurer B, Lawson M, Jenne DS, Manalang D, Baca E, Polagye B (2022) Cost-optimal wave-powered persistent oceanographic observation. Renew Energy 181:504–521

Druault P, Gaurier B, Germain G (2022) Spatial integration effect on velocity spectrum: towards an interpretation of the- 11/3 power law observed in the spectra of turbine outputs. Renew Energy 181:1062–1080

Forbush D, Cavagnaro RJ, Donegan J, McEntee J, Polagye B (2017) Multi-mode evaluation of power-maximizing cross-flow turbine controllers. Int J Mar Energy 20:80–96

Garavelli L, Hemery L, Rose D, Farr H, Whiting J, Copping A (2024) 2024 State of the science report—Chapter 3: Marine renewable energy: stressor–receptor interactions. Pacific Northwest National Laboratory (PNNL). https://doi.org/10.2172/2438589

Goring D, Nikora V (2002) Despiking acoustic Doppler velocimeter data. J Hydraul Eng 128:117–126

Hamilton A, Cazenave F, Forbush D, Coe R, Bacelli G (2021) The MBARI-WEC: a power source for ocean sensing. J Ocean Eng Mar Energy 7:189–200

Hand B, Kelly G, Cashman A (2021) Aerodynamic design and performance parameters of a lift-type vertical axis wind turbine: a comprehensive review. Renew Sustain Energy Rev 139:110699

Harding S, Hall K, Vavrinec J, Harker-Klimes G, Richmond M (2016) Field characterization of Triton tidal site: vessel-mounted ADCP survey of Sequim Bay inlet. Technical report, Report No. PNNL-25284 (Pacific Northwest National Laboratory, Richland, WA)

Hunt A, Strom B, Talpey G, Ross H, Scherl I, Brunton S, Wosnik M, Polagye B (2024) An experimental evaluation of the interplay between geometry and scale on cross-flow turbine performance. Renew Systain Energy Rev 206:114848

Li Q, Maeda T, Kamada Y, Murata J, Furukawa K, Yamamoto M (2015) Effect of number of blades on aerodynamic forces on a straight-bladed vertical axis wind turbine. Energy 90:784–795

Marsh P, Ranmuthugala D, Penesis I, Thomas G (2015) Numerical investigation of the influence of blade helicity on the performance characteristics of vertical axis tidal turbines. Renew Energy 81:926–935

Medina OD, Schmitt FG, Calif R, Germain G, Gaurier B (2017) Turbulence analysis and multiscale correlations between synchronized

flow velocity and marine turbine power production. Renew Energy 112:314–327
Miller MA, Duvvuri S, Brownstein I, Lee M, Dabiri JO, Hultmark M (2018) Vertical-axis wind turbine experiments at full dynamic similarity. J Fluid Mech 844:707–720
Pao LY, Johnson KE (2011) Control of wind turbines. IEEE Control Syst Mag 31(2):44–62
Polagye B, Joslin J, Murphy P, Cotter E, Scott M, Gibbs P, Bassett C, Stewart A (2020) Adaptable Monitoring Package development and deployment: lessons learned for integrated instrumentation at marine energy sites. J Mar Sci Eng 8(553):1–28
Polagye B, Thomson J (2013) Tidal energy resource characterization: methodology and field study in Admiralty Inlet, Puget Sound, US. Proc Inst Mech Eng Part A: J Power Energy 227:352
Polagye BL, Strom B, Ross H, Forbush DD, Cavagnaro RJ (2019) Comparison of cross-flow turbine performance under torque-regulated and speed-regulated control. J Renew Sustain Energy 11(4):044501
Rezaeiha A, Montazeri H, Blocken B (2018) Towards optimal aerodynamic design of vertical axis wind turbines: impact of solidity and number of blades. Energy 165:1129–1148
Sentchev A, Thiébaut M, Schmitt FG (2020) Impact of turbulence on power production by a free-stream tidal turbine in real sea conditions. Renew Energy 147:1932–1940
Shiono M, Suzuki K, Kiho S (2002) Output characteristics of Darrieus water turbine with helical blades for tidal current generations. In: ISOPE international ocean and polar engineering conference. ISOPE, Kitakyushu, Japan, pp ISOPE–I
Stringer C, Polagye B (2020) Implications of biofouling on cross-flow turbine performance. SN Appl Sci 2:464. https://doi.org/10.1007/s42452-020-2286-2
Strom B, Brunton S, Polagye B (2017) Intracycle angular velocity control of cross-flow turbines. Nat Energy 2:17103
Strom B, Johnson N, Polagye B (2018) Impact of blade mounting structures on cross-flow turbine performance. J Renew Sustain Energy 10(3):034504
Taylor G (1938) The spectrum of turbulence. Proc R Soc Lond 164:476–490
Thomson J, Polagye B, Durgesh V, Richmond M (2012) Measurements of turbulence at two tidal energy sites in Puget Sound, WA (USA). J Ocean Eng 37:363–374
Tobin N, Zhu H, Chamorro L (2015) Spectral behaviour of the turbulence-driven power fluctuations of wind turbines. J Turbul 16(9):832–846
Whitt C, Pearlman J, Polagye B, Caimi F, Muller-Karger F, Copping A, Spence H, Madhusudhana S, Kirkwood W, Grosjean L, Fiaz BM, Singh S, Singh S, Manalang D, Gupta AS, Maguer A, Buck JJH, Marouchos A, Atmanand MA, Venkatesan R, Narayanaswamy V, Testor P, Douglas E, de Halleux S, Khalsa SJ (2020) Future vision for autonomous ocean observations. Front Mar Sci 7:Article Number 697

PLOS One

RESEARCH ARTICLE

Observations of marine animal interactions with a small tidal turbine

Emma Cotter[1,2]*, **Christopher Bassett**[3], **Paul Murphy**[4], **Mitchell Scott**[4], **Alexa Runyan**[4], **Jood M. Almokharrak**[3], **Lucy G. Kao**[3], **Lillian M. Ovall**[4], **Suni A. McMillen**[3]

1 Coastal Sciences Division, Pacific Northwest National Laboratory, Sequim, Washington, United States of America, **2** Department of Mechanical Engineering, University of Washington, Seattle, Washington, United States of America, **3** Applied Physics Laboratory, University of Washington, Seattle, Washington, United States of America, **4** MarineSitu, Seattle, Washington, United States of America

* emma.cotter@pnnl.gov

OPEN ACCESS

Citation: Cotter E, Bassett C, Murphy P, Scott M, Runyan A, Almokharrak JM, et al. (2026) Observations of marine animal interactions with a small tidal turbine. PLoS One 21(1): e0338376. https://doi.org/10.1371/journal.pone.0338376

Editor: James K. Sheppard, San Diego Zoo Institute for Conservation Research, UNITED STATES OF AMERICA

Received: May 14, 2025

Accepted: November 20, 2025

Published: January 14, 2026

Peer Review History: PLOS recognizes the benefits of transparency in the peer review process; therefore, we enable the publication of all of the content of peer review and author responses alongside final, published articles. The editorial history of this article is available here: https://doi.org/10.1371/journal.pone.0338376

Abstract

The risk of collisions between animals and operating tidal turbines remains a concern in the scientific and regulatory communities. A sensor package including optical cameras was deployed to monitor animal interactions with a small-scale (1 m^2) cross-flow tidal turbine. The turbine was deployed in Washington State, USA for 141 days at a site with peak flow speeds of 2.5 m/s. We analyze optical camera imagery spanning 109 days of turbine operation. The analyzed images contain 1044 observations of fish, fish schools, seabirds, or seals in the vicinity of the turbine. No instances of collision with seabirds or seals were observed. Seabirds were only observed during daylight hours and while the turbine was stationary. Both seals and fish were observed during both day and night and while the turbine was stationary and rotating. Four fish were observed colliding with the moving turbine and in all but one case the animals swam away following the collision. Over the same period of time, over fifty times more fish (224 individual fish and 5 fish schools) were observed passing the moving turbine without collision. Fish encounters were likely under counted due to the difficulty in discerning small fish from plant matter in the water column. These observations represent the first optical camera imagery showing fish, bird, and marine mammal interactions with a tidal turbine in North America. In addition to quantitative and qualitative discussion of the implications of our observations for collision risk, we discuss lessons learned on sampling schemes and deployment of machine learning for detection of animals to inform future data collection strategies in future monitoring campaigns.

Introduction

In recent years, several projects have successfully demonstrated the feasibility of electrical power generation from tidal currents at grid scale [1]. At smaller scales, there is interest in leveraging analogous technologies for generating power at sea for

Data availability statement: Video data are available on the Marine and Hydrokinetic Data Repository here: https://mhkdr.openei.org/submissions/599. Metadata are included as Supporting information files.

Funding: The development and deployment of the Turbine Lander was sponsored by the Naval Facilities Engineering and Expeditionary Warfare Center (NAVFAC) under Naval Sea Systems Command contract N00024-20-F8708. Environmental monitoring data management was funded by the U.S. Department of Energy Water Power Technologies Office (WPTO) TEAMER program, and analysis of the collected data was funded by WPTO (award EE0007827). Development of the machine learning and data management tools used by MarineSitu for this work was supported by WPTO through the Small Business Innovation and Research project "Modular Instrumentation and Automated Data Processing for Marine Energy Monitoring" (Award DE-SC0021845). The funder provided support in the form of salaries for all authors, but did not have any additional role in the study design, data collection and analysis, decision to publish, or preparation of the manuscript. The specific roles of these authors are articulated in the 'author contributions' section.

Competing interests: Authors P.M., A.R., and L.O. are employed by MarineSitu or were employed by MarineSitu at the time of the study. This does not alter our adherence to PLOS One policies on sharing data and materials.

applications including scientific sampling, autonomous vehicle recharge, and aquaculture [2,3]. However, uncertainty surrounding the potential effects on marine animals remains a barrier to development of both grid- and small-scale tidal energy [4–7]. Potential effects include electromagnetic fields, underwater sound, physical effects on the surrounding environment (e.g., scour), and animal injury or mortality associated with collisions between animals and operating tidal turbines [6,7]. Notably, the limited volume of data to inform assessments of the risk of collision to fish, marine mammals, and diving seabirds has hindered tidal energy consenting processes globally.

Garavelli et al. [6] defines several terms that describe how animals might behave in the vicinity of a tidal turbine that will be used throughout this paper. An animal is deemed to have *avoided* a turbine if it responds to the presence of a turbine and moves away from it at a distance greater than 5 times the turbine diameter. Conversely, an animal *encounters* a turbine if it comes within a range of 5 turbine diameters. If an animal encounters a turbine, it might *evade* the turbine (i.e., change its behavior to avoid contact with the turbine) or experience *collision* (i.e., come in contact with a moving component of the turbine). While there have been no observations of collision between fish, marine mammals, or diving seabirds and tidal turbines reported in the literature to date, previous studies offer some insight into animal behavior around turbines.

In several studies, fish have been observed avoiding tidal turbines while they are operating [8–11], and evasion behavior by those fish that do encounter a tidal turbine has also been observed [9,11–13]. Based on a mobile echosounder survey, Grippo et al. [8] observed a decrease in fish abundance within 140 m of a tidal turbine deployed in Cobscook Bay, Maine (USA) while it was operating (avoidance), and this decrease was not observed while the turbine was stationary. Both Bevelheimer et al. [13] and Viehman and Zydlewski [12] used acoustic cameras to monitor fish activity in the vicinity of tidal turbines, and both observed decreased fish presence while the turbine was operating (i.e., avoidance) as well as instances of evasion behavior. In a fish release study conducted in a river in Sweden, Bender et al. [10] used an acoustic camera to observe that brown trout (*Salmo trutta*) rarely approached a turbine, regardless of operational state, and Atlantic salmon (*Salmo salar*) maintained a greater distance from the turbine while it was rotating. Similarly, Hammar et al. [11] used optical cameras to monitor a small tidal turbine, and observed fewer fish in the area when the turbine was operating (avoidance) as well as evasion behavior by several species that did encounter the turbine. Finally, in 4,000 hours of data recorded by motion-activated optical cameras mounted on a tidal turbine in Bluemull Sound (UK), 28 hours of which were acquired while the turbine was operating, Smith [9] observed fewer saithe (*Pollachius virens*) around the turbine during strong currents, and reported five instances of fish evading the moving turbine blades. No instances of fish passing through the rotor's swept area were reported.

Due to the relatively low abundance of marine mammals compared to fish, there have been fewer observations of marine mammal behavior around tidal turbines. Harbor seals (*Phoca vitulina*) were observed in the vicinity of the tidal turbine monitored in Smith [9], but they were rare (only 10 instances observed) and were never

observed when the turbine was operating. Using an array of hydrophones mounted to the base of a turbine deployed in Pentland Firth, UK, Gillespie et al. [14] found that harbor porpoises (*Phocoena phocoena*) that encountered a turbine effectively evaded the turbine blades, and only a single porpoise passed through the swept area (while the turbine was stationary) during 451 days of monitoring. Further analysis of the same data in Palmer et al. [15] indicates that harbor porpoises also avoided the turbine area while it was operating. Avoidance of turbines has also been demonstrated for harbor seals. At the same site as Gillespie et al. [14] and Palmer et al. [15], a multibeam sonar was used to study seal presence within tens of meters from a turbine, and found that fewer seals were present at flow speeds above the 1.2 m/s threshold for turbine operation. This number decreased even further when the turbine was operational [16]. Onoufriou et al. [17] observed a decrease in harbor seal abundance within 2 km of an array of tidal turbines while they were operating, and Hastie et al. [18] demonstrated an 11-41% reduction in seal presence near an acoustic projector simulating the sound of an operational tidal turbine.

Collision with turbines also presents a risk to diving seabirds, but there have been limited observations of seabirds around tidal turbines to date. Smith [9] observed European shag (*Phalacrocorax aristotelis*) and black guillemots (*Cepphus grylle*) in the vicinity of the monitored turbine. As with seals, these observations were rare (15 instances observed) and seabirds were only observed during periods when the turbine was not operating. Others have studied seabird habitat use in areas suitable for tidal energy development [19–21], but, to our knowledge, the only direct observations of seabird interactions with an operational tidal turbine to date are those described in Smith [9].

While existing studies indicate that many animals avoid the area surrounding operational tidal turbines, and some animals that do encounter tidal turbines are capable of evasion, the risk of collision remains a key concern. Further, most studies to date have investigated animal avoidance at larger scales, but there have been few reports of fine-scale evasion behavior in the immediate vicinity of a tidal turbine. In this work, we present observations made over several months of harbor seal, seabird, and fish encounters with a small tidal turbine designed to provide power for at-sea operations. Throughout the turbine deployment, sampling strategies were adjusted based on observations in the collected data and lessons learned. While this limits our ability to quantitatively evaluate animal encounter rates or long-term trends in animal presence, analysis of collected data provides insight into how different species behave in the presence of an operational tidal turbine. We also discuss lessons learned for effective data collection, automated data processing, and analysis to inform future monitoring campaigns.

Methods

Turbine lander

The Turbine Lander (Fig 1) is a marine energy converter system that includes a vertical axis, cross-flow turbine on a gravity foundation. The four-bladed rotor is 1.19 m tall and 0.85 m in diameter with blade chord lengths of 10.2 cm. The individual blades have a wet weight of approximately 1.5 kg and the turbine's moment of inertia is estimated to be approximately 2 kg m^2. When deployed, the bottom and top of the rotor are approximately 1.5 and 2.7 m above the seabed, respectively. While small, the system is considered full-scale as the target application is to provide modest amounts of power at sea where no cabled infrastructure exists. Environmental monitoring equipment (the Adaptable Monitoring Package) was distributed on several areas on the foundation.

During the deployment analyzed in this study, the turbine was primarily operated in speed control such that it maintained a constant tip-speed ratio near 2 (i.e., the tangential velocities of the rotor blades were approximately twice as fast as the inflow current speed). The minimum flow speed for turbine operation ("cut-in speed") was adjusted between 0.9 m/s and 1.0 m/s at different times throughout the deployment. Below the cut-in speed, the turbine rotor was programmed to be stationary. More information about the Turbine Lander's design and operation is can be found in Bassett et al. [22].

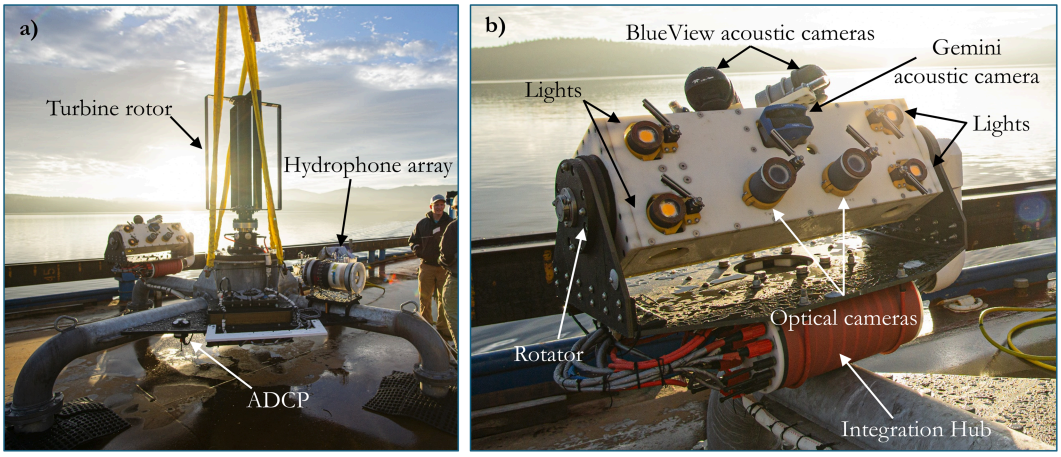

Fig 1. **Turbine and monitoring equipment**. (a) The Turbine Lander prepared for deployment. (b) The Adaptable Monitoring Package instrument head with sensors annotated. Photo credit: Abigale Snortland.

https://doi.org/10.1371/journal.pone.0338376.g001

Test site

The Turbine Lander was deployed on 18 October 2023 in the ~250 m wide tidal channel at the entrance to Sequim Bay, Washington, USA at 46° 4.761'N, 123° 2.589'W, adjacent to Pacific Northwest National Laboratory's (PNNL) Marine and Coastal Research Laboratory (Fig 2). Bathymetric data in Fig 2 were collected by C & C Technologies Survey Services and provided by Pacific Northwest National Laboratory. The deployment location is approximately 8 m deep at mean lower low water (MLLW) and characterized by mixed semi-diurnal tides that result in peak tidal velocities of approximately 2.5 m/s. The system was recovered on 7 March 2024, but the turbine was not operated after 11 February due to the

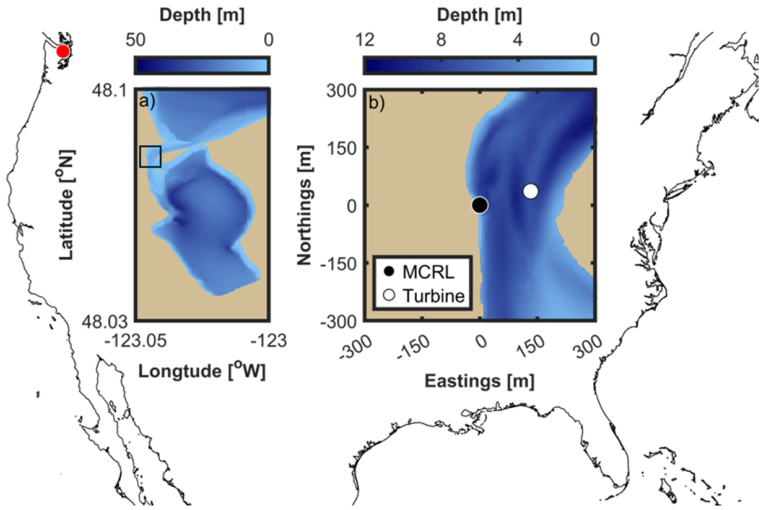

Fig 2. **Study site**. The background outlines central North America with the test site at the inlet to Sequim Bay, Washington (USA) highlighted by the red dot (upper right corner). (a) The bathymetry (MLLW) of Sequim Bay. The box at the constriction at the north end of the bay highlights the inlet, which is shown in (b). (b) The bathymetry of the inlet to Sequim Bay showing the locations of the PNNL Marine and Coastal Research Laboratory (MCRL) dock and the deployment location of the Turbine Lander and the Adaptable Monitoring Package (AMP).

https://doi.org/10.1371/journal.pone.0338376.g002

failure of two blades (see [22] for details). The system was cabled to shore, where shore-side computers handled environmental data acquisition and turbine control.

Sequim Bay is a habitat for fish, marine mammals, and seabirds [23]. Harbor seals are frequently observed in the area. Since 2021, more than 15 species of diving seabirds have been reported in the vicinity of PNNL-Sequim, including several species of waterfowl, three species of cormorant, and two species of auk [23]. Several forage fish species including Pacific herring (*Clupea pallasi*), surf smelt (*Hypomesus pretiosus*), and Pacific sand lance (*Ammodytes personatus*) are known to spawn in Sequim Bay, and are the most abundant forage fish species in the region [24,25]. Multiple species of salmonids and rockfish are also found in the area, with several species listed as endangered or threatened [23]. Among other species commonly observed in the area are sculpin, snailfish, flatfish, and perch.

Adaptable monitoring package

An integrated sensor system, the Adaptable Monitoring Package (AMP), which is described in detail in Polagye et al. [26] and available commercially through MarineSitu, was installed on one leg of the Turbine Lander platform to monitor animal activity in the vicinity of the turbine (Fig 1). The AMP included an optical camera system and three acoustic cameras. The optical camera system consisted of two Allied Vision Technologies Manta G-507b board level cameras in custom housings with KOWA lenses (LM5JC1M, 82° field of view). Four custom-built strobe lights that contained Cree CXB 3590 white LEDs provided artificial illumination for the optical cameras. The acoustic cameras on the AMP included two Teledyne BlueViews (M900-2250) and a Tritech Gemini (720is). The BlueView acoustic cameras were both configured with a 10 m maximum range and the Gemini was configured with a 15 m maximum range. The BlueView acoustic cameras were operated in their higher frequency mode (2250 kHz). To facilitate imaging of animals both up and downstream of the turbine during both flood and ebb tides, the BlueViews were oriented perpendicular to each other such that their beams overlapped by approximately 45° at the rotor. The Gemini was oriented such that the rotor was centered in its field of view. The AMP software triggered acquisition of the acoustic images with short time delays (e.g., < 50 ms) to avoid crosstalk while minimizing elapsed time between images.

Optical and active acoustic sensors were mounted on a tilt motor such that the field of view of the sensors could pan up and down in the water column. Throughout the deployment, the orientation was occasionally shifted up or down during system health checks, but the full turbine rotor was maintained within the field of view except for these short manual interventions (no more than a few minutes). In addition to the sensors on the AMP, a small passive acoustic array consisting of four hydrophones (custom data acquisition, HTI 90-HF hydrophones) was installed on one leg of the foundation and an acoustic Doppler current profiler (ADCP; Nortek Signature1000) was installed on a mounting plate between two legs of the foundation to measure flow speeds.

In this study, we focus on data from the optical cameras. Data from the acoustic cameras are referred to for additional context, and data from the ADCP are used to evaluate trends in animal presence with tidal currents. A detailed description of the acoustic camera data can be found in Bassett and Cotter [27].

Optical camera datasets

Two optical camera data acquisition strategies were used during the deployment: 1) scheduled data acquisition, and 2) data acquisition when animals were predicted to be present by real-time detection models operating on either the optical camera or acoustic camera data. Data acquisition methods varied over the course of the deployment as collected data were reviewed and informed more optimal approaches. Lessons learned are discussed in detail in the Discussion section.

Scheduled data were either acquired on a user-specified duty cycle (e.g., 5 s every 1 min) at a high frame rate (20-24 Hz) or continuously at 1 Hz. The strobe lights were activated during duty cycle data acquisition, but not during

continuous data acquisition. Continuous optical camera data collection was never implemented at night when artificial illumination would have been required because of concerns that continuous operation of the strobe lights would influence animal behavior.

Detection models operated in real time on each image by the cameras. When the models predicted that an animal was present (i.e., detected an animal in the image), data from 5 s before and 5 s after the frame detected by the model were archived with a frame rate of at least 20 Hz. Additionally, strobe lights were activated for 2.5 s following each model detection. We call each archived window of data a "detected event".

Both optical camera and acoustic camera models were developed using MarineSitu's commercial license of the Ultralytics YOLO model [28] and developed using MarineSitu deployment software. Models were iteratively trained and redeployed as more images were acquired and annotated throughout the deployment. The optical camera detection model was trained to detect seals, diving seabirds, and fish, however it only reliably detected seals and diving seabirds, possibly due to the fact that large fish were infrequently observed and, in many cases, small fish appeared similar to drifting debris, especially at farther ranges from the cameras. Because illumination was not constant, optical camera models were only able to detect animals during daylight hours or when the strobe lights were illuminated on a duty cycle. When detection occurred at night during duty cycle acquisition, artificial illumination was activated after each frame in which the animal was detected (i.e., the detected event might be longer than the scheduled duty cycle window).

Acoustic camera detection models (only deployed after 1 February) were trained to detect seals and diving birds, but did not perform well. During some periods, the model was tuned too permissively such that nearly all detections were false positives resulting from detritus in the water column or reflections from the moving turbine (e.g., 34,287 detections on the night of 2 February). During other periods, the acoustic camera model was tuned too conservatively such that it did not capture most animals of interest (e.g. 64 detections on the night of 10 February). Despite this poor performance, optical camera data collected as a result of either correct or incorrect detections from the acoustic camera model are included in our analysis because they contained many interesting observations of animal behavior around the moving turbine at night, when our sampling was otherwise limited.

We analyzed all optical camera images collected during periods of continuous recording and all detected events from 1 November 2023 to 17 February 2024, five days after the turbine was shut down. Because data collection methods were varied, these data are broken into three distinct subsets for analysis, which are indicated in Fig 3 and are described in the subsequent paragraphs. The first two subsets are comprised of scheduled data collection (duty cycle and/or continuous acquisition), and the third subset is comprised of detected events. Table 1 provides an overview of the duration of data recorded in each data subset, including the total number of hours in the sampling period, the total number of hours in the sampling period when the turbine was operational, the total number of hours with optical camera data recorded at a frame rate of at least 1 Hz, and the total number of hours with optical camera data recorded at a frame rate of at least 1 Hz while the turbine was operational.

Data subset 1 consists of scheduled data collection from 1-8 November. Data were acquired continuously at a frame rate of 1 Hz during the day, and for 3 s every 1 min with artificial illumination at night. No data were collected on 17 November between 13:04 and 18:00 (local time) when the turbine and AMP were shut down for maintenance.

Data subset 2 consists of scheduled data collection between 25 January and 17 February. Data were collected at 1 Hz during daylight hours, and no scheduled data collection was employed at night. The turbine was no longer operating during the last 5.5 days of this review period (after 11 February at 4:30 local time), and no data were collected on 6 February from 9:21 to 14:18 (local time) during system maintenance. We note that during collection of both data subset 1 and data subset 2, occasional network interruptions resulted in lost frames (i.e., frame rate < 1 Hz).

Data subset 3 is comprised of all detected events from the automatic detection models from 1 November to 17 February. Detection models were disabled from 8-17 November, so no events captured in data subset 1 are contained in data subset 3. Conversely, detection models were operating in concert with continuous data acquisition in data subset 2, so

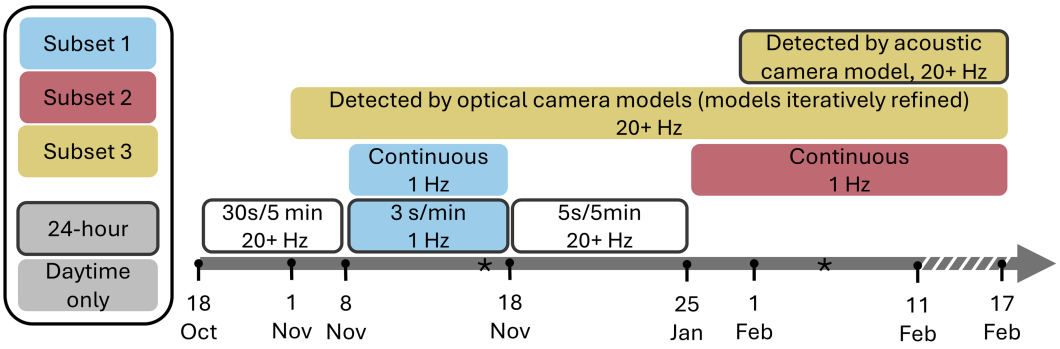

Fig 3. Timeline summarizing data collection. The three data subsets that were analyzed are indicated. Periods with a dark border include nighttime data, while periods without a dark border were only collected during daylight hours. Periods of data in white were not analyzed, and asterisks (*) indicate periods where the AMP was offline for up to 5 hours for system maintenance. The dashed portion of the timeline after 11 February indicates the period when the turbine was deployed, but not operating. Note that the timeline is not to scale.

https://doi.org/10.1371/journal.pone.0338376.g003

Table 1. Data summary. Summary of the data contained in each subset, including the total number of hours contained in each sampling window, the total number of hours in the sampling window when the turbine was operating, the total number of hours of recorded data at at least 1 Hz, and the total number of hours of data recorded at a frame rate of at least 1 Hz while the turbine was rotating.

	Total Hours	Total Hours with Turbine Operating	Hours Recorded	Hours Recorded with Turbine Rotating
Subset 1	240.0	88.8	81.5	8.0
Subset 2	552.0	126.3	208.9	28.6
Subset 3	2616.0	776.8	61.1	21.4

https://doi.org/10.1371/journal.pone.0338376.t001

events contained in data subset 2 that were automatically detected are also contained in data subset 3. However, only data subset 3 contains high frame rate recordings of these events.

Even though the automatic detection models did not effectively detect fish, many interesting observations of fish are included in data subset 3. These events were largely captured due to false positive detections by the detection models (e.g., the model detected a piece of kelp entrained on the turbine). We include these observations in this paper because they represent some of the first observations of fine-scale fish behavior around a moving tidal turbine. However, while our observations of fish offer insights into fish behavior around a moving tidal turbine, they cannot be used to quantitatively assess the number of fish that encountered the turbine or the probability of collision.

Data review and analysis

Every optical camera image included in data subsets 1, 2, and 3 was initially reviewed by at least one member of team of five human reviewers (authors C.B., J.A., L.K., L.O., and S.M.). We grouped observations into four classes for analysis: individual fish, fish schools, seabirds, and seals (harbor seals were the only observed species of marine mammal). Whenever one of the four classes was observed, the timestamps of the first and last images in which the animal or fish school was visible were logged as an event. During initial review, reviewers included any events containing ambiguous targets that could potentially be animals in the log. In some cases, an animal was not classifiable in an individual frame (e.g., edge of a flipper is the only part of a seal in view), but was classified based on observations in other images. Fish schools were logged as a single event when individual fish within the school were too numerous to reasonably count. With the exception of fish schools, two separate events were logged when two animals of interest were simultaneously detected, and if the same animal left the frame and then reentered, one event was logged. This required some subjective interpretation as seabirds and seals regularly left the frame and then reentered shortly thereafter. For seals, a threshold of 60 s was used to determine if a new event should be logged. The same threshold was used for seabirds unless it was

observed swimming to the surface and another dive was observed within the 60 s threshold (this would be logged as two events). Reviewers indicated whether each event was recorded during dark or light conditions, which was distinguished by whether or not artificial illumination was deemed necessary to observe the animal. This also required some subjectivity for events captured during dawn or twilight when light conditions were rapidly changing and artificial illumination was used but may not have been required to identify the animal. Initial annotation of events was conducted by five separate reviewers.

After initial annotation, each event was analyzed in detail by a single reviewer (C.B.). Events appearing in more than one data subset were consolidated such that they are represented in each subset in which they appeared, but the aggregated event counts presented in the Results section reflect only unique events. Taxonomic classification was performed to the lowest level possible for each animal, and qualitative observations of animal behavior were logged. These annotations are considered the final dataset that are discussed in the Results section and included in the Supplemental Data. Observations of fine-scale animal behavior, like evasion, were only possible for the events in data subset 3 due to the higher frame rate (20+ Hz). A more detailed description of this review process can be found in S4 Detailed Description of Human Review Process.

Lastly, concurrent acoustic camera data were reviewed for all events where animals were observed evading or colliding with the turbine. While the emphasis of this study is on the optical camera imagery, acoustic camera data were reviewed to determine if they provided additional context for these animal behaviors of interest.

After analysis of all annotated events, we evaluated trends in animal presence and behavior. Because fish were not automatically detected, our analysis of fish behavior is limited to qualitative observations. For seals and seabirds, which were detected by the real-time detection model, we analyze trends in animal presence with respect to flow speed, turbine operating state, and tidal elevation. Tidal elevation was measured by a tide gauge on the nearby research pier, and are referenced to the North American vertical datum of 1988 [29]. Flow speed was measured by the ADCP on the Turbine Lander, and was calculated as the 2-minute moving average at an elevation of 3.1 m above the seabed (approximately 40 cm above the top of the rotor). For each class, we determined the total number of events (n), the number observed when there was ambient light (n_{light}); the number observed when it was dark and artificial illumination was required (n_{dark}); the number observed when the turbine was rotating (n_{turb}); and the number observed when flow speeds exceeded the lowest turbine cut-in speed of 0.9 m/s (n_{cutin}). We note that n_{cutin} and n_{turb} differ because of tidal cycles when the turbine was not operational at the end of the deployment and one instance when the turbine was rotating during slack tide due to a communication failure with the ADCP.

Finally, we compared the trends in seal and bird observations in data subset 3 to those identified through human review of the continuously acquired data in subset 2 to assess model performance. Because the detection model was iteratively updated with newly acquired training data throughout the deployment, we cannot rigorously assess model performance or use the triggered events to quantitatively assess animal abundance or encounter rates. However, comparison with continuously acquired data offers some insight into whether the model reliably detected seals and seabirds.

Results

Review of the images in the three data subsets identified 1044 distinct events containing observations of fish, seals, or seabirds. While our analysis focuses on fish, seals, and seabirds due to regulatory interest, we note that kelp crabs (*Pugettia producta*), jellyfish, shrimp, euphausiids (krill), and sea slugs (order Nudibranchia) were also observed in the imagery. An overview of observed taxa, performed at the lowest level possible given the quality of the images, is included in S1 Species Table. The achieved level of taxonomic identification varied depending on ambient light, range to the animal, water clarity, and animal size. Species-level identification was straightforward for harbor seals, sometimes difficult for similar bird species, and typically not possible for small fishes. Water clarity varied throughout the deployment, which affected the ability to detect animals that were farther from the cameras than the turbine. In some conditions, the water

surface was visible (4+ m from the cameras), while at other times, the top of the turbine was not well defined despite being less than 2 m from the cameras.

An overview of the total number of events corresponding to each class in each data subset is included in Table 2. Fig 4 shows the distribution of events containing seals and seabirds in each data subset with respect to time of day, flow speed, and tidal elevation with the distribution of environmental conditions during all times with reviewed images in each data subset indicated for comparison. A representative time series of events from 2-8 February 2024 is shown in Fig 5. Among the patterns present in this time series are that bird detections were most common at high tides during daylight hours and that fish and seals were observed under a broad range of conditions. These trends are discussed in the subsequent sections and a full list of all annotated events, from all three data subsets, can be found in S2 Event Data. Below, we provide qualitative descriptions of the observations of each animal class. Videos of all fish collision and evasion events and representative bird and seal events are available online [30]. For a list of videos corresponding to each figure containing optical camera data, see S3 Videos.

Individual fish

The annotated events contained 524 unique instances of individual fish (342 had high frame rate data). While discrimination between species of fish was difficult, no listed threatened or endangered fish species known to occur in the area (e.g., rockfish, salmonids, or sturgeon) were observed and identified. We note, however, that distinguishing Pacific eulachon (*Thaleichthys pacificus*), whose Southern Distinct Population Segment is listed as threatened, from other forage fishes is difficult. Thus, we cannot unambiguously state that they were not observed.

Reviewers identified 229 events containing fish encountering the turbine while it was rotating (Table 2). We note that identification of individual small fish in the imagery was challenging, particularly when fish were moving passively with the flow during periods with high volumes of plant matter in the water column, and only events where a confident classification could be made are included in this count. Fig 6 shows representative examples of fish detected while the turbine was operating. During periods of sufficiently strong flow for the turbine to be rotating, nearly all observed fish were classified as unidentified forage fishes or perch-like species, which are relatively small (<25 cm). Only two larger fish were observed while the turbine was rotating, and both were swimming high in the water column above the rotor and could not be identified (Fig 6b, 6c). While the turbine was rotating, fish were most commonly observed moving passively with the

Table 2. Summary of all individual fish, fish schools, birds, and seals detected in data subsets 1, 2, and 3. Note that some events in data subset 2 are also contained in data subset 3.

	Subset 1 (81.5 hrs recorded)				
	n	n_{light}	n_{dark}	n_{turb}	n_{cutin}
Fish	129	29	100	77	76
Fish Sch.	11	8	3	2	2
Bird	12	12	0	0	0
Seal	7	0	7	1	0
	Subset 2 (208.9 hrs recorded)				
	n	n_{light}	n_{dark}	n_{turb}	n_{cutin}
Fish	109	109	–	2	2
Fish Sch.	0	0	–	0	0
Bird	195	195	–	0	2
Seal	12	12	–	0	0
	Subset 3 (61.1 hrs recorded)				
	n	n_{light}	n_{dark}	n_{turb}	n_{cutin}
Fish	342	65	277	162	175
Fish Sch.	8	1	7	3	5
Bird	294	294	0	0	1
Seal	84	36	48	8	7

https://doi.org/10.1371/journal.pone.0338376.t002

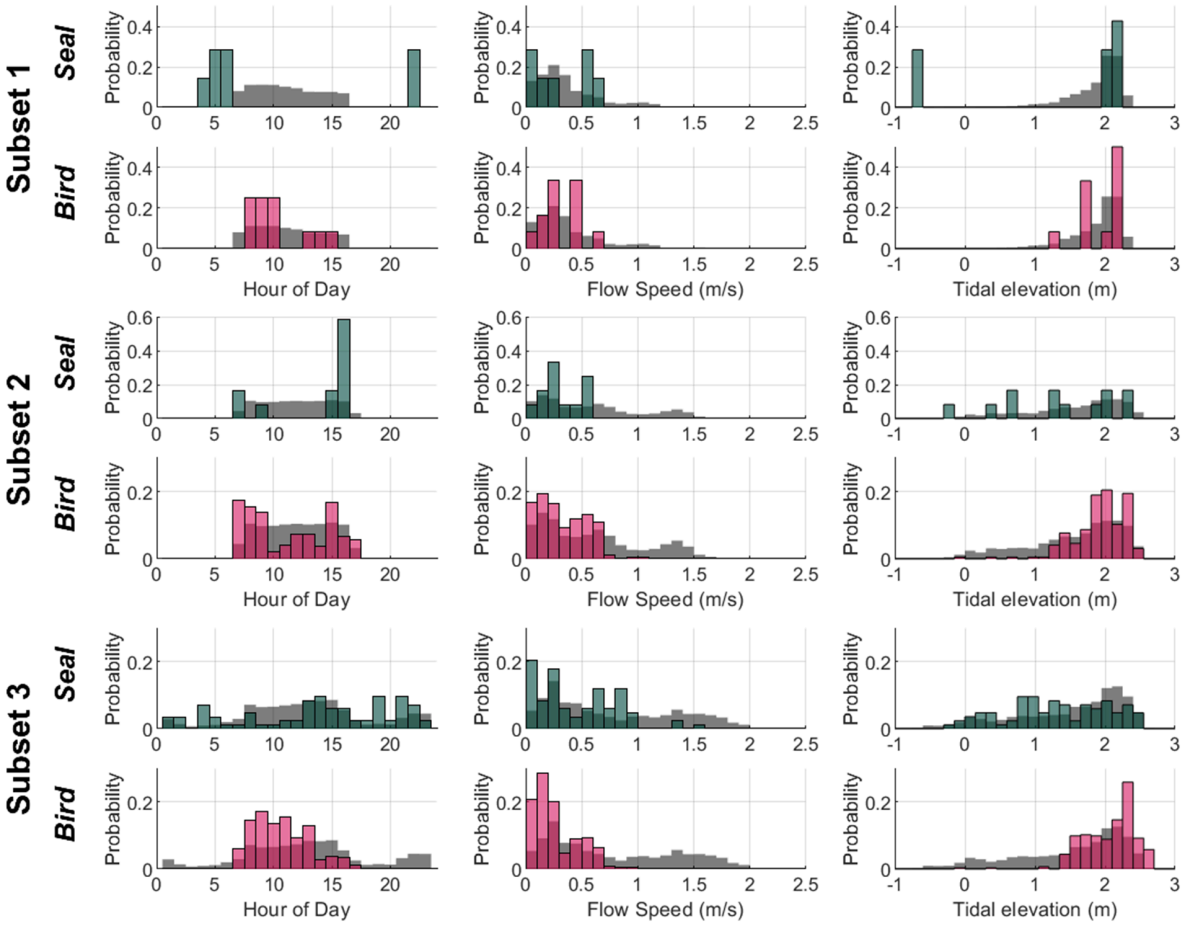

Fig 4. Distribution of seal and bird events. Distribution of events containing seals and seabirds in each data subset with respect to hour of day (local time), flow velocity, and tidal elevation (colored bars). Gray bars in the background of each histogram indicate the distribution of each environmental covariate throughout all images that were recorded and reviewed. Note that the y-axis scale differs between classes and data subsets.

https://doi.org/10.1371/journal.pone.0338376.g004

flow (e.g., Fig 6a, 6d), although examples of fish swimming against the current or roughly perpendicular to it were also observed. We observed four instances of fish colliding with the moving turbine blades (1.7% of total identified fish encounters with the moving turbine). In 50 events (21.7%), fish exhibited behavior consistent with evasion (i.e., when on course to collide with the turbine or enter the area swept by the moving turbine blades, they made an apparent change in trajectory). The remaining 175 fish that encountered the turbine while it was rotating passed without collision, but were not categorized as evasion because they did not exhibit a discernible change in trajectory within the field of view of the cameras. These counts exclude events classified as fish schools, in which additional examples of evasion, but not collision, occurred.

All four observed instances of collision with the moving turbine involved relatively small fish (less than approximately 20 cm long based on their size relative to the blade's chord length). In three of the four events, the fish were oriented normally in the water column and swam away after collision (i.e., no mortality). An example fish collision is shown in Fig 7. The flow speeds during these collision events were 1.0, 0.9, and 2.0 m/s (blade speeds of approximately 2, 1.8, and 4 m/s), respectively, and fish were observed both moving with and against the currents before collision. In the fourth event, the fish did not appear to be moving after the collision and sank towards the seafloor out of view (i.e., potential mortality).

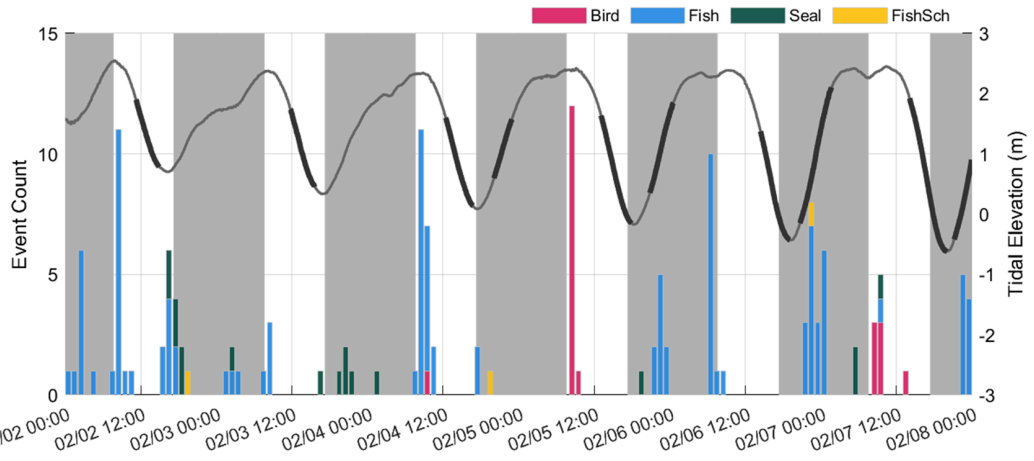

Fig 5. **Representative timeseries of events**. Number of events associated with each class per hour for a representative week of data. Events from both data subset 2 (continuous acquisition) and data subset 3 (detected events) are shown. Hours between sunset and sunrise are indicated in gray, and the tidal elevation is shown for reference. The darker regions of the tidal elevation time series indicate periods when the turbine was rotating.

https://doi.org/10.1371/journal.pone.0338376.g005

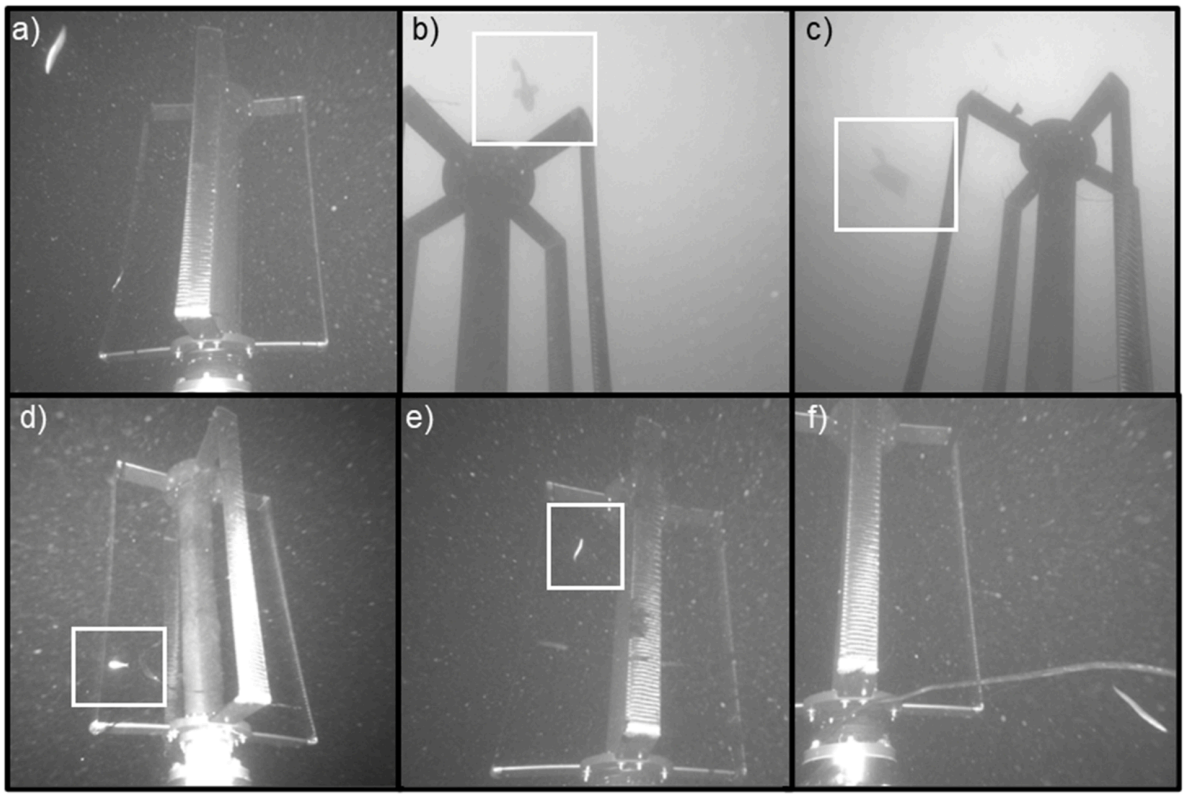

Fig 6. **Examples of individual fish when the turbine was rotating.** (a) Small fish drifting, head down, between AMP and rotor. (b) Large, unidentified fish swimming above rotor. (c) Flatfish drifting above moving rotor. (d) Perch-like species drifting with current between AMP and rotor. (e) Fish swimming within moving rotor. (f) Fish swimming away from rotor after collision.

https://doi.org/10.1371/journal.pone.0338376.g006

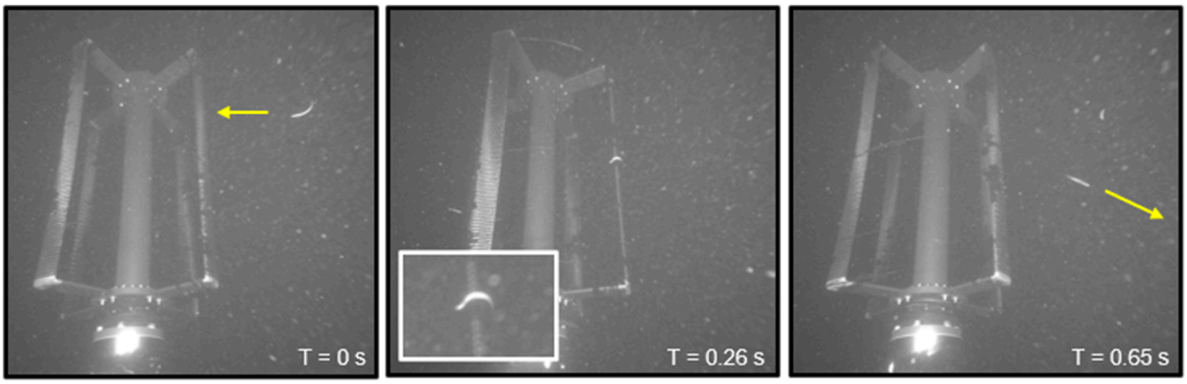

Fig 7. **Example of a collision between a fish and the turbine blades**. The yellow arrows approximate the direction the fish was moving in a given frame, and times are presented relative to the first frame. The inset in the middle frame shows a larger view of the collision seen on the blade on the right-hand side of the image.

https://doi.org/10.1371/journal.pone.0338376.g007

The flow speed during this event was 1.5 m/s, and the fish was swimming with the currents before the collision. We note that a fifth instance of fish collision was observed with the stationary turbine (inflow speed of 0.9 m/s). The fish was drifting passively, without moving, when it collided with the blade and then swam away. Review of the concurrent acoustic camera data revealed that prior to two of the collision events (one while the turbine was moving during 1.0 m/s currents, and one while the turbine was stationary), a seal had pursued the fish towards the turbine. In both events, the seal abandoned the pursuit and changed directions before entering the optical camera field of view.

Annotated imagery showing four of the 50 cases of observed evasion behavior by fish, and one of a seal, are shown in Fig 8. Like collision events, fish were observed moving both with and against the currents when they encountered the turbine before evasion. Four types of evasion behavior were observed: 1) swimming then changing trajectory to move around the turbine rotor, 2) diving towards the seafloor or swimming upwards to pass under or over the rotor, 3) swimming against the current to move away from the rotor, or 4) evading the turbine blades and entering and then exiting the turbine rotor without collision. Evasion of the moving turbine was observed at flow speeds ranging from 1-2.2 m/s. In two events, seals were observed in the same image sequence, and pursued the fish towards the turbine before the fish exhibited evasion behavior. Review of the acoustic camera data identified that two of these fish evasion events were related to seal/fish predator/prey interactions where the seal was beyond the optical camera field of view. Additionally, in one event, a small perch-like fish exhibited evasion behavior while the turbine was stationary (0.5 m/s flow speed). The fish was observed passively drifting towards the Turbine Lander, then suddenly swam down and under the rotor.

Fish schools

Nineteen total fish schools were recorded (Fig 9). Fish schools were observed both while the turbine was rotating and while it was stationary (Table 2). While the turbine was stationary, fish schools were observed dispersing and changing direction around the turbine rotor (e.g., Fig 9a, 9b). The five schools observed during turbine rotation were composed of unidentified small fish. In all five cases, the fish that encountered the turbine rotor effectively evaded it by swimming upstream and away from the rotor, ultimately passing between cameras and the turbine, or by diving down below the rotor (e.g., Fig 9d). Review of concurrent acoustic camera data indicated that the school shown in Fig 9d was considerably larger than was visible in the optical cameras and that most fish in the school avoided the rotor outside of the optical camera field of view. The individual fish associated with fish schools that evaded the rotor could not be readily counted and are therefore not included in the evasion/collision metrics presented for individual fish.

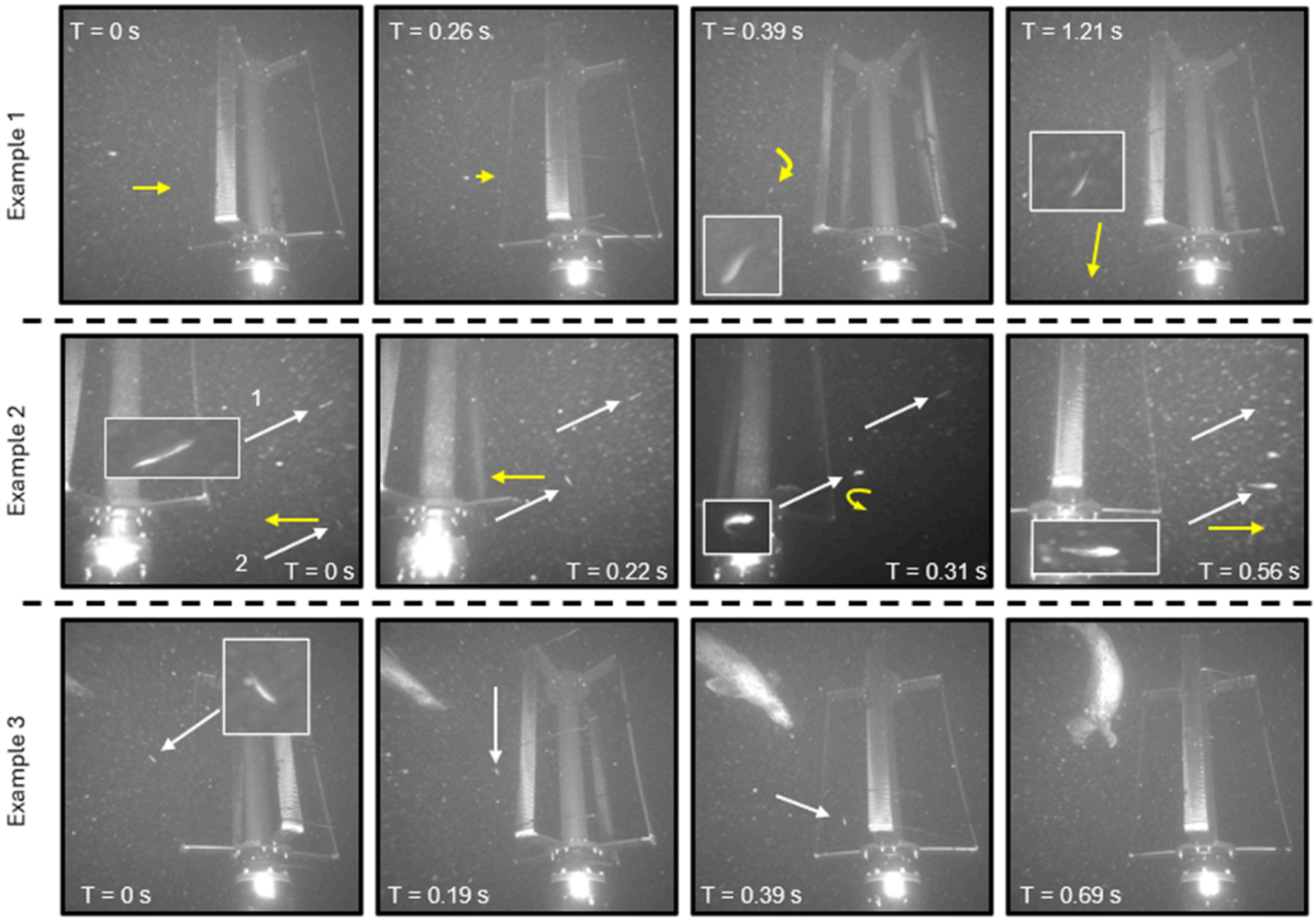

Fig 8. **Examples of evasion events while the turbine was operational**. In the images, the white arrows point to the fish and the yellow arrows approximate the direction of travel in optical images. Times are presented relative to the first frame. (Example 1) An evasion event with a single small fish. The fish approaches the rotor before turning and diving down away from the rotor. (Example 2) Two fish evading the turbine rotor using different tactics. Fish 1 swims against the current and moves out of the field of view. Fish 2, swimming with the current, executes a turn and swims away from the rotor. (Example 3) A seal pursuing a fish. The fish swims into and out of the rotor, evading a collision with the moving rotor in the process. As the seal approaches the moving rotor it stops pursuing the fish, slows down, and swims away from the rotor.

https://doi.org/10.1371/journal.pone.0338376.g008

Seabirds

A total of 406 unique events containing seabirds, including pigeon guillemots, double-crested cormorants, and possibly pelagic cormorants, were recorded (see examples in Fig 10). Of the observed seabirds, 74% (299) were identified as cormorants and 26% (105) were identified as pigeon guillemots. One event could not be attributed to either species because the bird was too close to the camera to identify distinguishing features.

Diving seabirds were exclusively observed when the turbine was not operating (Table 2), and were most frequently observed at high tide, when there were the longest periods of near-slack water (Fig 4). Seabirds were only detected at flow speeds greater than the minimum turbine cut-in speed of 0.9 m/s on two occasions. On 7 February, a pigeon guillemot was observed swimming towards the water surface between the turbine and the AMP when the flow speed was

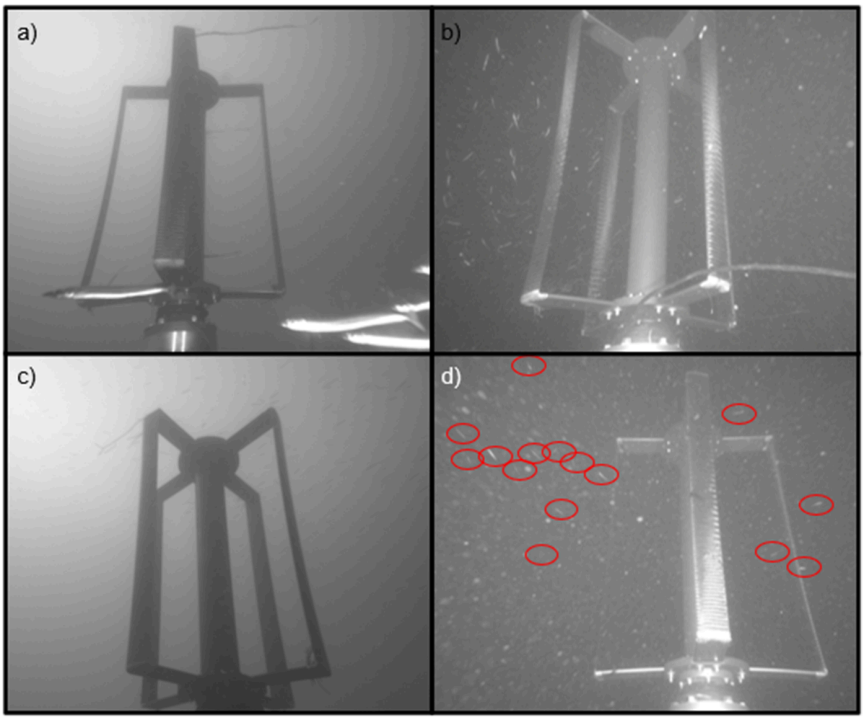

Fig 9. **Examples of fish schools**. (a–b) A small school of forage fish near the AMP. (b) A fish school near the rotor. Most fish swim up or around the backside of the rotor although several swim between the rotor and the camera. (c) A fish school near the surface while the turbine was stationary. (d) A fish school evading the turbine rotor at night while the turbine was rotating. Red circles highlight the individual fish.

https://doi.org/10.1371/journal.pone.0338376.g009

approximately 0.9 m/s. The turbine cut-in speed was adjusted to 1 m/s at this time, so the turbine was not rotating. At the end of deployment, when the turbine was no longer operational (12 February), a cormorant was observed diving at a shallow angle (across the frame) in the background when the flow speed was 1.02 m/s and the turbine would have recently started to rotate had it not been shut down. All observations of diving seabirds were during the day, and seabirds were observed diving through the camera field of view towards the base of the Turbine Lander and resurfacing with prey (fish), indicating that they were likely foraging around the base of the turbine.

Seals

Harbor seals were observed in 92 unique events (Table 2). Most seals (90%) were detected during periods when the turbine was not operating, and no instances of collision were observed. Seals were observed during all hours of the day, but more frequently when it was dark (58%; Fig 4). This is particularly notable given the lack of automatic detection models and limited sampling at night for much of the deployment. We also note that observations of seals were not evenly distributed in time; seals were observed on 44 unique days, with up to 22 events on a single night (3-4 November 2023).

Seals were observed encountering the turbine while it was moving on nine occasions. Three of these events were instances when the turbine was operating due to a system error and flow speeds were below 0.9 m/s, four were at flow speeds between 0.9 and 1 m/s, and two were at flow speeds between 1.3 and 1.4 m/s. Three types of seal behavior were observed while the turbine was rotating. In three events, the seal was observed in the background, and did not approach the moving turbine (Fig 11a). In four events, the seal approached the moving turbine rotor and swam in its wake with its head oriented towards the turbine before swimming away (Fig 11b). These interactions ranged in duration from a few

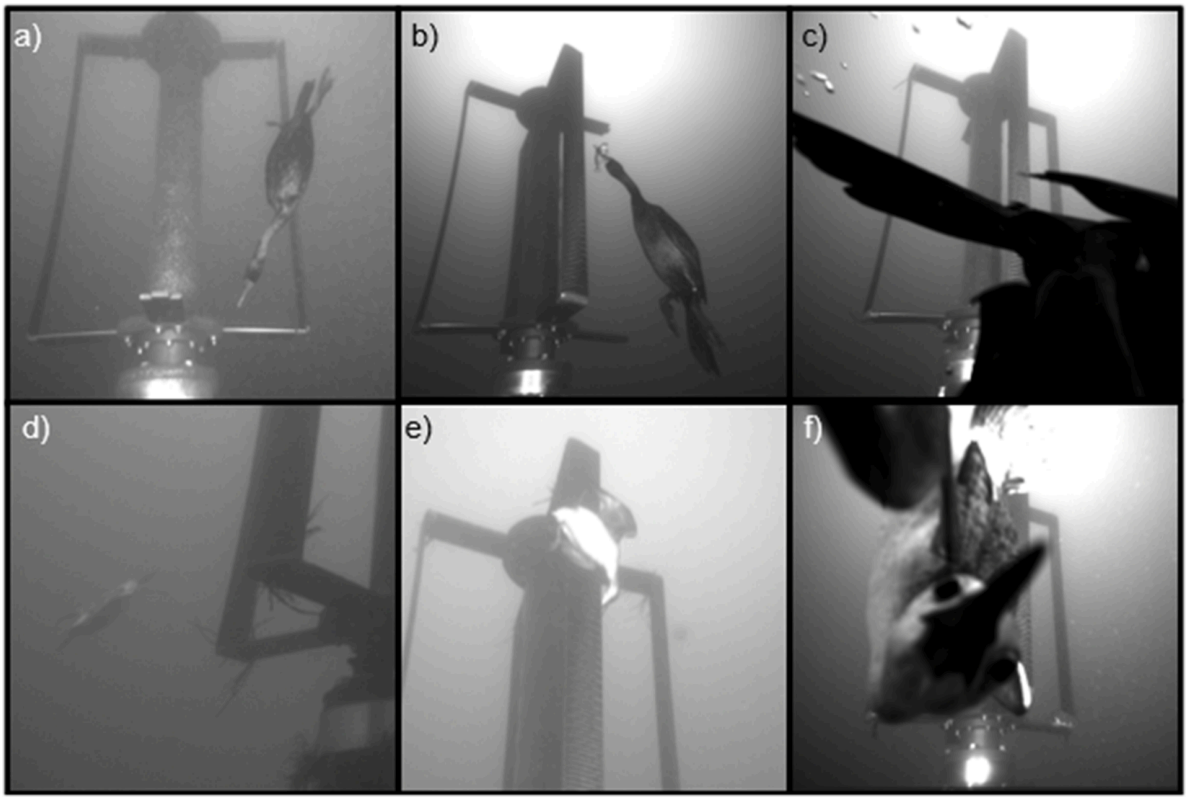

Fig 10. **Examples of seabirds**. (a–c) Cormorants diving, swimming to the surface, and presumably foraging in the vicinity of the AMP. (d-f) Pigeon guillemots swimming, picking at the rotor, and interacting with the AMP.

https://doi.org/10.1371/journal.pone.0338376.g010

seconds to several minutes. Lastly, in two events, the seal was pursuing fish prey. In one of these events, upon encountering the turbine, the seal stopped pursuing the fish and changed trajectory to avoid colliding with the moving turbine rotor (i.e., evasion). The fish then passed through the rotor, evading the blades without collision (Fig 8). In the other case, the full event was not captured but the recorded frames show the fish near the turbine and swimming away from the seal while the seal swims away behind the rotor. Review of the acoustic camera data concurrent with fish evasion and collision events identified seven additional events where seals were in the vicinity of the turbine while it was rotating, but did not approach the turbine and therefore were not observed in the optical cameras (including the five fish events previously discussed).

While the turbine was stationary, seals were observed both swimming past the turbine without changing trajectory (i.e., no attraction) and directly interacting with the turbine structure or the AMP (i.e., attraction). Instances of seals interacting with the stationary turbine structure included swimming between the turbine rotor blades and shaft or simply approaching different parts of the rotor (Fig 11c, 11d).

Comparison between continuously-acquired data and detected events

A comparison between the events in the overlapping period of data subsets 2 (daytime continuous data collection) and 3 (detected events) offers some insight into the performance of the real-time detection model for bird and seal detection. Due to a software bug introduced when continuous acquisition was enabled on 25 January, real-time detection models were not running reliably between 25 and 31 January. After the bug was resolved on 31 January, 94 of the 123 (76%)

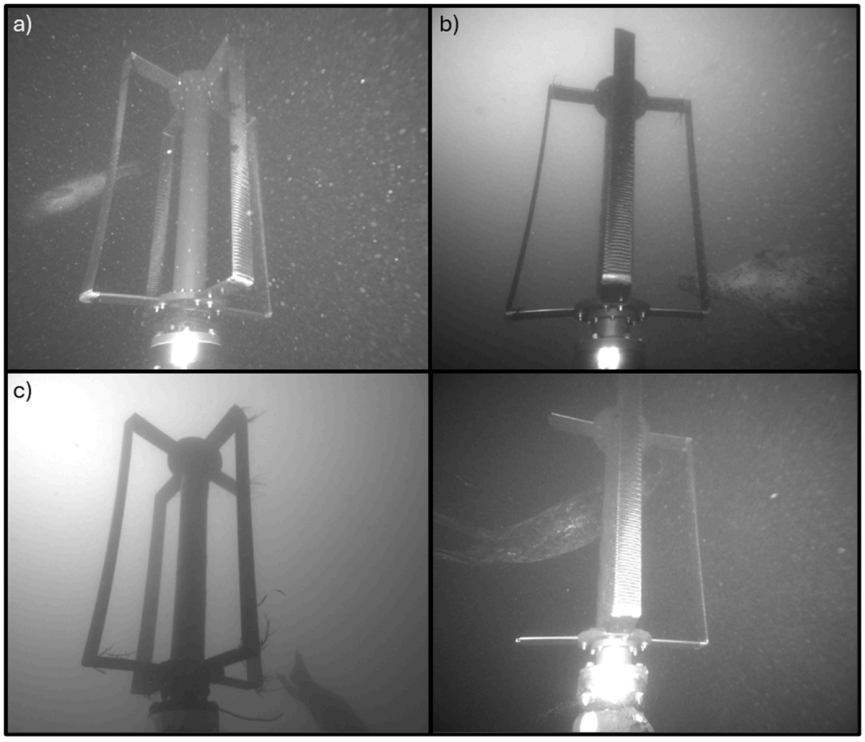

Fig 11. **Examples of seals**. a) Seal swimming behind the moving rotor at night. b) Seal approaching the moving rotor in the wake during the day. c) A seal diving towards the seabed. d) A seal entering the rotor's swept area and bending around the shaft. In both (c) and (d) the rotor was stationary.

https://doi.org/10.1371/journal.pone.0338376.g011

events containing seabirds and 9 of the 11 (82%) events containing seals that were identified in the continuously acquired data comprising data subset 2 were also contained in data subset 3 (i.e., were detected by the real-time detection model). In 14 of the 29 bird events and both of the seal events that were missed by the detection model, the animal was only faintly visible in the background of the image beyond the turbine or near the edge of the camera field of view. This indicates that the detected events in data subset 3 likely contain most events where seabirds and seals approached the turbine rotor during periods with sufficient illumination for optical detection, though we cannot quantitatively assess performance throughout the deployment since the model was iteratively retrained. However, retraining was generally found to have a more significant effect on reducing the false positive rate (number of images archived that did not contain an animal of interest) than the false negative rate (number of animals missed).

In addition, Fig 4 shows that the trends in bird and seal presence with respect to time of day, flow velocity, and tidal elevation remain fairly consistent between the data subsets comprised of scheduled data acquisition (subsets 1 and 2) and the data subset comprised of detected events (subset 3). This indicates that, while we cannot quantitatively assess the total number of animals that encountered the turbine, our analysis of the conditions under which seabirds and seals encountered the turbine is likely representative.

Discussion

Limitations of this study and implications for collision risk

In the review of optical camera imagery spanning 109 days, we observed four instances of fish collision with the moving turbine (out of 229 individual fish and 5 fish schools observed encountering the moving turbine). No instances of collision with seabirds or marine mammals were observed. Several important limitations of this study must be considered when

interpreting the results. First, the real-time detection model that triggered data collection at a sufficiently high frame rate to resolve fine-scale fish behavior did not effectively detect fish. Therefore, our observations of fish offer insights into fish behavior around the turbine, but we cannot draw conclusions about trends in fish behavior or the total number of fish that encountered, evaded, or collided with the turbine. Second, sampling was limited at night, when the turbine was most frequently rotating due to local tidal forcing, indicating that many animal interactions with the moving turbine at night were likely not recorded. Finally, because optical camera observations are limited to the near-field, our results offer insight into the conditions under which animals encountered the moving turbine and their behavior around the turbine structure. We are not able to draw conclusions about avoidance behavior at ranges beyond the field of view of the cameras.

To our knowledge, this paper presents the first observations of fish collisions with a tidal turbine in the literature, though fish collision with a riverine turbine has previously been observed [31]. In three of the four cases of collision with the moving turbine, the fish appeared to swim away after the blade strike event. While we cannot quantify the total number of collisions that occurred, our observations indicate that the probability of collision for fishes is low (225 fish of the 229 fish observed encountering the moving turbine did not experience collision). Further, our observations indicate that even relatively small fish are capable of evasion at flow speeds exceeding 2 m/s. For these small fish, flow speeds during turbine operation typically exceed a value of 10 body lengths per second. This threshold corresponds to the upper limit of swimming speeds that most fish can achieve for short periods of time (burst swimming), while sustained swimming speed thresholds would be expected to be lower [32,33]. We hypothesize that the inability of small fish to swim against the current in a sustained manner may explain why most fish observed during turbine operation were small (i.e., large fish with stronger swimming capabilities may have avoided the turbine outside of the camera field of view). If true, burst swimming speeds, in conjunction with the speed of a turbine's blades, could be used to evaluate fish evasion capabilities. Finally, observations of seals pursuing fish immediately before those fish either collided with or evaded the turbine indicates that predator-prey interactions may be drivers of fine-scale fish behavior around a moving turbine.

The total number of fish encounters with the turbine that were identified by reviewers is likely a significant underestimate of the actual number of fish encounters during the reviewed time periods. Distinguishing between drifting plant matter and fish in the optical data was difficult for human reviewers because many fish were observed to be drifting without actively swimming. In these cases, lacking fish-like motion to unambiguously distinguish between plant matter and fish, we chose to limit positive identification of fish events to cases where the imagery was unambiguous due to fish-like characteristics (e.g., fins). In several cases, objects were observed that were not initially identified as fish when they entered the field of view, but were only determined to be fish after they exhibited evasion behavior when they approached the turbine rotor. We also speculate that fish were more readily discernible at night due to reflection of the direct light from the strobes. However, even at night, the orientation of the animals influenced detectability. Fish oriented perpendicular to the camera lens scattered relatively little light and appeared only as small dots with no discernible features unless their orientation changed during sampling.

Because evasion and collision both involve the fish actively moving, changing orientation, or interacting with a turbine blade, we feel confident that all of the clear instances of these interactions were logged. Instances of evasion that involved subtle changes to trajectory to avoid interactions may have been under-counted due to difficulties identifying the behavior. However, we believe it is reasonable to speculate that an order of magnitude more small fish were likely present in recorded images than were counted. If true, this would considerably decrease the fraction of fish encounters with the moving turbine that involved evasion or collision. Unfortunately, we cannot recommend any specific sampling or processing approaches to mitigate these biases in optical camera imagery unless conditions are suitable for color imagery. The challenges in optical detection could be mitigated, in part, through the use of acoustic cameras, though detection of fish in the vicinity of a moving turbine is not straightforward and there are many other challenges associated with detection of fish in acoustic camera imagery [34].

Because over 99% of seabirds were observed during periods with currents below the minimum turbine cut-in speed of 0.9 m/s, and all seabirds were detected when the turbine was not operating, our observations suggest that the risk of

collision for seabirds during this turbine deployment was low. This is consistent with studies of the foraging patterns of black guillemots in tidal channels conducted in Scotland, UK [20,21]. However, a study conducted in the same geographic region as the Turbine Lander deployment (Vancouver Island, Canada) found higher abundance, but no increase in diving behavior, of pigeon guillemots and pelagic cormorants during periods of high flow [35], and other species of seabirds have been shown to forage in strong currents [20]. We also only observed diving seabirds during daylight hours. This is consistent with previous observations of cormorants [36] and pigeon guillemots [37], but cormorants have been observed foraging at night in regions with seasonally low ambient light [38] and nocturnal foraging behavior has been reported for other species of guillemots [37]. The variability of trends in seabird behavior reported in the literature indicates that collision risk will vary between species and may vary between locations for the same species or family of seabirds. We note that subsurface observations are not necessary to determine temporal patterns in bird foraging; telemetry or visual surveys may provide much of the necessary information to assess this risk if the bird foraging depths are known.

Harbor seals most frequently encountered the turbine while it was stationary, though nine instances of seal interaction with the moving turbine were recorded. Three of these observations occurred during periods when the turbine was rotating at flow speeds below the turbine cut-in speed due to a software error. The fact that we detected most seals when the turbine was not operational is consistent with a recent study that used a multibeam sonar to monitor seal presence around a grid-scale tidal turbine in the Pentland Firth, Scotland [16]. When we observed seal encounters with the turbine while it was rotating, their behavior indicated that they were capable of evasion, even when pursuing prey. This would suggest that even though harbor seals may have exhibited attraction to the turbine, they were at low risk of collision. The highest risk may occur at turbine start-up if a seal is present and interacting with the stationary rotor. To mitigate this risk, devices could be programmed with a "soft start" wherein the turbine ramps up to its operating state slowly, giving any animals present the time to move away from the device. Alternatively, a deterrence device could be activated for a short period before turbine start-up.

Lastly, in considering the implications of this study for a broader understanding of collision risk, it is important to consider that design of a tidal turbine (e.g., cross-flow versus axial-flow) influences the risk of collision. Specifically, cross-flow turbines like the one in this study operate most efficiently at lower tip-speed ratios than axial-flow turbines [39]. For the majority of the deployment, the Turbine Lander blades moved at approximately two times the flow speed (tip-speed ratio of 2), resulting in peak blade speeds of less than 5 m/s. Axial flow turbines typically operate at tip-speed ratios between 4 and 6, meaning that, at the Sequim Bay test site, the tips of the blades of an axial flow turbine would be moving over 10 m/s during peak flow speeds, more than twice as fast as the cross-flow turbine studied here. Animals may be less capable of evading faster-moving blades, and the consequence of collision (i.e., severity of injury or mortality) with a faster moving blade would potentially be higher.

Lessons learned and recommendations for future studies

While the optical camera imagery collected using the AMP offers many insights into how animals behaved in the vicinity of the Turbine Lander, we cannot draw conclusions about animal encounter rates or the probability of collision. There are several reasons for this, including our decision to focus our analysis on the optical camera imagery and the variable sampling strategies used throughout the deployment. In the sections that follow, we discuss lessons learned from this study and how they can inform future efforts.

Trade-offs of optical vs. acoustic cameras. As has been well established in previous work [40,41], no single sensor can provide all of the necessary information to characterize animal behavior around turbines. While optical cameras, like those used in this study, are the only sensor that can provide high-resolution information sufficient to characterize fine-scale animal behavior and facilitate species-level identification, they have limited range and are reliant on optical clarity and availability of light. While a single optical camera captured the entire Turbine Lander in its field of view, this is typically not possible for grid-scale turbines (e.g., [9]). Conversely, acoustic cameras can detect animals at the longer ranges

(tens of meters) necessary to monitor larger turbines and observe avoidance behavior. Acoustic cameras, depending on their operating frequency, can also operate in more turbid waters and without illumination, but their low resolution and frame rates (depending on range requirements) limit behavior classification capabilities for small animals, and even for larger animals at greater ranges. Our goal before deploying the Turbine Lander was to leverage the advantages of both sensor types for multi-sensor, 24-hour monitoring, but, we ultimately prioritized human review and development of automatic detection models for the optical camera data. While time and budget constraints were a factor, this approach was also driven by the fact that the position of the AMP on the Turbine Lander resulted in more compelling optical imagery. The optical cameras captured the entire turbine rotor, while the close range of the acoustic cameras meant that only a "slice" of the rotor was captured in the field of view. As a result of the narrow beamwidth at the range of the turbine, larger animals (i.e., seabirds and seals) took up a sufficiently large fraction of the beam to cause processing artifacts that partially obscured the image if the animal was near the turbine. Further, clutter in the acoustic camera imagery from the turbine structure and entrained sediment and plant matter made it difficult to interpret fine-scale animal behavior around the turbine.

Our focus on the optical cameras severely limited our observations at night. Because continuous operation of artificial illumination for nighttime monitoring with optical cameras, whether white or red light, can bias animal behavior [42, 43], we only enabled artificial illumination at night on a sparse duty cycle or when animals were detected in the acoustic camera data. A duty cycle is likely to miss interactions of interest, making acoustic camera-triggered artificial illumination ideal. However, deployment of automatic detection models on the acoustic camera imagery was not attempted until late in the deployment (February), and they did not perform well due to the large number of false positive detections resulting from the motion of the turbine and debris in the water column. Ultimately, better positioning of the acoustic cameras and the development of more effective strategies for real-time detection of animals in the presence of a moving turbine will be a high priority for future deployments of the AMP. While there are existing methods for the real-time, automatic detection of animals in acoustic camera data (e.g., [44]), the task is further complicated in the presence of a moving turbine structure because it introduces significant frame-to-frame variability even when animals of interest are not present. The development of effective algorithms for real-time acoustic camera detection of animals in the presence of a turbine will likely require a combination of advanced background subtraction methods, target tracking, and other classification models.

Sampling strategies and automatic detection. Many lessons were learned about how to balance conflicting priorities for data collection and about how to train and evaluate machine learning models for real-time animal detection throughout the Turbine Lander deployment. We initially adopted a high frame rate duty cycle to assess system performance and collect training data for real-time detection models (Fig 3). Our primary reason for this was that high frame rate data are required to evaluate fine-scale animal behavior, including collision and evasion, in either optical or acoustic camera imagery. For example, if an animal is moving with the currents at a flow speed of 2 m/s, and data are acquired at a low frame rate of 1 Hz, the animal will move 2 m between frames, a distance longer than the turbine rotor diameter. However, if data were acquired at 20 Hz, the animal would move 10 cm between frames, a distance similar to the chord length of one of the turbine blades. Because acquiring data continuously at such a high frame rate would accrue unwieldy volumes of data (over 175 GB per day if data were acquired at 20 Hz from one of the AMP cameras), we initially identified a duty cycle as the best solution for data collection before automatic detection was enabled.

In practice, we quickly identified that the duty cycle did not capture a sufficient number of events to train an automatic detection model or to gain a comprehensive understanding of the types of animals that were interacting with the turbine. Further, while the duty cycle produced many images of the animals that were recorded (e.g., 20 images of the same seal), it was preferable to have fewer images of many animals (e.g., two images each of 10 different seals) to build a more robust machine learning model for animal detection. Therefore, we switched to low frame rate, continuous acquisition on 8 November. This approach was effective in building a more robust training data set, and after just over a week, an automatic detection model was redeployed on 17 November. At this point, we disabled continuous data acquisition and began

duty cycle acquisition again. However, when faced with evaluating the false negative rate of the model (i.e., number of missed targets), we realized that the continuous, low frame rate data acquisition would again be preferable for the same reasons, and began continuous recording again on 25 January. Ultimately, our ability to quantitatively assess the performance of the models deployed in real-time before 25 January was limited, meaning that we cannot use our results to assess the rates of animal encounter, evasion, or collision.

Based on these experiences, and with the advantage of hindsight, we recommend the following strategy for future optical camera data collection campaigns with cabled instrumentation systems. Initially, low frame rate, continuous acquisition is recommended during daylight hours. If artificial illumination is available, a high duty cycle at night should be considered. While we acknowledge this may bias animal behavior, the benefits of sampling during periods when data are otherwise unavailable may outweigh the benefits of collecting an unbiased sample with few relevant observations. Further, sampling more frequently or even continuously at a high frame rate during periods when the turbine is rotating should also be considered, as these data are significantly more valuable than data collected while the turbine is stationary. Data should be reviewed and annotations used to train a detection model for identification of animal classes (e.g., fish, seabirds). This is time-intensive, but necessary, to enable subsequent reductions in data volume and associated processing requirements. If the model achieves suitable performance in testing, continuous data acquisition can be disabled, although low duty cycle data acquisition is still recommended. If the model is re-trained or updated during the deployment, the initial period of continuously acquired data, in addition to newly acquired duty-cycled data, can be used as a baseline to assess model performance and false negative rates. Depending on the species of interest and the image quality, in some cases, suitable model performance may not be achievable. For example, reliable detection of small fish was challenging for human reviewers in our dataset, and it is unlikely that a machine learning algorithm will be able to detect them reliably. In this case, high duty cycles or continuous data acquisition are recommended. A similar strategy would be recommended for acoustic cameras, but continuous data acquisition could be utilized during all hours of the day.

When evaluating the performance of detection models, we recommend using different evaluation metrics than are used for many applications of machine learning. In this application, the machine learning model is being used to identify periods of data to archive for human review, not to count the total number of frames that animals are identified in. For example, if a seal enters the field of view, there may be frames where only part of the seal is visible that might be missed by automatic detection algorithms. However, if the seal is detected by the model later in the sequence, data stored in a ring buffer can be archived to capture the entire event. This indicates that frame-by-frame assessment of model performance is not the most representative metric for model performance. Rather, model performance should be evaluated on an event basis - an event can be considered “captured” if the animal was detected in at least one frame that would be archived and flagged for human review. Further, for many applications of machine learning, correct and incorrect detections are weighted equally, but for this application, models should be tuned to favor a high true positive rate over a low false positive rate. The “cost” of an incorrect detection is additional human review and data storage, while the “cost” of a missed event is potentially lost knowledge of animal interactions of interest. As long as the cost imposed by false positives is acceptable, which would typically be measured by the time to archive and review them, relatively high false positive rates are not inherently problematic.

Conclusions

While there are several limitations to the presented data, the observations of animal interactions with an operational tidal turbine reported in this study provide new insight into animal behavior around tidal turbines. Seabirds were likely at low risk for collision, given that they were frequently observed when the turbine was stationary but were never observed while it was operating. While this result may be limited to the specific species and site, it is the most comprehensive set of observations of seabird interactions with a tidal turbine to date. Seals were occasionally observed while the turbine was rotating, but exhibited strong swimming capabilities indicating that they are capable of evading collision. While four fish

collision events with the moving turbine were observed, more than 10 times more fish were observed evading the moving turbine blades, including during periods when flow speeds exceeded 2 m/s. Further, many more fish were likely present in the imagery that encountered the turbine without collision but were difficult or impossible to identify.

Supporting information

S1 Species Table. List of all animal families and species observed. SpeciesTable.xlsx includes all observed animals, reviewer confidence in taxonomic classification, and qualitative notes on general behavior observed for each species or family. Confidence was assessed subjectively based on the clearly identifiable characteristics including size, shape, and patterns. The notes describe the confidence of the classification and frequency with which the animals were observed.
(XLSX)

S2 Event Data. Metadata for all annotated events. Events.zip contains CSV files listing the start time, end time, animal class, flow speed, and ambient light conditions for each annotated event. Qualitative notes on animal species and behavior are also included.
(ZIP)

S3 Videos. Corresponding videos for figures. Corresponding_videos.csv contains the file name of the video file corresponding to each figure in the paper containing camera imagery. All videos can be found at [30].
(CSV)

S4 Detailed Description of Human Review Process. Written overview of image review process Review Process.pdf provides a more detailed overview of the human review process for optical images described in the manuscript.
(PDF)

Acknowledgments

The authors wish to thank Lenaïg Hemery for assistance with species identification, Garrett Staines for reviewing an early version of this manuscript, the Pacific Northwest National Laboratory dive team for maintenance of the Turbine Lander, and MarineSitu team members James Joslin, Emily Paine, and Sadie Kass for their contributions to AMP data collection strategy, system deployment and recovery, and data management and data delivery systems. Lastly, we would like to thank the reviewers for their thoughtful reviews of the manuscript.

Author contributions

Conceptualization: Christopher Bassett.

Data curation: Alexa Runyan, Jood M. Almokharrak, Lucy G. Kao, Lillian M. Ovall, Suni A. McMillen.

Formal analysis: Emma Cotter, Christopher Bassett, Mitchell Scott.

Funding acquisition: Christopher Bassett.

Investigation: Emma Cotter.

Methodology: Christopher Bassett.

Project administration: Christopher Bassett, Alexa Runyan.

Software: Paul Murphy, Mitchell Scott.

Validation: Paul Murphy.

Visualization: Emma Cotter.

Writing – original draft: Emma Cotter, Christopher Bassett.

Writing – review & editing: Paul Murphy, Mitchell Scott, Alexa Runyan, Jood M. Almokharrak, Lucy G. Kao, Lillian M. Ovall, Suni A. McMillen.

References

1. IEA-OES. Annual Report: An Overview of Ocean Energy Activities in 2023. 2024. https://www.ocean-energy-systems.org/publications/oes-annual-reports/document/oes-annual-report-2023/
2. Whitt C, Pearlman J, Polagye B, Caimi F, Muller-Karger F, Copping A, et al. Future vision for autonomous ocean observations. Front Mar Sci. 2020;7. https://doi.org/10.3389/fmars.2020.00697
3. Cavagnaro RJ, Copping AE, Green R, Greene D, Jenne S, Rose D, et al. Powering the blue economy: progress exploring marine renewable energy integration with ocean observations. mar technol soc j. 2020;54(6):114–25. https://doi.org/10.4031/mtsj.54.6.11
4. Hutchison ZL, Lieber L, Miller RG, Williamson BJ. Comprehensive Renewable Energy (2nd Edn). Oxford: Elsevier; 2022. p. 258–90.
5. Copping AE, Hasselman DJ, Bangley CW, Culina J, Carcas M. A probabilistic methodology for determining collision risk of marine animals with tidal energy turbines. JMSE. 2023;11(11):2151. https://doi.org/10.3390/jmse11112151
6. Garavelli L, Hemery LG, Rose DJ, Farr JM, Copping AE. OES-environmental 2024 state of the science report: environmental effects of marine renewable energy development around the world. 2024. https://doi.org/10.2172/2438585
7. Ascher SE, Gray IM, Collins CM (Tilly). Misplaced fears? What the evidence reveals of the ecological effects of tidal power generation. Ecol Sol and Evidence. 2025;6(4):e70124.https://doi.org/10.1002/2688-8319.70124
8. Grippo M, Zydlewski G, Shen H, Goodwin RA. Behavioral responses of fish to a current-based hydrokinetic turbine under mutliple operational conditions. Environ Monit Assess. 2020;192(10):645. https://doi.org/10.1007/s10661-020-08596-5 PMID: 32939667
9. Smith K. Shetland tidal array monitoring report: subsea video monitoring. Nova Innovation; 2021.
10. Bender A, Langhamer O, Francisco F, Forslund J, Hammar L, Sundberg J, et al. Imaging-sonar observations of salmonid interactions with a vertical axis instream turbine. River Research & Apps. 2023;39(8):1578–89. https://doi.org/10.1002/rra.4171
11. Hammar L, Andersson S, Eggertsen L, Haglund J, Gullström M, Ehnberg J, et al. Hydrokinetic turbine effects on fish swimming behaviour. PLoS One. 2013;8(12):e84141. https://doi.org/10.1371/journal.pone.0084141 PMID: 24358334
12. Viehman HA, Zydlewski GB. Fish interactions with a commercial-scale tidal energy device in the natural environment. Estuaries and Coasts. 2014;38(S1):241–52. https://doi.org/10.1007/s12237-014-9767-8
13. Bevelhimer M, Scherelis C, Colby J, Adonizio MA. Hydroacoustic assessment of behavioral responses by fish passing near an operating tidal turbine in the East River, New York. Trans Am Fish Soc. 2017;146(5):1028–42. https://doi.org/10.1080/00028487.2017.1339637
14. Gillespie D, Palmer L, Macaulay J, Sparling C, Hastie G. Harbour porpoises exhibit localized evasion of a tidal turbine. Aquatic Conservation. 2021;31(9):2459–68. https://doi.org/10.1002/aqc.3660
15. Palmer L, Gillespie D, MacAulay JDJ, Sparling CE, Russell DJF, Hastie GD. Harbour porpoise (Phocoena phocoena) presence is reduced during tidal turbine operation. Aquatic Conservation. 2021;31(12):3543–53. https://doi.org/10.1002/aqc.3737
16. Montabaranom J, Gillespie D, Longden E, Rapson K, Holoborodko A, Sparling C, et al. Seals exhibit localised avoidance of operational tidal turbines. Journal of Applied Ecology. 2025;62(2):242–52. https://doi.org/10.1111/1365-2664.14844
17. Onoufriou J, Russell DJF, Thompson D, Moss SE, Hastie GD. Quantifying the effects of tidal turbine array operations on the distribution of marine mammals: implications for collision risk. Renewable Energy. 2021;180:157–65. https://doi.org/10.1016/j.renene.2021.08.052
18. Hastie GD, Russell DJF, Lepper P, Elliott J, Wilson B, Benjamins S, et al. Harbour seals avoid tidal turbine noise: implications for collision risk. Journal of Applied Ecology. 2017;55(2):684–93. https://doi.org/10.1111/1365-2664.12981
19. Slingsby J, Scott BE, Kregting L, McIlvenny J, Wilson J, Yanez M, et al. Using Unmanned Aerial Vehicle (UAV) imagery to characterise pursuit-diving seabird association with tidal stream hydrodynamic habitat features. Front Mar Sci. 2022;9. https://doi.org/10.3389/fmars.2022.820722
20. Couto A, Williamson BJ, Cornulier T, Fernandes PG, Fraser S, Chapman JD, et al. Tidal streams, fish, and seabirds: understanding the linkages between mobile predators, prey, and hydrodynamics. Ecosphere. 2022;13(5). https://doi.org/10.1002/ecs2.4080
21. Johnston D, Furness R, Robbins A, Tyler G, McIlvenny J, Masden E. Tidal stream use by black guillemots Cepphus grylle in relation to a marine renewable energy development. Mar Ecol Prog Ser. 2021;669:201–12. https://doi.org/10.3354/meps13724
22. Bassett C, Gibbs P, Wood H, Cavagnaro RJ, Cunningham B, Dosher J, et al. Lessons learned from the design and operation of a small-scale cross-flow tidal turbine. J Ocean Eng Mar Energy. 2025;11(4):909–29. https://doi.org/10.1007/s40722-025-00411-y
23. Thompson SW, Snyder SF, Duberstein CA, Norris ES, Barnett JM, Blake JL. Pacific Northwest National Laboratory Annual Site Environmental Report for Calendar Year 2023. PNNL-36464. Pacific Northwest National Laboratory; 2024. https://doi.org/10.2172/2476873
24. Washington Department of Fish and Wildlife WDFW. 2024. https://wdfw.wa.gov/fishing/management/marine-beach-spawning#herring
25. Penttila D. Marine forage fishes in puget sound. Washington Department of Fish and Wildlife. 2007. https://wdfw.wa.gov/sites/default/files/publications/02193/wdfw02193.pdf

26. Polagye B, Joslin J, Murphy P, Cotter E, Scott M, Gibbs P, et al. Adaptable monitoring package development and deployment: lessons learned for integrated instrumentation at marine energy sites. JMSE. 2020;8(8):553. https://doi.org/10.3390/jmse8080553
27. Bassett C, Cotter E. Observation of fish, birds, and harbor seals around an operating cross-flow turbine. Proc EWTEC. 2025;16. https://doi.org/10.36688/ewtec-2025-907
28. Jocher G, Qiu J, Chaurasia A. Ultralytics YOLO. 2023. https://github.com/ultralytics/ultralytics
29. Whiting JM, Cotter ED, McVey JR, Williams NG, Zimmerman SA, Vavrinec J, et al. Data fusion to enhance quality control and analysis with instruments at the marine and coastal research laboratory. Pacific Northwest National Laboratory; PNNL-32294; 2021. https://doi.org/10.2172/1842840
30. Bassett C, Cotter E. Turbine Lander, Sequim Bay (2023-2024) Environmental Observations and Data. 2025. https://mhkdr.openei.org/submissions/599
31. Courtney MB, Flanigan AJ, Hostetter M, Seitz AC. Characterizing sockeye salmon smolt interactions with a hydrokinetic turbine in the Kvichak River, Alaska. North American Journal of Fisheries Management. 2022;42(4):1054–65. https://doi.org/10.1002/nafm.10806
32. Bainbridge R. The speed of swimming of fish as related to size and to the frequency and amplitude of the tail beat. Journal of Experimental Biology. 1958;35(1):109–33. https://doi.org/10.1242/jeb.35.1.109
33. Sambilay JVC. Interrelationships between swimming speed, caudal fin aspect ratio, and body length of fishes. Fishbyte. 1990;8(3):16–20.
34. Cotter E, Staines G. Observing fish interactions with marine energy turbines using acoustic cameras. Fish and Fisheries. 2023;24(6):1020–33. https://doi.org/10.1111/faf.12782
35. Holm KJ, Burger AE. Foraging behavior and resource partitioning by diving birds during winter in areas of strong tidal currents. Waterbirds. 2002;25(3):312–25. https://doi.org/10.1675/1524-4695(2002)025[0312:fbarpb]2.0.co;2
36. King DT, Harrel JB, Dorr B, Reinhold D. Observations of nocturnal foraging in the double-crested cormorant. Colonial Waterbirds. 1998;21(2):234. https://doi.org/10.2307/1521911
37. Ewins PJ. Pigeon Guillemot (Cepphus columba), version 2.0. In: Poole AF, Gill FB, editors. The Birds of North America. vol. 1. Ithaca, NY: Cornell Lab of Ornithology; 1993. p. 123–30.
38. White CR, Butler PJ, Grémillet D, Martin GR. Behavioural strategies of cormorants (Phalacrocoracidae) foraging under challenging light conditions. Ibis. 2008;150(s1):231–9. https://doi.org/10.1111/j.1474-919x.2008.00837.x
39. Aslam Bhutta MM, Hayat N, Farooq AU, Ali Z, Jamil ShR, Hussain Z. Vertical axis wind turbine – a review of various configurations and design techniques. Renewable and Sustainable Energy Reviews. 2012;16(4):1926–39. https://doi.org/10.1016/j.rser.2011.12.004
40. Cotter E, Murphy P, Polagye B. Benchmarking sensor fusion capabilities of an integrated instrumentation package. International Journal of Marine Energy. 2017;20:64–79. https://doi.org/10.1016/j.ijome.2017.09.003
41. Hasselman DJ, Barclay DR, Cavagnaro RJ, Chandler C, Cotter E, Gillespie DM, et al. Environmental Monitoring Technologies and Techniques for Detecting Interactions of Marine Animals with Turbines. In: Copping AE, Hemery LG, editors. OES-Environmental 2020 State of the Science Report: Environmental Effects of Marine Renewable Energy Development Around the World. Report for Ocean Energy Systems (OES); 2020. pp. 176–213. https://doi.org/10.2172/1633202
42. Rooper CN, Williams K, De Robertis A, Tuttle V. Effect of underwater lighting on observations of density and behavior of rockfish during camera surveys. Fisheries Research. 2015;172:157–67. https://doi.org/10.1016/j.fishres.2015.07.012
43. Geoffroy M, Langbehn T, Priou P, Varpe Ø, Johnsen G, Le Bris A, et al. Pelagic organisms avoid white, blue, and red artificial light from scientific instruments. Sci Rep. 2021;11(1):14941. https://doi.org/10.1038/s41598-021-94355-6 PMID: 34294780
44. Cotter E, Polagye B. Automatic classification of biological targets in a tidal channel using a multibeam sonar. Journal of Atmospheric and Oceanic Technology. 2020;37(8):1437–55. https://doi.org/10.1175/jtech-d-19-0222.1